Phycocyanin Protects INS-1E Pancreatic Beta Cells against Human Islet Amyloid Polypeptide -induced Apoptosis through Attenuating Oxidative Stress and Mitochondrial Dysfunction

LI, Xiaoling

A Thesis Submitted in Partial Fulfilment
of the Requirements for the Degree of
Doctor of Philosophy
in
Medical Sciences

The Chinese University of Hong Kong
August 2010

Declaration of Originality

The work contained in this thesis is the original research performed by the author at the Department of Medicine and Therapeutics, The Chinese University of Hong Kong. No part of the work described in this thesis has already been or is being currently submitted for any such degree, diploma or other qualification.

Acknowledgements

Foremost, I would like to thank my supervisor, Prof. Juliana C.N. Chan and Prof. Gang Xu, for their patience, continuing encouragement and elaborate guidance. Aside from helping me formulate hypothesis, design experiments and interpret results, they have also been most kind and supportive during my study and research.

I am also deeply grateful to Prof. Y.S. Wong, Dr. Tianfeng Chen and Ms. Iris Tong in the Department of Biology, The Chinese University of Hong Kong, for their thoughtful suggestions, valuable technical support, assistance and encouragement in the past years.

I would like to express my gratitude to all my other senior colleagues and labmates in Li Ka Shing Institute of Health Sciences, who have shared their experience during my completion of this project. They include Dr. Hailu Zhao, Mr. Rocky Fan, Dr. Xuemei Gu, Miss. Kuan Li, Miss. Lucy Xu, Mr. Yaohui Nie and Mr. Zhangfang Kang. Without their help, my research could not have been completed.

Finally, my gratitude to my family for their wholehearted support and understanding is beyond the description by words.

Abstract

It is widely accepted that human islet amyloid polypeptide (hIAPP) aggregation plays an important role in the loss of insulin-producing pancreatic beta cells. Insulin secretion impairment and cell apoptosis can be due to mitochondrial dysfunction in pancreatic beta cells. hIAPP-induced cytotoxicity is mediated by the generation of reactive oxygen species (ROS). Phycocyanin (PC) is a natural compound from blue-green algae that is widely used as food supplement. Currently, little information is available about the effect of hIAPP on mitochondrial function of beta cells and protection of PC against hIAPP-induced cytotoxicity. In this thesis, I hypothesize that hIAPP may impair beta cell function with the involvement of mitochrondrial dysfunction, and this effects could be attenuated by PC. Therefore, the aim of this study was to investigate the role of mitochondria in hIAPP-induced apoptosis, the *in vitro* protective effects of PC and explore the underlying mechanisms.

Our results showed that hIAPP inhibited the INS-1E cell growth in a dose-dependent manner. However, cytotoxicity of hIAPP was significantly attenuated by co-incubation of the cells with PC. hIAPP induced DNA fragmentation and chromatin condensation, which were key characteristics of cell apoptosis. These changes were inhibited by PC as examined by TUNEL assay and DAPI staining. Moreover, PC significantly prevented the hIAPP-induced overproduction of intracellular ROS and malonaldehyde (MDA), as well as changes of activities of

superoxide dismutase (SOD) and glutathione peroxidase (GSH-Px) enzymes. Furthermore, hIAPP triggered the activation of mitogen-activated protein kinases (MAPKs) such as c-Jun N-terminal kinase (JNK) and p38 kinase, and these effects were effectively suppressed by PC.

It was found that hIAPP induced apoptosis in INS-1E cells with the disruption of mitochondrial function, as evidenced by ATP depletion, mitochondrial mass reduction, mitochondrial fragmentation and loss of mitochondrial membrane potential ($\Delta\Psi m$). Further molecular analysis showed that hIAPP induced changes in the expression of Bcl-2 family members, release of cytochrome c and apoptosis-inducing factor (AIF) from mitochondria into cytosol, activation of caspases and cleavage of poly (ADP-ribose) polymerase. Interestingly, the hIAPP-induced mitochondrial dysfunction in INS1-E cells was effectively restored by co-treatment with PC.

Additionally, cyclosporin A, an inhibitor of the mitochondrial permeability transition (MPT) pore, failed to prevent hIAPP-induced $\Delta\Psi m$ collapse, cytochrome c and AIF release and caspase-3 activation, indicating that the MPT pore was not involved in hIAPP-induced apoptosis. On the other hand, potential crosstalk between the extrinsic and intrinsic apoptotic pathways was demonstrated by cleavage of Bid by caspase-8 in the apoptotic process triggered by hIAPP.

Taken together, I have demonstrated for the first time the involvement of mitochondrial dysfunction in hIAPP-induced INS-1E cell apoptosis, which was

attenuated by PC through attenuating oxidative stress, modulating JNK and p38 pathways and reducing mitochondrial dysfunction.

摘要

胰淀素（hIAPP）在 2 型糖尿病发病过程中起着重要作用。线粒体功能损伤是 beta 细胞胰岛素分泌功能障碍及细胞凋亡的主要原因。hIAPP 介导的细胞毒性与活性氧（ROS）有关。藻蓝蛋白（PC）是一种从保健食品螺旋藻中分离出来的具有新颖生物活性的天然化合物。但是，关于 PC 拮抗 hIAPP 毒性及 hIAPP 对 beta 细胞线粒体的功能的作用的研究未见报导。故此，本课题的将研究线粒体在 hIAPP 诱导的 beta 细胞凋亡中的作用，并在此模型中研究 PC 对 hIAPP 毒性的拮抗作用及分子机制。

结果显示：在 INS-1-E 大鼠胰岛细胞模型中，hIAPP 对胰岛细胞的生长具有呈剂量效应的抑制作用，细胞呈现亚二倍体（Sub-G1）凋亡峰、DNA 断裂及染色质的固缩等凋亡特征。相关的分子机制研究发现，hIAPP 处理可提高胰岛细胞内细胞内活性氧（ROS）、丙二醛（MDA）水平以及超氧化物歧化酶（SOD）活性，降低谷胱甘肽过氧化物酶（GSH-Px）活性，诱导 c-Jun N 端激酶(JNK) 和 p38 蛋白激酶磷酸化，Caspase 家族蛋白的活化，提示 hIAPP 通过氧化应激和激活 JNK 和 p38 蛋白激酶通路诱导胰岛细胞凋亡。PC 能有效的抑制 hIAPP 诱导的 INS-1-E 细胞凋亡，降低细胞内活性氧和丙二醛水平，并阻断 MAPK 通路。

基于线粒体在细胞生命活动中的重要性，我们研究了 hIAPP 所诱导的 INS-1-E 细胞线粒体功能损伤。结果发现，hIAPP 能显著的诱导细胞 ATP 耗竭、线粒体膜电位和线粒体质量的下降。同时，hA 通过调控 Bcl-2 家族蛋白的表达而导致细胞中 Cytochrome-c 及 AIF 的转位释放。PC 能有效的抑制 hIAPP 诱导的 INS-1-E 细胞线粒体功能障碍，从而保护细胞，拮抗 hA 的毒性作用。环孢霉

素 A（Cyclosporin A），一种特异性线粒体渗透性转换（MPT）孔抑制剂，未能阻止 hIAPP 诱导的线粒体膜通透性的增加、细胞 Cytochrome-c 及 AIF 的释放和 Caspase-3 活化，提示此细胞凋亡未涉及 MPT 孔的启动。更有趣地，我们发现了在 hIAPP 介导的细胞凋亡中，内源性和外源性凋亡通路通过 Bcl-2 家族蛋白 Bid 而相互窜扰。此项研究首次阐述了线粒体凋亡通路在 hIAPP 的毒性作用中的重要，同时研究了 PC 的保护作用和分子机制。

综上结果，PC 有望成为以 hIAPP 为作用靶点的新型药物在 2 型糖尿病的预防和治疗中发挥作用。关于 hIAPP 诱导胰岛细胞凋亡的分子机制的研究，对于探讨 2 型糖尿病发病机理，寻找以 hIAPP 为作用靶点的 2 型糖尿病治疗药物提供实验和科学依据。

List of Abbreviations

AIF	Apoptosis-inducing factor
BCA	Bicinchoninic acid
BH-3	Bcl-2-homology domain-3
Cdks	Cyclin-dependent kinases
CKIs	Cdk inhibitors
CsA	Cyclosporin A
DAPI	4',6-Diamidino-2-phenyindole
DCF-DA	2′,7′-dichlorofluorescein diacetate
DMEM	Dulbecco's modified Eagle's medium
DMSO	Dimethylsulfoxide
DR	Death receptor
EDTA	Ethylenediaminetetraacetic acid
ERK	Extracellular-regulated kinase
FACS	Fluorescence-activated cell sorting
FBS	Fetal bovine serum
GSH-Px	Glutathione peroxidase
IAPP	Islet amyloid polypeptide
IC_{50}	50 % inhibition concentration values
JC-1	5,5′,6,6′-tetrachloro-1,1′,3,3′-tetraethylimidacarbocyanine iodide
JNK	c-Jun NH_2-terminal kinase
LDH	Lactate dehydrogenase
MAPK	Mitogen-activated protein kinase
MMP	Mitochondrial membrane potential
MTT	3-(4,5-dimethylthiazol-2-yl)-2,5-diphenyl tetrazolium bromide
NADH	Nicotinamide adenine dinucleotide

PARP	Poly (ADP-Ribose) Polymerase
PBS	Phosphate buffered saline
PC	Phycocyanin
PI	Mropidium iodide
ROS	Reactive oxygen species
SAPK	Stress-activated protein kinase
SOD	Superoxide dismutase
TUNEL	TdT-mediated dUTP-biotin nick end labeling
T1DM	Type 1 diabetes mellitus
T2DM	Type 2 diabetes mellitus
UCP-2	Uncoupling protein-2
ΔpH	Transmembrane proton gradient
$\Delta \Psi m$	Mitochondrial membrane potential

Table of Contents

Chapter 1: Introduction

1.1 Diabetes mellitus

Diabetes mellitus is a complex disease characterized by insulin deficiency and/or resistance leading to chronic hyperglycaemia due to inadequate transport of glucose from the vasculature into peripheral tissues, notably fat and muscle. Diabetes is an increasing worldwide health problem and the number of people suffering from diabetes is on the increase due to population growth, aging, urbanization, and increasing obesity and physical inactivity. The prevalence of diabetes worldwide was estimated to be 2.8 % in 2000 and 4.4 % in 2030. The total number of people with diabetes is anticipated to rise from 171 million in 2000 to 366 million in 2030 (Wild et al., 2004). Prevalence of diabetes is higher in developed than in developing countries, but the major increase in people with diabetes will occur in developing countries. Currently, India, China, and the United States are the countries with the largest number of people with diabetes. The majority of people with diabetes in developing and developed countries are in the age range of 45–64 and 65 years, respectively. There are more women than men with diabetes, especially in developed countries.

Diabetic patients have high blood glucose level due to insufficient insulin production or insufficient cellular response to insulin action. Insulin is a hormone

produced by pancreatic islets which promotes glucose entry into the cells for storage or energy production. Insufficient insulin actions can lead to hyperglycemia and other metabolic derangements (such as dyslipidemia, oxidative stress, inflammation) which alter the cellular microenvironment culminating in various organ damages. These include diabetic nephropathy, neuropathy, retinopathy and accelerated atherosclerosis causing ischaemic heart and cerebrovascular disease (Rother, 2007).

Diabetes mellitus can be classified as type 1 (T1DM) and type 2 (T2DM) diseases. T1DM accounts for about 10 % of all cases, while T2DM is a more prevalent form. There is now an explosive increase in the prevalence of T2DM affecting more than 170 million people worldwide. An estimated equal number of people have prediabetes with impaired glucose tolerance who are at high risk for developing T2DM and cardiovascular diseases.

People with T1DM have severe deficiency of insulin production making them susceptible to acute hyperglycemia and ketosis, which can be fatal. Thus, T1DM patients need life long insulin treatment to avoid acute metabolic decompensation. In T1DM, there is selective apoptotic destruction of beta cells in the islets of Langerhans of the pancreas (Atkinson and Eisenbarth, 2001). This type of diabetes can be further classified as immune-mediated or idiopathic. The majority of T1DM patients have autoimmune disease where beta cell loss is due to T-cell mediated

attack (Rother, 2007). There is no known preventive measure against T1DM which accounts for approximately 10 % of all cases of diabetes in North America and Europe.

Type 2 diabetes is the most common metabolic disease in the world. In the United States, it is the leading cause of blindness, end-stage renal disease, and non traumatic loss of limb, with associated health care costs estimated to exceed $130 billion per year. Of even greater concern, T2DM is rapidly becoming a global pandemic. It has been projected to afflict more than 300 million individuals worldwide by the year 2025, with most of the increase occurring in Asia, especially China and India. Although the primary cause of this disease is unknown, primary beta cell defect appears to be an important culprit, often unmasked by insulin resistance due to acquired factors such as obesity (Zimmet et al., 2001).

Diabetes has long been treatable since insulin became medically available in 1921. However, the cure of diabetes is still far from reality. The main treatment for hyperglycaemia in T1DM patients is insulin replacement, typically by injection of the recombinant hormone. Although pancreatic transplantation was able to aboragate or reduce insulin requirement, the procedure requires major surgery and long-term immunosuppression (Gruessner et al., 1997). In morbidly obese T2DM patients, gastric bypass surgery has been successful in causing remisson of disease although

the underlying mechanisms remain uncertain. Although undiagnosed or suboptimally managed diabetes can lead to lethal and devastating complications, there is a large body of evidence showing that lifestyle modification can prevent progression from prediabetes to diabetes and that intensive risk factor control can reduce new onset of all diabetes-related complications (Clark et al., 1988; Gaede et al., 2008; Li et al., 2008; Tuomilehto et al., 2001).

1.2 Islet amyloid polypeptide

1.2.1 Islet amyloid

T2DM is characterized by beta cell dysfunction, reduced beta cell mass, and deposition of islet amyloid derived from islet amyloid polypeptide (IAPP, also known as amylin) (Butler et al., 2003a; Kahn, 2003). IAPP is a 37 amino acid peptide co-secreted with insulin from the beta cells of pancreatic islets in both diabetic and non-diabetic subjects. Under normal circumstances, IAPP is released into the circulation and excreted via the kidney. In contrast to human IAPP, rat IAPP does not form fibrils which is due to lack of proline amino acid residue which has given the hIAPP the propensity to aggregate and form amyloid fibrils (**Fig. 1.1**).

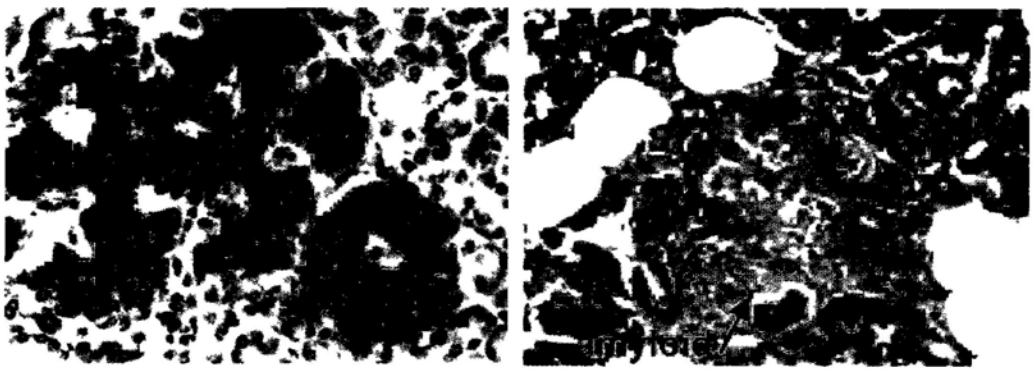

Fig. 1.1 Human islets from T2DM subjects (right) have fewer beta cells than those from nondiabetic subjects and contain deposits of amyloid (arrow) derived from IAPP. Human islets were stained for insulin (Matveyenko and Butler, 2006).

1.2.2 Physiological functions of IAPP

Islet amyloid polypeptide is co-expressed with insulin by pancreatic beta cells. The peptide is also co-secreted with insulin in response to beta cell stimulation by both glucose and non-glucose secretagogues (Haataja et al., 2008). In healthy people, plasma IAPP concentrations range between 4 pmol/l (fasting) and 25 pmol/l (postprandial). The physiological function(s) of IAPP is still not completely understood. Proposed biological actions of IAPP include suppression of food intake, promotion of gastric emptying and augmentation of arginine-stimulated glucagon secretion from pancreatic alpha-cells. Supraphysiological concentrations of IAPP have been shown to have inhibitory effects on both insulin secretion and action but the physiological relevance of these findings has been questioned (Gebre-Medhin et al., 2000).

Application of 10 nM hIAPP to rat soleus muscle strips has been shown to inhibit insulin-mediated glucose uptake. Based on these findings, the authors argued that the large amyloid deposits in the islet in T2DM might be associated with high circulating levels of IAPP, which in turn contributed to insulin resistance. In reality, the circulating concentrations of IAPP (5–20 pM) were found to be far lower than that required to inhibit insulin action (in nanomoles). Furthermore, plasma IAPP levels in T2DM were not found to be elevated compared with nondiabetic controls. While IAPP have been reported to have direct paracrine effect on beta cells to inhibit insulin secretion, delay gastric emptying and suppress appetite, it remains uncertain whether these physiological actions occur within normal circulating levels of IAPP or only in response to pharmacological IAPP concentrations (Haataja et al., 2008).

1.2.3 IAPP and T2DM

IAPP in humans, monkeys and cats is amyloidogenic and these species are known to develop spontaneously T2DM. In contrast, rats and mice do not develop T2DM, since IAPP in rat and mouse is non-amyloidogenic and appears not to be toxic to cultured cells. Importantly, transgenic mice and rats that express hIAPP may develop T2DM especially in the presence of high expression rates of hIAPP, typically in an obesogenic background (Butler et al., 2004; Janson et al., 1996).

In autopsy studies, amyloid is commonly found in T2DM but not in T1DM

since destruction of islet beta cells in the latter removes the source of IAPP. The role of islet amyloid in the pathogenesis of T2DM remains controversial. Accumulating evidence suggests that islet amyloid deposits may play an important role in the loss of beta cells and contribute to the progressive decline in insulin secretion, characteristic of T2DM. Firstly, islet amyloid has been reported in 40-90 % of T2DM patients at autopsy. Although the degree of amyloid deposition correlated with the severity of human disease in most of these case series, negative findings have also been reported (Butler et al., 2003a). Secondly, loss of beta cell mass in both diabetic human and non-human primates is related to islet amyloid formation. Thirdly, amyloid lesion precedes the onset of hyperglycemia in monkeys, suggesting a possible causal role (Marzban et al., 2003). However, there is emerging evidence supporting the beta cell toxicity of hIAPP oligomers rather than amyloid fibrils. Transgenic rodent models that expressed hIAPP developed spontaneous diabetes with loss of islet beta cells in the absence of islet amyloid visible by light microscopy (Janson et al., 1996; Wong et al., 2008). In obese hemizygous hIAPP transgenic mice that developed diabetes, extensive islet amyloid was found, but there was no relationship between the extent of islet amyloid and frequency of beta cell apoptosis (Butler et al., 2003b).

1.2.4 hIAPP induced beta cell death

In *in vitro* studies, both intracellular and extracellular accumulation of hIAPP are associated with beta cell death, although the mechanisms are likely to be different. Exposure to hIAPP fibrils induces death of both human and rat islet beta cells *in vitro* (Lorenzo et al., 1994). While synthetic hIAPPs can spontaneously aggregate into fibrils *in vitro* which are toxic to beta cells, synthetic rodent IAPP does not form fibrils and is not toxic to beta cells (Hiddinga and Eberhardt, 1999; Lorenzo et al., 1994). Besides, the oligomeric aggregates formed by misfolded hIAPP seem to be more cytotoxic than mature amyloid fibrils (Meier et al., 2006). Transgenic mice models with high expression of hIAPP developed diabetes accompanied by decreased beta cell mass and cell dysfunction (Butler et al., 2004; Butler et al., 2003a). In T2DM autopsy cases, extensive islet amyloid depositions may contribute to loss of beta cell and impairment of insulin secretion (Butler et al., 2003a; Clark et al., 1988; Zhao et al., 2003). Taken together, these findings suggest that only aggregated (fibrillar or oligomers) but not soluble forms of IAPP is toxic to beta cells.

In *in vitro* studies, cytotoxic hIAPP fibrils cause formation of ion-permeable pores in lipid bilayer membranes. This results in disruption of ionic homeostasis across the cell membrane which may induce apoptosis and cell death (Anguiano et al., 2002). Accumulating evidence also indicates that the cytotoxicity of hIAPP is

associated with membrane disruption, formation of non-specific ion channels, endoplasmic reticulum (ER) stress and oxidative stress (Haataja et al., 2008; Hoppener and Lips, 2006). However, the sequence of events and the inter-relationships of these proposed molecular mechanisms in causing cell death remain to be fully elucidated.

1.3 Apoptosis and the signaling pathways

In multicellular organisms, apoptosis is a normal component of the cell cycle and tissue remodelling process in response to a cellular "insult", such as ultraviolet light, chemical or physical damage or a viral infection. This insult starts with a cascade of events which culminate into cellular destruction. This mechanism is often referred to as "programmed cell death" as it is an innate response of the cell to protect the rest of the organism from a potentially harmful agent. Apoptosis involves a series of biochemical events with characteristic morphological changes (**Fig. 1.2**). These include blebbing, cell membrane changes such as loss of membrane asymmetry and attachment, cell shrinkage, nuclear fragmentation, chromatin condensation, chromosomal DNA fragmentation and formation of apoptotic bodies (**Fig. 1.3**) culminating in disposal of cellular debris without damaging the organism.

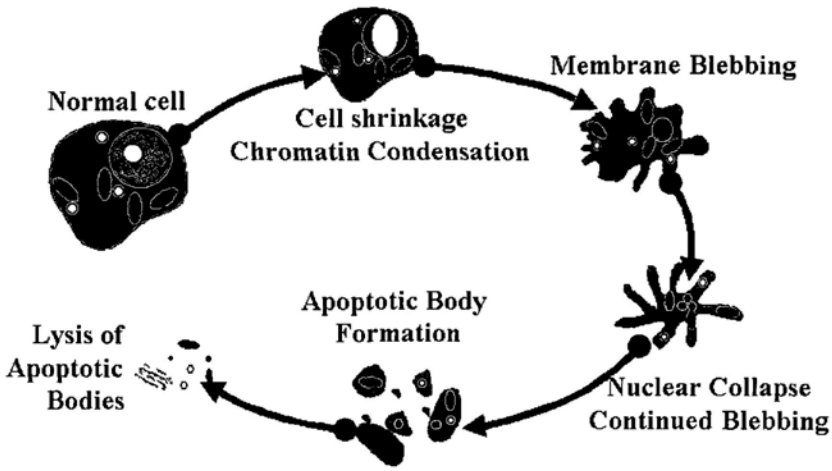

Fig. 1.2 The process of apoptosis (programmed cell death)

(http://www.microbiologybytes.com/virology/kalmakoff/baculo/baculohostinteract.html).

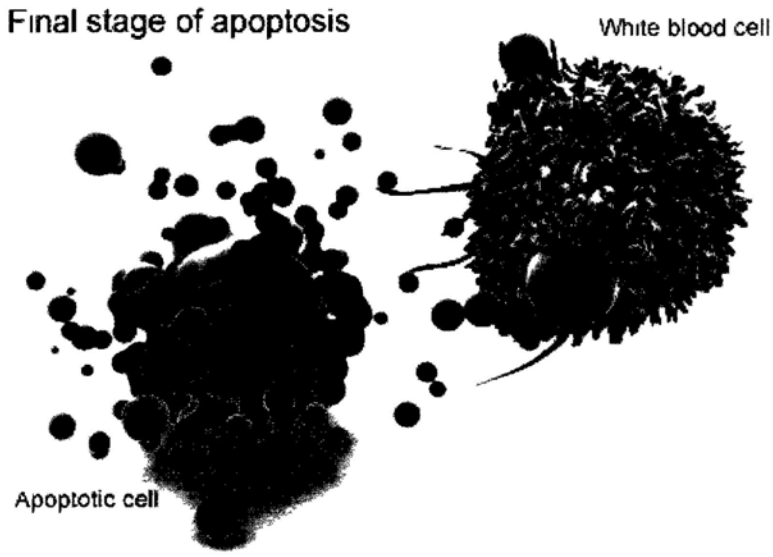

Fig. 1.3 Formation of apoptotic bodies in the final stage of apoptosis. White blood cells called macrophages consume apoptotic bodies, which removes the damaged cell and protects the organism.
(http://ghr.nlm.nih.gov/handbook/illustrations/apoptosismacrophage).

There are a number of mechanisms that can lead to cell apoptosis and the

sensitivity of a cell to apoptoic stimuli depends on many factors. These include expression of pro- and anti-apoptotic proteins (e.g. caspase family members, Bcl-2 family proteins, p53, p21), inhibitor of apoptosis proteins, severity of the stimulus and the stage of cell cycle. Generally, apoptosis may occur via the death receptor (extrinsic) pathway (Nagata, 1997) and /or mitochondrial (intrinsic) pathway (Li et al., 1997).

1. 3.1 Death receptor (extrinsic) pathway

The extrinsic pathway is triggered by the formation of death inducing signaling complex, which subsequently activates initiator caspase-8 and cleaves executioner caspases (Nagata, 1997; Zapata et al., 2001). As shown in **Fig. 1.4**, in extrinsic apoptotic pathway, the signaling ligands, which are released by other cells, bind to transmembrane death receptors on the target cell and induce cell apoptosis. For instance, the natural killer cells in immune system possess Fas ligand (FasL) on their surface. The binding of the FasL to Fas receptors on the cell membranes will trigger multiple receptors to aggregate on the cell surface. Binding of these receptors will recruit an adaptor protein known as Fas-associated death domain protein (FADD) on the cytoplasmic side of the receptors. FADD, in turn, causes the formation of the death-inducing signaling complex (DISC), activation of caspase-8 (cysteinyl aspartate-specific protease) and triggering of the proteolytic caspase cascade (Igney

and Krammer, 2002). Alternatively, activation of caspase-8/-10 cleaves a Bcl-2-homology domain 3 (BH3) family protein, BID, into its active form tBid (truncated BID), which provides a cross-talk between the extrinsic (death receptor-activated) and intrinsic (mitochondrial) pathway. Of note, cleaved Bid acquires a strong propensity to mitochondria and promotes the mitochondrial permeability transition (Buytaert et al., 2007).

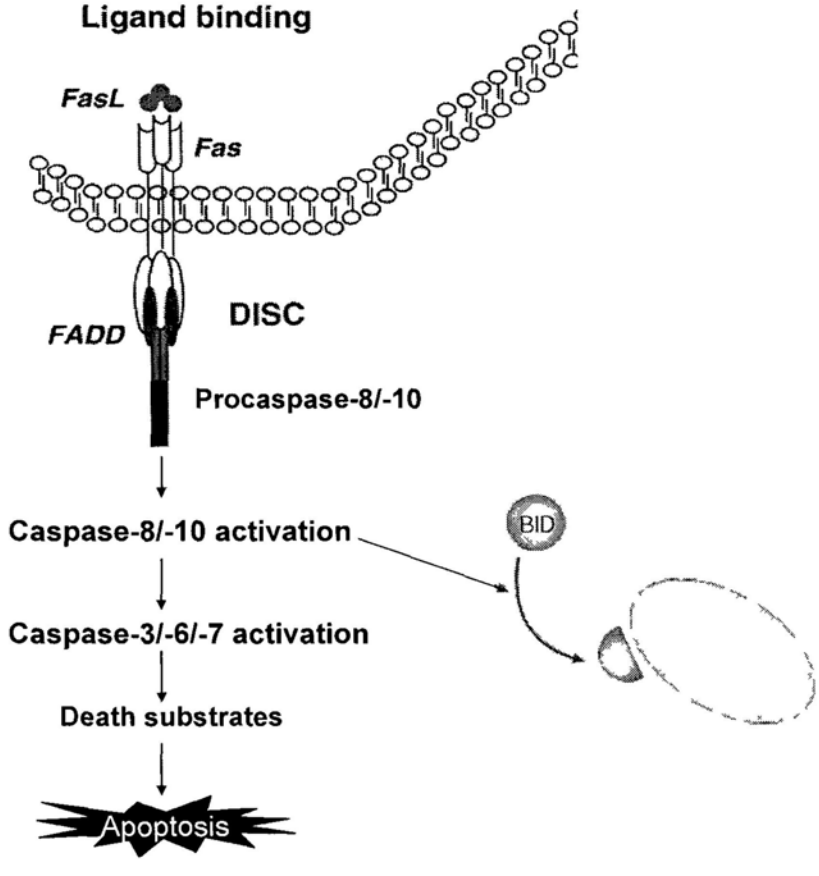

Fig. 1.4 Apoptosis occurs through death receptor (extrinsic) pathway. The extrinsic apoptosis pathway is triggered by binding of the death ligand (FasL) to their cell surface death receptor (Fas).This induces formation of the death-inducing signaling complex, the oligomeric platform which leads to the activation of initiator caspase-8/-10. The caspase can either directly activate the effector caspase-3 or

cleave Bid to recruit the mitochondrial apoptosis pathway. Both of them eventually converge to the activation of the effector caspases leading to cell death (Buytaert et al., 2007).

1.3.2 Mitochondrial (intrinsic) pathway

The mitochondrial pathway is mediated by the Bcl-2 family proteins, which disrupt the mitochondria membrane potential ($\Delta\Psi m$). This results in release of apoptogenic factors from the mitochondria to the cytosol, such as cytochrome c, Smac/Diablo and apoptosis-inducing factor (AIF). Cytochrome c in cytosol would form an apoptosome with apoptosis activating factor 1 and caspase-9, and then activate the downstream apoptotic signals (Kim, 2005; Li et al., 1997). As shown in **Fig. 1.5**, mitochondria play a central role in the intrinsic pathway of apoptosis. Although mitochondria are life-essential organelles for the production of metabolic energy in the form of ATP, numerous intrinsic and extrinsic cell death stimuli converge on mitochondria to induce the permeabilization of mitochondrial membranes. Depletion of $\Delta\Psi m$ results in the mitochondrial release of apoptogenic factors. This cellular event has been regarded as the point-of-no-return in cell apoptosis. Interestingly, AIF and EndoG in the cytosol can translocate to the nucleus and trigger chromatin condensation and large-scale DNA fragmentation resulting in caspase-independent apoptosis (Igney and Krammer, 2002).

The mitochondria-mediated apoptotic pathway is tightly regulated by Bcl-2

family proteins that comprise both proapoptotic proteins (**Table 1.1**), such as Bax, Bad and Bid, and antiapoptotic proteins, such as Bcl-2 and Bcl-xL. Bcl-2 and Bcl-xL bind to the outer membrane of mitochondria and block cytochrome c efflux. However, upon apoptotic stimulation, Bax specifically translocates to the mitochondria membrane and forms membrane integrated homo-oligomers with Bak, which permeabilize the outer mitochondrial membrane and trigger the loss of $\Delta\Psi m$, followed by release of apoptogenic factors into cytoplasm.

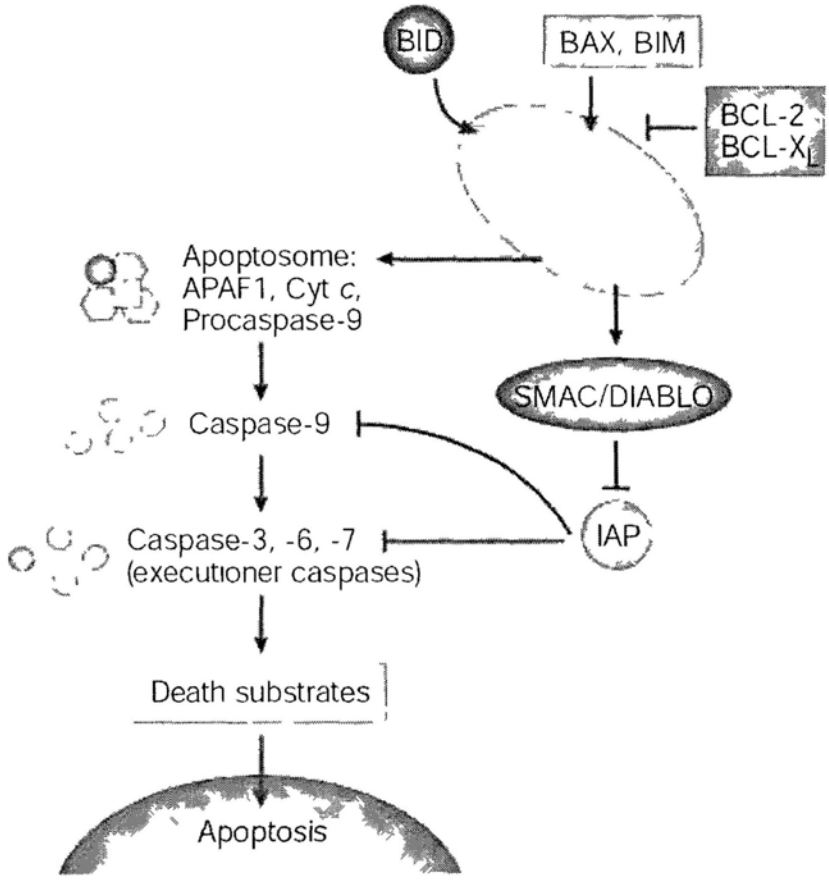

Fig. 1.5 Apoptosis occurs through mitochondrial (intrinsic) pathway. The mitochondrial pathway is mediated by Bcl-2 family proteins, which regulate the mitochondria membrane potential ($\Delta\Psi m$). The loss of $\Delta\Psi m$ induces release of

apoptogenic factor such as Cyto c from the mitochondrial inner space to cytosol. Once in the cytosol, Cyto c binds to apoptotic protease activating factor-1(APAF-1) and activates caspase-9. Caspase-9, in turn, activates the effector caspases-3/-6/-7, and eventually leads to cell apoptosis (Igney and Krammer, 2002).

Table 1.1 Bcl-2 family members

Bcl-2 family (Pro-Survial)		Bax family (Pro-Apoptosis)	BH3-only family (Pro-Apoptosis)	
Bcl-2	A1/Bfl1	Bax	Bik	Hrk
Bcl-xL	Mcl-1	Bak	Bim	Puma
Bcl-w		Bok	Bad	Noxa
			Bmf	Bid

1.3.3 Roles of caspases

After the activation of extrinsic and intrinsic apoptotic pathways, the final pathway that leads to execution of the death signal is the activation of a series of proteases termed caspases. Caspases are a family of cysteine proteases that cleave their substrates specifically following an aspartate residue (Kumar, 2007). Nowadays, about 14 caspase family members have been identified in mammalian cells, of which 11 enzymes are known in humans. These enzymes are synthesized as inactive precursors. However, upon receiving apoptotic signals, caspases undergo processing to generate proteolytical subunits containing the active enzymes. Recent studies have revealed that all activated caspases can be detected as cleaved fragments in apoptotic cells (Fuentes-Prior and Salvesen, 2004). The caspase family comprises of two

subtypes: the initiator caspases (caspase-2, -8, -9 and -10) and effector caspases (caspase-3, -6 and -7). The intrinsic and extrinsic apoptotic pathways can converge on caspase-3, which then cleaves the inhibitor of the caspase-activated deoxyribonuclease, thereby activating the latter to cause nuclear apoptosis. The upstream caspases that activate caspase-3 are caspases-9 and -8 in the intrinsic and extrinsic pathways, respectively. Other caspase family members, like caspase-1, -4, -5, -11, -12 and -14, are mainly involved in cytokine maturation and inflammation (Vermeulen et al., 2005).

1.4 Apoptosis and diabetes mellitus

Apoptosis is a coordinated series of events in inducing programmed cell death, and plays an important role in the maintenance of homeostasis in multicellular organisms. Defects in apoptosis regulating machinery can result in abnormal cellular growth, which may lead to cancer development. Excess apoptosis may also contribute to cell loss in other human diseases such as Alzheimer's disease, Parkinson's disease, and diabetes mellitus (Lee and Pervaiz, 2007). There are several lines of evidence showing that apoptosis is an important mode of cell death in diabetes. In both T1DM and T2DM, loss of pancreatic beta cells is pathologocial hallmarks. While the triggering factors may differ in T1DM and T2DM, apoptotic destruction of the insulin-producing pancreatic beta cells plays a key role in the

complete or partial loss of insulin production in these subjects.

T1DM is characterized by progressive loss of islet beta cells. Typically, 70–80 % of beta cells are lost at the time of diagnosis, through a T-cell mediated autoimmune reaction. The latter is determined by a combination of genetic susceptibility and exposure to external stressors, such as viral infections. Apoptotic signals come from high concentrations of inflammatory cytokines or T cells in the islet microenvironment (Lee and Pervaiz, 2007). In the majority of T2DM patients, insulin resistance is a key feature often due to visceral obesity with increased production of free fatty acids and adipocytokines (Despres and Lemieux, 2006). This is accompanied by hyperinsulinemia which contribute to hypertension and dyslipidemia to increase cardiovascular risk, so called metabolic syndrome. In predisposed subjects with beta cell insufficiency, hyperglycemia eventually develop when the number and/or function of beta cells fails to provide further compensation to maintain euglycemia (Kahn et al., 2006; Mathis et al., 2001). Although the causes and molecular mechanisms of beta cell apoptosis is not yet clear, beta cell toxicity of glucose, saturated fatty acids, islet amyloid polypeptide (IAPP) and IL-1 beta have all been implicated. These stimuli have been shown to induce both oxidative and ER stress leading to apoptotic beta cell death (Lee and Pervaiz, 2007).

1.5 Mitochondrial dysfunction in T2DM

1.5.1 Mitochondria and insulin secretion

There is now strong evidence supporting failure of insulin secretion as the main culprit in T2DM (Muoio and Newgard, 2008). Recent genome wide association studies also indicate that nearly all newly discovered T2DM genes are implicated in beta cell structure and secretion. Thus, T2DM evolves when beta cells fail to produce and/or release appropriate amount of insulin to correct hyperglycemia and inhibit lipolysis.

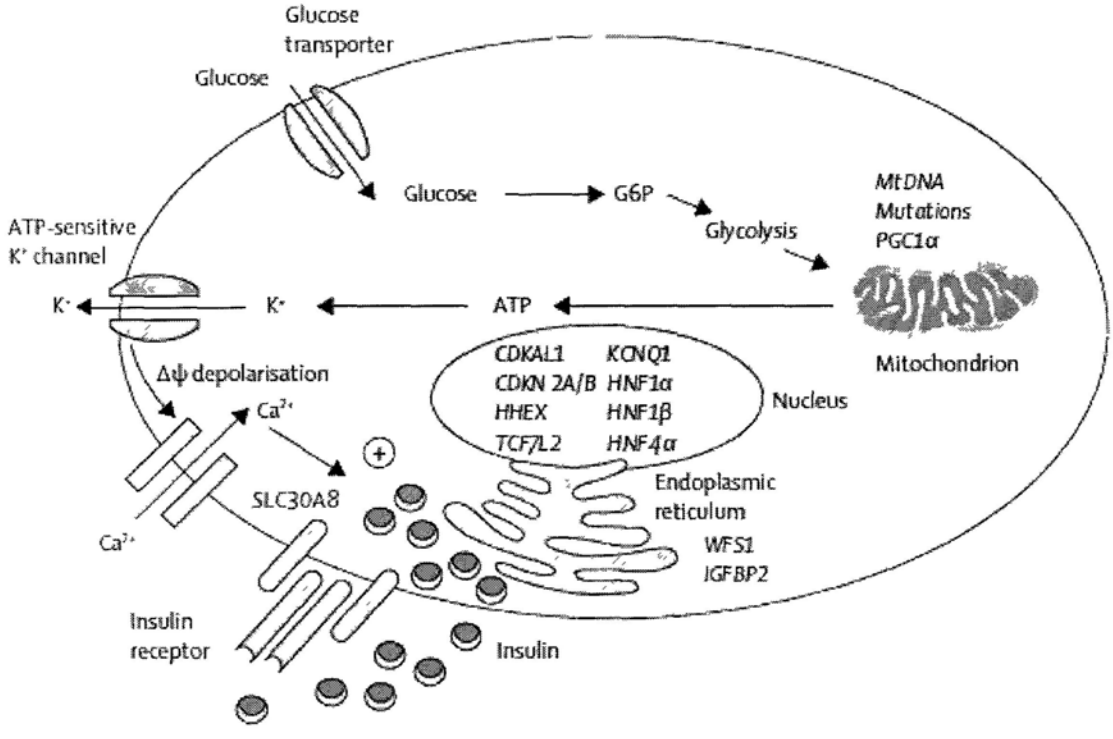

Fig. 1.6 The roles of type 2 diabetes genes and mitochondria in insulin secretion. Pancreatic beta cells genes associated with type 2 diabetes are in italics. The glucose uptake into beta cells increases substrate supply to drive mitochondrial oxidative phosphorylation to produce ATP. This results in closure of ATP-sensitive K^+ channel, plasma membrane depolarization, Ca^{2+} influx following activation of voltage-gated

Ca^{2+} channels, and Ca^{2+}-mediated stimulation of granule exocytosis (Ramachandran et al., 2010).

Insulin secretion is an energy dependent process with glucose as an important metabolic fuel (Muoio and Newgard, 2008). Other factors such as circulating hormones, paracrine and autocrine mechanisms, and neuronal (autonomic and sensory) control, also play important roles in modulating insulin secretion. During these processes, mitochondria plays a particularly important role (Wollheim, 2000). As shown in **Fig. 1.6**, entry of metabolic fuel such as glucose into the beta cells is followed by oxidation to produce reducing equivalents, which drive the mitochondrial respiratory chain to produce ATP via oxidative phosphorylation (OXPHOS). The rise in the ATP:ADP ratio closes the ATP-sensitive K^+ channel (KATP), which results in depolarization of the plasma membrane, opening of voltage-gated Ca^{2+} channels and subsequently exocytosis of insulin/amylin containing vesicles (Mulder and Ling, 2009). It has been reported that mitochondria also plays a critical role in the KATP-independent pathway to sustain insulin secretion (Maechler et al., 2006). In this connection, metabolites from mitochondria, reducing equivalents or metabolite fluxes are believed to account for the sustained phase of insulin secretion, which cannot be upheld by raised intracellular Ca^{2+} alone, for instance, the product of the triggering pathway. Thus, mitochondria play a pivotal role in the control of insulin secretion which is the deciding pathogenetic event in

T2DM. As such, metabolic dysregulation can lead to mitochondrial dysfunction resulting in failure of insulin secretion and sets up a vicious cycle.

1.5.2 Mitochondria and beta cell mass

Mitochondria also play a critical role in the control of beta cell mass. Available data suggest that increased apoptosis underlies the loss of beta cell mass observed in islets from patients with T2DM (Butler et al., 2003a; Trifunovic and Larsson, 2008). Indeed, the apoptotic pathways converge in mitochondria, where the processes of caspase-3 activation and cytochrome c export participate in these events. Besides, aging is a major determining factor in the pathogenesis of T2DM. Here, several lines of evidence show the intimate relationships between aging and mitochondrial metabolism (Lee and Pervaiz, 2007; Trifunovic and Larsson, 2008). Other studies have indicated that mitochondrial dysfunction caused accelerated apoptosis of pancreatic beta cells and loss of beta cell mass (Trifunovic and Larsson, 2008).

1.5.3 Oxidative phosphorylation and ROS generation in mitochondria

Oxidative stress is a state of imbalance that favors the production of reactive oxygen species (ROS) over antioxidant enzymes. By definition, ROS include superoxide (O_2^-), hydroxyl radical (•OH) and the non-radical species, hydrogen peroxide (H_2O_2). Mitochondria are considered to be a major source of ROS, the

formation of which is inevitable during normal oxidative metabolism which can further increase in pathological conditions. The contribution of mitochondria to clinical manifestation of disease is ascribed largely to the production of ROS. ROS generation within mitochondria is closely associated with the primary function of these organelles, namely respiration, oxidative metabolism and ATP synthesis (Adam-Vizi and Chinopoulos, 2006). Most bioenergetic factors, such as complex-I in the respiratory chain, nicotinamide adenine dinucleotide (NADH) and ATP, modulate mitochondrial ROS generation via their effects on transmembrane proton gradient (ΔpH) and $\Delta\Psi$m (Lambert and Brand, 2004).

As shown in **Fig. 1.7**, the cellular metabolism of substrates such as glucose and free fatty acids generates electrons (e^-) in the form of the reduced hydrogen carriers-NADH and FADH2. NADH and FADH2 donate electrons to the electron-transport chain, which comprises protein complexes that are located in the mitochondrial inner membrane. Electrons are ultimately transported to molecular oxygen, which is reduced to water in the last step of the electron-transport chain. As electrons are transferred along the electron-transport chain, a fixed number of protons (H^+) are pumped from the mitochondrial matrix into the mitochondrial intermembrane space, which establishes a proton gradient across the mitochondrial inner membrane. The energy that is conserved in this proton gradient drives the

synthesis of ATP from ADP and inorganic phosphate (Pi) by ATP synthase as protons are transported back from the intermembrane space into the mitochondrial matrix. ATP is then made available to the cell for various processes that require energy. Proton leak, partly mediated by the uncoupling proteins (UCPs), uncouples the processes of electron transport/proton-gradient generation on the one hand, and ATP synthesis on the other. Moreover, studies have showed that addition of purine nucleotides to freshly prepared mitochondria from brown adipose tissues reduced the high rate of uncoupled respiration in these mitochondria (Nicholls, 2001). Purine-nucleoside di- and triphosphates, such as ATP, ADP, GTP and GDP, but not purine-nucleoside monophosphates, such as AMP and GMP, bind with high affinity to UCPs. Nucleotide binding usually occurs on the cytosolic side of the mitochondrial inner membrane (Nicholls, 1976). Theoretically, physiological millimolar concentrations of ATP and ADP should completely inhibit UCP1 activity in intact cells (Nicholls, 2001).

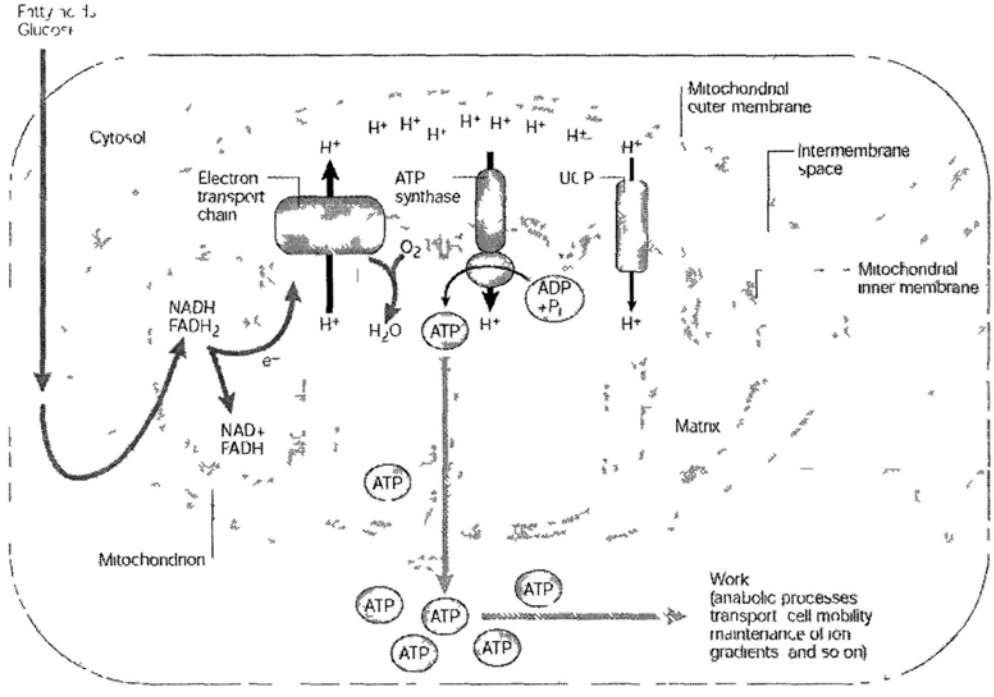

Fig. 1.7 Substrate oxidation and oxidative phosphorylation in mammalian cells (Zhang et al., 2001).

1.5.4 Functional roles of UCPs

UCP family is a superfamily of mitochondrial anion-carrier proteins. The genes encoding the members of UCPs have been described across various animal and plant species. Mammals express five UCPs, named UCP1–UCP5. A number of hypotheses have been proposed to explain the functional roles of UCPs in diabetes. One of these hypotheses, discussed below, focuses on changes in the expression and function of UCP-2, an inner mitochondrial membrane protein that diminishes the proton gradient generated by the respiratory chain (Lowell and Shulman, 2005). The production of superoxide is positively correlated with the mitochondrial membrane potential (Korshunov et al., 1997), due to the 'random' single-electron-transfer

reactions from components of the electron-transport chain to molecular oxygen. Higher mitochondrial membrane potential increases superoxide production in the mitochondrial electron-transport chain. This event induces UCP-dependent proton leak, thereby decreasing mitochondrial membrane potential and, consequently, superoxide production in an autoregulatory feedback loop (Duval et al., 2002; Negre-Salvayre et al., 1997). However, overexpression of UCP-2 in beta cells could attenuate ATP synthesis and insulin secretion in response to glucose, whereas islets isolated from UCP-2 deficient mice exhibit enhanced ATP generation and insulin secretion upon glucose exposure (Zhang et al., 2001). In a high-fat diet-induced T2DM model, the lack of UCP-2 improves blood glucose levels and insulin secretory capacity (Joseph et al., 2002). Taken together, these findings suggest that UCP-2 may play an important role in the pathogenesis of beta cell dysfunction and that UCP-2 inhibitors may be used to prevent or treat T2DM.

1.6 Oxidative stress in T2DM

Oxidative stress is widely accepted as playing a key mediatory role in the development and progression of diabetes and its complications due to increased production of free radicals and impaired antioxidant defenses (Rolo and Palmeira, 2006). Cellular ROS signaling has been frequently linked to cell death pathways, either by inducing apoptosis, or by contributing to the above described stress

responses. Thus, ROS activity represents another candidate in triggering the stress responses in beta cells with metabolic overload. The weak expression of natural enzymatic defences, like catalase and superoxide dismutase, renders beta cells particularly susceptible to ROS (Maechler et al., 1999). In rodents, compared to other tissues, pancreatic islets have low levels of superoxide dismutase (SOD) and glutathione peroxidase (GSH-Px) and no detectable level of the enzyme catalase. These low levels of antioxidant enzymes may explain the increased sensitivity of beta cells to cytokines (Tiedge et al., 1997).

Other researchers have shown that production of ROS in beta cells was linked to mitochondrial metabolism and that ROS content in isolated islets of Zucker diabetic fatty rats was higher than that in Zucker lean control islets under resting conditions (Bindokas et al., 2003). ROS can also elicit beta cell apoptosis leading to decreased beta cell mass (Mandrup-Poulsen, 2001). In a rat model of intrauterine growth retardation with development of diabetes in adulthood, investigators reported increased production of ROS which was associated with damaged mitochondrial DNA. The latter can lead to further production of ROS resulting in progressive loss of beta cell function and development of T2DM in the adult rat (Simmons et al., 2005). Taken together, these observations indicate that ROS may participate in the impairment of glucose-induced insulin secretion observed in association with ageing

and T2DM.

Overexpression of antioxidants, including catalase, GSH-Px , Cu/ZnSOD, MnSOD, metallothionein or combinations of these molecules reduce susceptibility of islets and beta cells to cytokine and inducers of oxygen radicals by blocking oxidation of cellular proteins (Mysore et al., 2005). In streptozotocin-treated mice, systemic treatment with antioxidants or transgenic expression of combinations of antioxidants protected against diabetes, and improved the survival of islet grafts (Mysore et al., 2005). In sum, antioxidant therapeutic interventions might contribute to preservation of beta cell function (Robertson et al., 2003).

1.7 *Spirulina* and phycocyanin

1.7.1 *Spirulina*

Spirulina (**Fig. 1.8**) is free-floating filamentous cyanobacteria characterized by cylindrical, multicellular trichomes in an open left-hand helix, which live in both sea and fresh water. *Spirulina* is the common name for human food supplements produced primarily from two species of cyanobacteria: *Spirulina platensis*, and *Spirulina maxima*. *Spirulina* occurs naturally in tropical and subtropical lakes with high pH and high concentrations of carbonate and bicarbonate. *Arthrospira platensis* occurs in Africa, Asia and South America, whereas *Arthrospira maxima* is confined to Central America. *Spirulina* is mostly cultivated in open-channel raceway ponds,

with paddle-wheels used to agitate the water. The largest commercial producers of *Spirulina* are located in the United States, Japan, Thailand, India, Taiwan, China, Pakistan and Burma.

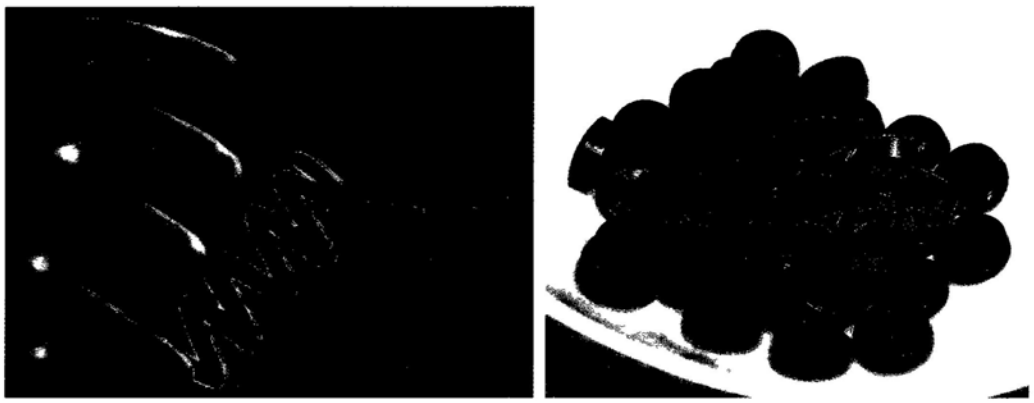

Fig. 1.8 *Spirulina* cells and tablets.
(See http://commons.wikimedia.org/wiki/File:*Spirulina*_tablets.jpg; and http://www.herbalorganics.biz/Spirulina-Arthrospira-platensis-Latin/)

Spirulina contains high amount of protein which accounts for 55-77 % of its dry weight. It is considered as a complete protein containing all essential amino acids. *Spirulina* is also rich in other nutrients, such as vitamins, beta-carotene, vitamin E, carotenoids, manganese, zinc, copper, iron, selenium, and gamma linolenic acid (Campanella et al., 1999). Moreover, *Spirulina* lacks cellulose cell walls and therefore can be easily digested. Thus, *Spirulina* has long been grown photoautotrophically in the production of algal health food (Chen et al., 2006). Currently, *Spirulina* can be found in health food stores and is sold mainly as a dietary supplement in the form of health drinks or tablets.

1.7.2 Applications of *Spirulina*

Spirulina possess antioxidant, antiviral, anticancer, anti-diabetes, immunomodulating, weight reducing and lipid-lowering properties, which make them useful in some clinical conditions (Parikh et al., 2001; Rodriguez-Hernandez et al., 2001).

Antioxidant and anticancer effects: *Spirulina* contains high amount of bioactive components, like phycobiliproteins, carotenoids and essential fatty acid, which have been shown to process antioxidant and anticancer activities (Wu et al., 2005). The combined antioxidant and immune modulating characteristics of *Spirulina* may cause tumor destruction to prevent cancer (Parikh et al., 2001; Rodriguez-Hernandez et al., 2001). Although many *in vivo* and *in vitro* studies have been conducted, there has been only one trial in human subjects in Kerala, India (Mathew et al., 1995). In this study, researchers have reported specifically the chemopreventive effects of *Spirulina* on oral carcinogenesis, in particular leukoplakia. For instance, complete regression of lesions was observed in 20 of 44 (45%) evaluable subjects supplemented with *Spirulina* (1 g/day for 12 mos). When stratified by types of leukoplakia, the response was more pronounced in homogeneous lesions with complete regression in 16 of 28 (57%) subjects with homogeneous leukoplakia. Moreover, supplementation with *Spirulina* did not result

in increased serum concentration of retinol or beta-carotene, nor was it associated with toxicity (Mathew et al., 1995). Recent study also showed that selenium-enriched *Spirulina platensis* extract could inhibit the growth of human breast cancer cells through induction of G1 cell cycle arrest and mitochondria-mediated apoptosis (Chen et al, in press).

Anti-diabetes and cholesterol-lowering activities: *Spirulina maxima* has been reported to prevent formation of fatty liver in alloxan-induced diabetic mice (Rodriguez-Hernandez et al., 2001). Supplementation of *Spirulina* showed beneficial effect on controlling blood glucose and improving the lipid profile of T2DM patients (Parikh P et al, 2001). Other studies have shown that administration of *Spirulina* supplements in patients with ischemic heart disease had lower blood cholesterol, triglycerides and LDL cholesterol than the control group (Mathew et al., 1995). In another small study involving 15 type 2 diabetic patients, patients treated with *Spirulina* had reduced LDL:HDL ratio compared to the control group. These proof-of-concept studies or anedoctal reports suggest that *Spirulina* may have a role in the prevention or treatment of diabetes, dyslipidemia or ischemic heart disease although larger scale studies are clearly needed.

Immunomodulation and anti-viral activities: In Japan, scientists analyzed the effects and molecular mechanism of *Spirulina* on human immune capacity by

examining the blood cells of volunteers before and after oral administration of hot water extract of *Spirulina platensis*. The results showed that *Spirulina* activated the human innate immune system through augmentation of interferon production and Nature killer cytotoxicity. Treatment with *Spirulina* also enhanced IgA production in human saliva, suggesting a pivotal role of microalga in mucosal immunity (Hirahashi et al., 2002).

The active component of the water extract of *Spirulina*, sulfated polysaccharide, calcium *Spirulina* (Ca-Sp), has been shown to inhibit the *in vitro* replication of several enveloped viruses, including Herpes simplex type I, human cytomegalovirus, measles and mumps virus, influenza A virus and human immunodeficiency virus-1 virus (HIV-1) (Hayden et al., 2005). In another *in vitro* experiment, aqueous extract of *S. platensis* has been shown to inhibit HIV-1 replication in human T-cells, peripheral blood mononuclear cells and Langerhan cells (Ayehunie et al., 1998).

1.7.3 Phycocyanin and its applications

Spirulina is an important source of phycocyanin (PC, **Fig. 1.9**), a blue photosynthetic pigment that has been described as a natural agent with novel antioxidant activity (Bhat and Madyastha, 2000; Bhat and Madyastha, 2001). Many *in vitro* and *in vivo* studies suggest that PC may have potential usage in

biotechnology, diagnostics, foods and medicine (Chen and Wong, 2008a; Romay et al., 2003; Vadiraja et al., 1998).

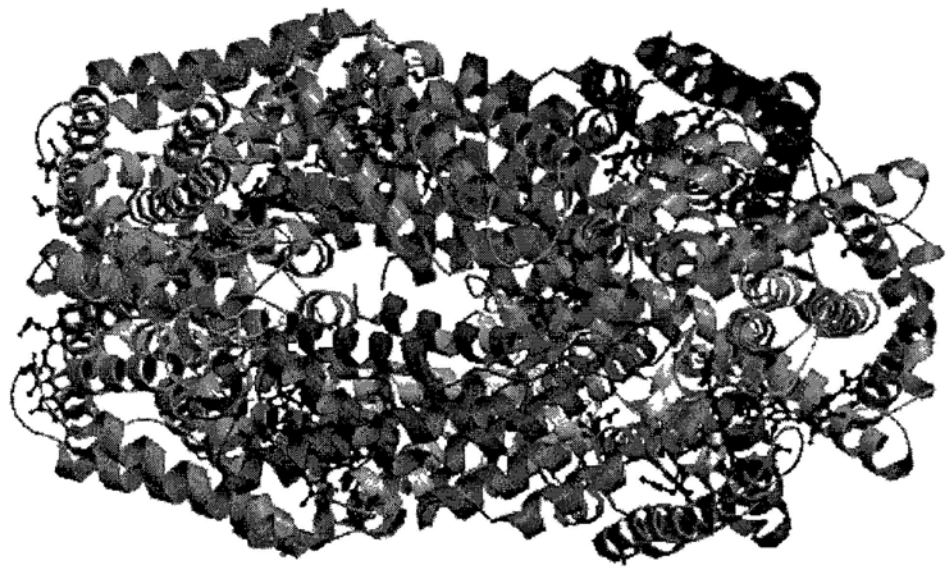

Fig. 1.9 Crystal structure of phycocyanin from *Spirulina Platensis* (http://www.rcsb.org/pdb/explore.do?structureId=1ha7)

Nutraceutical and pharmaceutical: PC has been shown to possess antioxidant, antiproliferative, anti-inflammatory, antimutagenic, antiviral, cardio-protective and anticarcinogenic activities in both *in vitro* and *in vivo* studies (Bhat and Madyastha, 2000; Bhat and Madyastha, 2001; Eriksen, 2008; Farooq et al., 2004; Gonzalez et al., 1999). For instance, PC reduces oxidative stress, inhibits activities of NADH oxidase and other enzymes, and alters gene regulation in mammalian cell lines and hamsters (Cherng et al., 2007; Madhyastha et al., 2006). Other studies suggested that PC inhibited the growth of various cancer cells via induction of apoptosis (Reddy et al., 2003; Roy et al., 2007; Subhashini et al., 2004).

In support of this action, recombinant PC beta-subunit has been shown to inhibit cell proliferation and cause apoptosis in carcinoma cells (Wang et al., 2007). Other researchers have shown that the antioxidant and antiproliferative activities of PC can be enhanced through incorporation of selenium (Chen and Wong, 2008a). These observations have motivated research in PC as a nutraceutical or pharmaceutical with anticarcinogenic properties and other possible health benefits.

Food additive and health food: PC from *Spirulina* has been marketed as food additive and health food in many countries including Japan and USA. Studies have addressed the functionality of PC in foods with regards to colour stability and rheological properties (Eriksen, 2008). PC is now being used as a natural pigment in food such as chewing gum, dairy products and jellies. Despite its lower stability to heat and light, compared to gardenia and indigo, PC is considered a more versatile colorant and gives jelly gum and coated soft candies a bright blue color. They are also used to color other food products such as fermented milk products, ice creams, soft drinks, desserts, sweet cake decoration, milk shakes and cosmetics. Whole cyanobacteria were suggested to stimulate the immune defense system and possess antioxidant activity and cholesterol-lowering effect, partly because of their PC contents.

Fluorescent probe: As compared with other fluorophores, phycobiliproteins

including PC have higher molar extinction coefficients and fluorescence quantum yields (Eriksen, 2008). Phycobiliproteins conjugated to immunoglobulins, protein A and avidin through amino and carboxyl groups have been developed into fluorescent probes widely used in histochemistry, fluorescence microscopy, flow cytometry, fluorescence-activated cell sorting and fluorescence immunoassays. PC trimer can be chemically stabilized by crosslinking of peptide chains, thus enhancing its extinction coefficients (Sun et al., 2006). These chemically stabilized PC trimers can be used as fluorescent probes with spectral properties different from other phycobiliproteins.

1.8 Aims of this project

It is well known that misfolded hIAPP in the pancreatic islets is associated with loss of insulin-secreting beta cells in T2DM patients. Insulin secretion impairment and cell apoptosis are due to mitochondrial dysfunction in pancreatic beta cells. However, the role of mitochondria in hIAPP-induced cytotoxicity has not been well elucidated. Given the link of hIAPP-cytotoxicity and mitochondrial dysfunction in T2DM, I hypothesized that hIAPP-induced apoptotic cell death might induce mitochondrial dysfunction in pancreatic beta cell through generation of ROS. Given the antioxidant effect of PC which is a widely used naturally occurring food

supplement extracted from blue-green algae, I further explored the effects of PC on beta cells in the presence of hIAPP.

Therefore, the aim of my thesis was to investigate the role of mitochondria in hIAPP-induced apoptosis, and the *in vitro* protective effects of PC against hIAPP-induced apoptotic cell death and the underlying mechanisms.

Chapter 2: Materials and Methods

2.1 Materials

Human islet amyloid polypeptide was synthesized using t-boc chemistry and purified by reverse phase high performance liquid chromatography (HPLC) in the Yale University. Phycocyanin (PC) was extracted from *Spirulina platensis* by ultrasonication and purified by liquid chromatography as previously described (Chen et al., 2006). The fractions with purity ratios (A620/A280) > 4.5 were collected and lyophilized to solid powder for further use. The molecular masses of PC were determined as 35671.8 Da, by matrix-assisted laser desorption/ionization time-of-flight/time-of-flight analysis (Chen et al., 2006). Thiazolyl blue tetrazolium bromide (MTT), 1,1,1,3,3,3-hexafluoro-2-propanol (HFIP), 4',6-Diamidino-2-phenyindole (DAPI), Propidium iodide (PI), cyclosporin A (CsA), 5,5′,6,6′-tetrachloro-1,1′,3,3′-tetraethylimidacarbocyanine iodide (JC-1), ATP bioluminescence assay kit, 2′,7′-dichlorofluorescein diacetate (DCF-DA), SP600125 and bicinchoninic acid (BCA) kit for protein determination were purchased from Sigma. 5-bromo-2'-deoxyuridine (BrdU) ELISA kit, lactate dehydrogenase (LDH) assay kit and terminal transferase dUTP nick end labeling (TUNEL) assay kit were obtained from Roche Applied Science (Basel, Switzerland). MitoTracker Green FM, MitoTracker Red CMXRos, and MitoProbe transition pore assay kit were purchased

from Invitrogen, Molecular Probes (Eugene, OR, USA). Caspase-8 inhibitor (z-IETDfmk) and caspase-9 inhibitor (z-LEHD-fmk) were obtained from Merck. Caspase-3 substrate (Ac-DEVD-AMC) was purchased from Biomol (Germany). SP600125 (JNK inhibitor), SB203580 (p38 inhibitor) and U0126 (ERK inhibitor) were obtained from Calbiochem (San Diego, CA). RPMI 1640 medium and fetal bovine serum (FBS) were purchased from Gibco BRL (Gaithersburg, MD). General caspase inhibitor (z-VAD-fmk), caspase-9 substrate (Ac-LEHD-AFC) and caspase-8 substrate (IETD-AFC) were purchased from Calbiochem. PathScan® Cleaved poly (ADP-ribose) polymerase (PARP) (Asp214) Sandwich ELISA Kit, and all antibodies (except for tBid antibody which was obtained from Invitrogen) used in this study were purchased from Cell Signaling Technology (Beverly, MA). Superoxide anion radical ($O_2^{\cdot-}$), hydroxyl radical (·OH), superoxide dismutase (SOD), glutathione peroxidase (GSH-Px) enzymes and malonaldehyde (MDA) were assayed using kits from Nanjing Jiancheng Bioengineering Institute (Nanjing, China). The polyclonal rabbit antiamyloid oligomer antibody (A11) was purchased from Chemicon International (Temecula, Calif). The water used in all experiments was ultrapure, supplied by a Milli-Q water purification system from Millipore.

2.2 Cell culture and treatment

INS-1E rat insulinoma cell line was a gift from Dr. P. Maechler (University of

Geneva, Switzerland). Cells were grown in monolayer cultures in RPMI-1640 medium supplemented with 10 mmol/L HEPES, 10 % FBS, 2 mmol/L L-glutamine, 1 mmol/L sodium pyruvate, 50 μmol/L mercaptoethanol, 100 U/ml penicillin, and 100 μg/ml streptomycin, at 37 °C in a humidified (5 % CO_2, 95 % air) atmosphere. The passage number of the INS-1E cells was 68-73 in the present study.

For peptide treatment, lyophilized hIAPP was dissolved in HFIP, which was removed by evaporation under N_2 as previously described (Konarkowska et al., 2006). The resulting peptide was dissolved in sterile water to a stock concentration of 500 μM and then applied to cultured cells. All hIAPP solutions used in experiments were prepared freshly.

The cells were seeded in 96-well microplate at a density of 5×10^4 cells per well for MTT and Brdu assays. For other assays, cells were seeded in 6-well plates at a density of 9×10^5 cells per well. Cells were incubated with hIAPP (2.5-30 μM) for 24 h to examine the effects of hIAPP on INS-1E cells. In addition, cells were pretreated with or without PC (1.25-5 μM) for 2 h and then co-incubated with 20 μM hIAPP for another 24 h to evaluate the protective effects of PC.

2.3 Antiproliferative activity

2.3.1 MTT assay

MTT assay was used to examine the effect of hIAPP and PC on INS-1E cells

growth. The cells seeded in 96-well microplate at a density of 5 x 10^4 cells/well were cultured at 37 °C in a humidified atmosphere for 48 h. Cells were incubated with hIAPP (2.5–30 μM) for 24 h to examine the effects of hIAPP on INS-1E cells. In addition, cells were pretreated with or without PC (1.25–5 μM) for 2 h and then co-incubated with 20 μM hIAPP for another 24 h to evaluate the protective effects of PC. After treatment, 20 μl/well of MTT solution (5 mg/ml in PBS buffer) was added and incubated for 5 h. The medium was aspirated and replaced with 150 μl/well of dimethyl sulphoxide (DMSO) to dissolve the formazan salt. All the wells were then mixed by pipetting until all crystals were dissolved completely. The color intensity of the formazan solution, which reflects the cell growth condition, was measured at 570 nm using a microplate spectrophotometer (SpectroAmax^{TM} 250). The growth inhibitory activity was expressed as percentage (%) of cell viability in the treatment group relative to the control group.

2.3.2 Cell proliferation ELISA-BrdU (chemiluminescence) assay

BrdU assay is a chemiluminescence immunoassay used in quantification of cell proliferation. This assay is based on the incorporation of the pyrimidine analogue BrdU instead of thymidine into the DNA of proliferating cells.

DNA synthesis was assessed by a BrdU ELISA kit according to the

manufacturer's instruction. Briefly, The cells seeded in 96-well Nunc White Microwell™ Plates at a density of 5×10^4 cells/well were cultured at 37 °C in a humidified atmosphere for 48 h. Cells were incubated with hIAPP (2.5-30 μM) for 24 h to examine the effects of hIAPP on INS-1E cells. In addition, cells were pretreated with or without PC (1.25-5 μM) for 2 h and then co-incubated with 20μM hIAPP for another 24 h to evaluate the protective effects of PC. After treatment, BrdU was added at final concentration of 10 μM and further incubated for 2 h. The labeling medium was then removed. The labeled cells were dried in 50 °C oven and were further incubated with 200 μL/well FixDenat solution for 30 min to denature DNA. The FixDenat solution was then removed and cells were stood for another 30 min. A volume of 100 μL/well anti-BrdU-POD solution was added and further incubated for 1 h at room temperature to allow the binding of antibody with BrdU that incorporated newly synthesized cellular DNA. The wells were washed 3 times with 200 μL washing solution. In each experimental setup, a negative control, a blank and a background control were also included. The cells of negative control were treated with PBS instead of hIAPP. In the blank, the well contents consisted of culture medium, BrdU labelling solution and anti-BrdU-POD. This well provided information about the non-specific binding of BrdU and anti-BrdU-POD conjugate to the microplate. The well contents of background control consisted of cultured cells

and anti-BrdU-POD solution which provided information about the non-specific binding of anti-BrdU-POD conjugate to cells in the absence of BrdU. Finally, 100 μL/well of substrate solution containing luminol and 4-iodophenol were added and shaken for at least 3 min. Light emission was measured by a microtiter plate luminometer (ML3000). The results were expressed as percentage (%) of cell proliferation in the treatment group relative to the control group, which was calculated by the following equation:

$$\text{Cell proliferation percentage} = \frac{\text{Average luminescence of treatment group}}{\text{Average luminescence of control group}} \times 100\%$$

2.3.3 Lactate dehydrogenase (LDH) assay

Release of cytoplasmic LDH is a marker of loss of cell membrane integrity and an indication of cytotoxicity. INS-1E cells seeded in 96-well microplate at a density of 5×10^4cells/well were cultured at 37 °C in a humidified atmosphere for 48 h. Cells were incubated with hIAPP (2.5–30 μM) for 24 h to examine the effects of hIAPP on INS-1E cells. In addition, cells were pretreated with or without PC (1.25–5 μM) for 2 h and then co-incubated with 20 μM hIAPP for another 24 h to evaluate the protective effects of PC. The cells of negative control were treated with PBS instead of hIAPP. At the end of each treatment, the cells were precipitated by

centrifugation (1500 g) for 10 min at room temperature. LDH activity was assayed using the cytotoxicity detection kit according to the manufacturer's guidelines. Aliquots (100 μL) of supernatants were transferred to a 96-well plate, and then incubated with 100 μL reaction mixture containing catalyst (Diaphorase/NAD+ mixture) and dye solution (INT and sodium lactate). After 30 min incubation in darkness, absorbance at 490 nm was taken using a microplate spectrophotometer (SpectroAmaxTM 250). The results were expressed as percentage (%) of LDH release in the treatment group relative to the control group.

2.3.4 Trypan blue exclusion assay

The trypan blue exclusion test was used to determine the number of viable cells. It is based on the principle that live cells possess intact cell membranes that exclude trypan blue dye, whereas dead cells do not. In this test, a viable cell will have a clear cytoplasm whereas a nonviable cell will have a blue cytoplasm.

INS-1E cells seeded in 12-well plates at a density of 50×10^4 cells/well were cultured at 37 °C in a humidified atmosphere for 48 h. Cells were incubated with hIAPP (2.5-30 μM) for 24 h to examine the effects of hIAPP on INS-1E cells. In addition, cells were pretreated with or without PC (1.25-5 μM) for 2 h and then co-incubated with 20 μM hIAPP for another 24 h to evaluate the protective effects of PC. At the end of each treatment, the cells were harvested using trypsin-EDTA

solution and resuspended in PBS. The cellular suspension was mixed with equal amounts of 0.1 % trypan blue solution and the trypan blue-excluded viable cells were counted using a hemacytometer under a microscope.

2.4 Morphological analysis of apoptosis

2.4.1 TUNEL enzymatic labeling assay

The TUNEL reaction is designed to detect and quantify apoptotic cell death at single cell level in cells and tissues. The TUNEL assay involves labeling of the 3'-hydroxyl DNA ends generated during DNA fragmentation by means of terminal deoxyribonucleotidyl transferase (TdT) and labeled dUTP.

This assay was performed according to the manufacturer's instructions. INS-1E cells seeded in on cover glass in six-well plates at a density of 80 × 10^4cells/well were cultured at 37 °C in a humidified atmosphere for 48 h. Cells were incubated with hIAPP (2.5-30 μM) for 24 h to examine the effects of hIAPP on INS-1E cells. In addition, cells were pretreated with or without PC (1.25-5 μM) for 2 h and then co-incubated with 20 μM hIAPP for another 24 h to evaluate the protective effects of PC. After treatment, cells were washed with PBS and air dried, and then fixed with freshly prepared fixation solution (4 % paraformaldehyde in PBS, pH 7.4) for 1 h at room temperature. After washes in PBS, cells were permeabilized with 0.1 % Triton X-100 for 2 min, and then incubated with TUNEL reaction mixture

containing nucleotide mixture and terminal deoxynucleotidyl transferase (TdT) for 60 min in a humidified atmosphere at 37°C in darkness. The negative control and the positive control were also included. For the negative control, the cells were incubated with nucleotide mixture in reaction buffer (without terminal transferase) instead of TUNEL reaction mixture. Prior to labeling procedures, DNA strand breaks were induced in positive control by incubating the fixed and permeabilized cells with DNase I, grade 1 (1U/ml in 10mM Tris-HCl, pH7.5 containing 1mM magnesium chloride and 1mg/ml BSA) for 10 min at room temperature. After that, stained cells were washed with PBS and observed using fluorescence microscopy (Nikon Eclipse 80i). For the evaluation of fluorescence microscopy, an excitation wavelength at 488 nm and emission wavelength at 515 nm were used. Fluorescence images were collected using a Bio-Rad Radiance 2100 system with LaserShape2000 software (Bio-Rad).

2.4.2 DAPI staining

DAPI (4'-6-Diamidino-2-phenylindole dihydrochloride) is a fluorescent dye which binds selectively to natural double-stranded DNA to form strongly fluorescent DNA-DAPI complexes. The chromatin condensation and nuclear shrinkage of apoptotic cells can be observed under fluorescence microscopy after appropriate staining of nuclei with DNA-specific fluorochromes.

INS-1E cells seeded in on cover glass in six-well plates at a density of 80 × 10^4 cells/well were cultured at 37 °C in a humidified atmosphere for 48 h. Cells were incubated with hIAPP (2.5–30 μM) for 24 h to examine the effects of hIAPP on INS-1E cells. In addition, cells were pretreated with or without PC (1.25–5μM) for 2 h and then co-incubated with 20 μM hIAPP for another 24 h to evaluate the protective effects of PC. After treatment, cells were washed with PBS and fixed with 4 % paraformaldehyde for 1 h at room temperature. After washes in PBS, cells were incubated with 1 μg/ml of DAPI for 15 min. Stained cells were washed with PBS and observed using fluorescence microscopy (Nikon Eclipse 80i).

2.5 Flow cytometric analysis of apoptosis

The cell cycle distribution was analyzed by flow cytometry. INS-1E cells seeded in six-well plates at a density of 80 × 10^4 cells/well were cultured at 37 °C in a humidified atmosphere for 48 h. Cells were incubated with hIAPP (2.5–30 μM) for 24 h to examine the effects of hIAPP on INS-1E cells. In addition, cells were pretreated with or without PC (1.25–5 μM) for 2 h and then co-incubated with 20 μM hIAPP for another 24 h to evaluate the protective effects of PC. After treatment, the cells were harvested, washed twice with PBS, and fixed in 70% ethanol at -20°C overnight. Fixed cells were then washed twice with PBS to remove ethanol. After that, cells were further washed with 1 % BSA and then stained with propidium iodide

(PI) (1.21 mg/ml Tris, 700 U/ml RNase, 50.1 μg/ml PI, pH 8.0) for 4 h in darkness. The stained cells were examined with Epics XL-MCL flow cytometer (Beckman Coulter, Miami, FL). Cell cycle distribution was analyzed using MultiCycle software (Phoenix Flow Systems, San Diego, CA). The proportion of cells in G0/G1, S, G2/M phases was represented as DNA histograms. Apoptotic cells with hypodiploid DNA content were detected by quantifying the Sub-G1 peak in the cell cycle pattern. For each experiment, 10,000 events per sample were recorded.

2.6 Determination of caspase activity

Caspase activity was measured using a fluorometric method. Briefly, treated cells were harvested and suspended in cell lysis buffer, and then incubated on ice for 1 h. After centrifugation at 10,000 × g for 10 min, supernatants were collected and immediately measured for protein concentration. For determination of caspase activity, cell lysates were placed in 96-well plates and then specific caspase substrates (Ac-DEVD-AMC for Caspase-3 substrate, Ac-IETD-AMC for caspase-8 and Ac-LEHD-AMC for caspase-9 substrate) were added. Plates were incubated at 37 °C for 1 h and caspase activity was determined by fluorescence intensity with the excitation and emission wavelengths set at 380 and 440 nm, respectively.

2.7 Analysis of Poly (ADP-ribose) polymerase

Poly (ADP-ribose) polymerase (PARP) cleavage in INS1-E cells was

examined using PathScan® Cleaved PARP (Asp214) Sandwich ELISA Kit, which could detect endogenous levels of cleaved PARP protein. Briefly, after incubation with the cell lysates, cleaved PARP protein was captured by the coated antibody on the microwells. Following extensive washing, PARP Rabbit antibody was added to detect the captured cleaved PARP according to the manufacturer's instructions.

2.8 Measurement of ROS generation

A fluorometric assay (DCF-DA assay) was used to determine the relative levels of ROS, such as superoxide radical, hydroxyl radical, and hydrogen peroxide, as described previously (Chen and Wong, 2009). 2′,7′-dichlorofluorescein diacetate (DCFF-DA) is a nonpolar compound that diffuses rapidly into the cells, where it hydrolyzes to the fluorescent polar derivative DCF, which is a reduced form. In the presence of esterases and ROS, the reduced form of DCF is oxidized to the highly fluorescent DCF. Briefly, the treated-cells were harvested and then incubated with DCFH-DA at a final concentration of 10 μM at 37°C for 30 min. Labeled cells were washed twice with PBS and suspended in PBS at cell density of 1×10^6 cells/ml for detection of fluorescence. The fluorescence intensity of DCF was measured by a Tecan SAFIRE multifunctional monochromator based microplate reader, with the excitation wavelength at 485 nm and emission wavelength at 535 nm respectively.

The induction of ROS was also monitored qualitatively by fluorescence

microscopy. Treated-INS-1E cells cultured on cover glass in six-well plates were loaded with 10 μM DCFDA for 30 min, and then examined under a fluorescence microscope (Nikon Eclipse 80i).

2.9 Measurement of O^{2-}, •OH, SOD, GSH-Px and MDA

Cells after treatments were harvested by centrifugation, washed with PBS, and lysed in lysis buffer (Cell Signaling Technology). Supernatants were collected after centrifugation at 13,000 ×g for 20 min. Aliquots of the samples were transferred into polyethylene tubes and stored at −80 °C until analysis. The protein concentrations were determined using BCA protein assay kit. The levels of O^{2-}, •OH, SOD, GSH-Px and MDA in the cell lysates were determined by different assay kits from Nanjing Jiancheng Bioengineering Institute (Nanjing, China), according to the manufacturer's manuals.

The superoxide anion radicals were generated by the xanthine/xanthine oxidase system and reacted with 2,4-iodiphenyl-3,4-nitrophenyl-5-phenyltetrazolium chloride to form formazan, a coloured compound which can be spectrophotometrically quantified at 550 nm. The production of formazan is proportional to the level of superoxide anion radicals in the tested samples. The final results were determined using the following equation:

Percentage of control (%) = (As-Ab)/(Ac-Ab)×100

Where As, Ac and Ab are the absorbances of the treated cells, control cells and blank, respectively.

Hydroxyl radicals were generated in the Fenton reaction, which reacted with Gress reagent to form mixed solution with red color. Absorbance of the solution was measured at 532 nm. The quantity of hydroxyl radicals is proportional to the degree of the color of mixed solution. The final results were expressed as percentage of control as determined by the above equation.

Determination of SOD activity was modified from the previous method (Chen et al., 2008). This method was based on xanthine and xanthine oxidase system to generate superoxide radicals. The superoxide radicals react with p-iodonitrotetrazlium violet to form a red formazan dye that was measured at 550 nm. One unit of SOD activity was defined as the amount of enzyme required to exhibit 50 % dismutation of superoxide radical.

GSH-Px activity was measured by quantifying the rate of oxidation of reduced glutathione (GSH) to oxidized glutathione (GSSG) by the hydrogen peroxide. One unit of GSH-Px activity was defined as the decrease in 1 mM GSH (except the effect of non-enzymatic reaction) in a system of enzymatic reaction of 1 mg protein per minute.

MDA content was measured by the thiobarbituric acid (TBA) method (Celik

and Suzek, 2008). This assay was based on the combination of MDA with TBA, which formed a chromogen compound whose absorbance was determined at 532 nm. The MDA content was expressed as nmol/mg protein.

2.10 Measurement of intracellular ATP content

The intracellular ATP content was determined using a bioluminescence somatic cell assay kit according to the manufacturer's instructions. After treatments, the cells were washed with cold PBS and then incubated in cold somatic cell ATP releasing reagent. The supernatants were collected and mixed with the luciferase reagent. ATP measurements were carried out using an Lmax luminometer (Molecular Devices). The calculated intracellular ATP value (pg/pl) was then normalized to total protein levels (pg/pl).

2.11 Measurement of mitochondrial mass

The mitochondrial mass was determined using the fluorescent dye Mitotracker Green FM as described previously (Nie and Wong, 2008). Briefly, the treated cells were trypsinized and resuspended in PBS buffer containing 100 nM of Mitotracker Green FM for 30 min. The staining cells were resuspended in PBS and then analyzed by flow cytometer.

2.12 Living cell staining and microscopy

The cells were grown to 60 % confluence on a glass coverslip. Mitochondria

and nucleuses were stained with 50 nM MitoTracker Red CMXRos and 1 ug/ml DAPA, respectively for 20 min. After washing with PBS twice, cells were cultured in suitable fresh medium on a thermo-cell culture FCS2 chamber (Bioptechs, Butler, PA, USA) mounted onto the adapter in the stage of an inverted fluorescence microscope Cell Observer (Carl Zeiss, Jena, Germany). Cell morphology was captured by differential internal reflection fluorescence microscopy. Drugs and culture medium were introduced to the cell culture chamber through the perfusion tubes (Bioptechs) connected to the cell chamber. Cell images were captured with a monochromatic CoolSNAP FX camera (Roper Scientific, Pleasanton, CA, USA) using a ×63 numerical aperture (NA) 1.4 Plan-Apochromat objective (Carl Zeiss), and analysed by using AxioVision 4.2 software (Carl Zeiss).

2.13 Determination of mitochondrial membrane potential

The mitochondrial membrane potential ($\Delta\Psi m$) was determined using the fluorescent probe JC-1 as described previously (Chen and Wong, 2008b). Briefly, the treated cells were trypsinized and resuspended in PBS buffer containing 10 μg/ml of JC-1. The cells were incubated at 37 °C in the incubator for 10 min, and then the staining solution was removed. The cells were resuspended in PBS and then analyzed by flow cytometer. The percentages of the cells that fluoresced green were used to represent the cells that lost $\Delta\Psi m$.

2.14 Measurement of mitochondrial permeability transition (MPT) pores

The opening of MPT pores was examined using the MitoProbe™ Transition Pore Assay Kit with minor modifications to the manufacturer's protocol (Dey et al., 2009). MPT pore opening was measured directly using a combination of calcein AM and $CoCl_2$. Calcein AM could passively diffuse into the cells and accumulate in cytosolic compartments, including the mitochondria. Once inside cells, calcein AM is cleaved by intracellular esterases to liberate the very polar fluorescent dye calcein, which does not cross the mitochondrial or plasma membranes in appreciable amounts over relatively short periods of time. The fluorescence from cytosolic calcein is quenched by the addition of $CoCl_2$, while the fluorescence from the mitochondrial calcein is maintained. When MPT is activated, the fluorescence from the mitochondrial calcein is also quenched by $CoCl_2$, resulting in reduced fluorescence intensity. In this study, INS1-E cells were harvested by trypsinization, and then resuspended at a concentration of 1×10^6 cells/ml in pre-warmed Hank's Balanced Salt Solution (HBSS) containing Ca^{2+}. The cells were incubated with 2 μM calcein AM and 400 μM $CoCl_2$ at 37 °C for 15 min in the dark, and then washed with HBSS/Ca to remove excess staining and quenching reagents. After centrifugation, cell pellets were resuspended in HBSS/Ca and analyzed by flow cytometry.

2.15 Immunoblot analysis

2.15.1 Preparation of protein lysates

To prepare whole cell lysates, the cells were harvested and suspended for 30 min on ice in lysis buffer (Cell Signaling Technology), supplemented with 1 mM PMSF (Phenylmethanesulfonyl fluoride, Sigma-Aldrich) After centrifugation at 13,000 × g at 4 ° C for 20 min to separate the cellular debris, the supernatant was collected and stored at −80 ° C until use.

2.15.2 Isolation of cytosol and mitochondrial fractions

To obtain cytosolic and mitochondrial fractions, the cells were incubated with hypotonic buffer (20 mM Hepes, 1 mM EDTA, 10 mM KCl, 1.5 mM $MgCl_2$, 1 mM EGTA, 1mM dithiothreitol, 250 mM sucrose, aprotinin, leupeptin and pepstatin 2 mg/ml each, pH 7.5) on ice for 30 min. After the cells were disrupted in a glass Dounce homogenizer by optimized gentle strokes, homogenates were centrifuged at 1000 × g for 10 min at 4 °C to remove unbroken cells and nuclei. The supernatants were further centrifuged at 12,000 × g at 4 °C for 30 min to separate the mitochondria and cytosol fractions.

2.15.3 Bicinchoninic acid (BCA) assay

The protein concentrations were determined using BCA protein assay kit (Sigma-Aldrich) according to the manufacturer's instructions. The standard curve was prepared with 0, 62.5, 125, 250, 500 and 1000 μg/ml bovine serum albumin per

25 μL/well in 96-well microplate for calibration. At the same time, 2 μL cell lysates was diluted with 23 μL ultrapure water for protein content measurement. 200 μL of freshly-prepared BCA assay working solution was added to each well and then incubated at 37 °C for 30 minutes. After that, the microplate was cooled to room temperature and the absorbance was measured at 562 nm by microplate spectrophotometer (SpectroAmaxTM 250 microplate spectrophotometer). A calibration curve was plotted with the absorbance of the standards and the protein concentration of cell lysate was therefore calculated.

2.15.4 Western blot analysis

Equal amounts of protein (30-100 μg) were mixed with Laemmli sample loading buffer (0.0625 M Tris-HCl, pH 6.8, 2 % SDS, 1 % b-mercaptoethanol, 10 % glycerol and 0.01 % bromophenol blue) (Bio-Rad) and heated at 99 °C for 5 min. Sodium dodecyl sulfate-polyacrylamide gel electrophoresis (SDS-PAGE) was carried out in 10 % tricine gels loading the obtained proteins at 70 V for 30 min and followed at 100 V for 90 minutes. Proteins were then transferred to nitrocellulose membrane at 110 V for 1 h. The membrane was blocked with 5 % non-fat milk in TBST buffer (50 mM Tris–HCl, pH 7.5, 150 mM NaCl, and 0.02 % Tween 20) for 1 h, and incubated with the primary antibodies at 1:1000 dilutions in 5 % non-fat milk at 4 °C overnight. The membrane was then incubated with a horseradish peroxidase

(HRP)-conjugated secondary antibody at 1:2000 dilutions at room temperature for 1 h, followed by three washes in TBST buffer. Specific bands were revealed by enhanced chemiluminescence reagent. Actin was used to confirm the equal loading and transfer of proteins.

2.16 Dot blot analysis

100 μg hIAPP was dissolved in 50 ul 0.04N NaOH and then diluted to a final volume of 500 μl by PBS. 10 μl hIAPP was mixed with 10 μl PBS or different dosage of PC. Rat IAPP (rIAPP) was prepared in the same way as hIAPP, and rIAPP were used as a negative control. All prepared samples were incubated at 37 °C for 24 h before detection. The dot blot experiment procedure was performed as described before (Zhao et al., 2009). Single dots (20 μL) of each sample were spotted on nitrocellulose membranes. Subsequently, the membranes were washed 5 times in TBST buffer and blocked with TBS that contained 0.2 % TBS-T at room temperature for 1 h. Then, the membranes were incubated for 30 min at room temperature with the antioligomer antibody at 1:2000 dilution in TBS with 0.05 % TBS-T.3 The membranes were washed 3 times for 5 min, each with TBS-T, incubated with horseradish peroxidase conjugated antirabbit IgG at 1:10,000 dilution, and incubated for 1 h at room temperature. The blots were washed 3 times with TBS-T and developed with enhanced chemiluminescence reagent.

2.17 Statistical analysis

Data are expressed as mean ± SD. Differences between two groups were analyzed by the Student's t test. One-way analysis of variance (ANOVA) was used in multiple group comparisons. These analyses were carried out by SPSS 12.0. Difference with $P<0.05$ (*) or $P<0.01$ (**) was considered statistically significant.

Chapter 3: Results

3.1 PC attenuates hIAPP-induced cytotoxicity in INS-1E cells

3.1.1 Evaluation of metabolic activity

Cellular growth was evaluated using MTT assay, which is a quantitative colorimetric assay based on the ability of viable cells to reduce the yellow tetrazolium salt MTT to a dark-blue formazan product. We first examined the cytotoxic effects of hIAPP and possible protective effects of PC on INS-1E cell using the MTT reduction assay. It was found that exposure of INS-1E cells to hIAPP resulted in time-and dose-dependent decrease in cell viability (**Fig. 3.1A**). Rat IAPP was used as a negative control. The time-dependent effects of different doses of rat IAPP (0 – 20 μM) on INS-1E cells at 24, 48 and 72 h were also examined. It was found that rat IAPP showed no cytotoxicity on INS-1E cells at various doses or at different time (**Fig. 3.1B**). When INS-1E cells were treated with hIAPP for 24 h, the cells treated with 20 μM of hIAPP showed reduced cell viability by approximately 50 % relative to control cells (**Fig. 3.2A**). This cytotoxic effect was significantly attenuated by co-treatment with PC in a dose-dependent manner (**Fig. 3.2B**). At concentrations of 2.5 and 5 μM, PC increased the cell viability of hIAPP-treated cells to 75 % and 86 %, respectively of the control cells. Cells treated with 5 μM of PC showed no difference in cell viability from that of control cells.

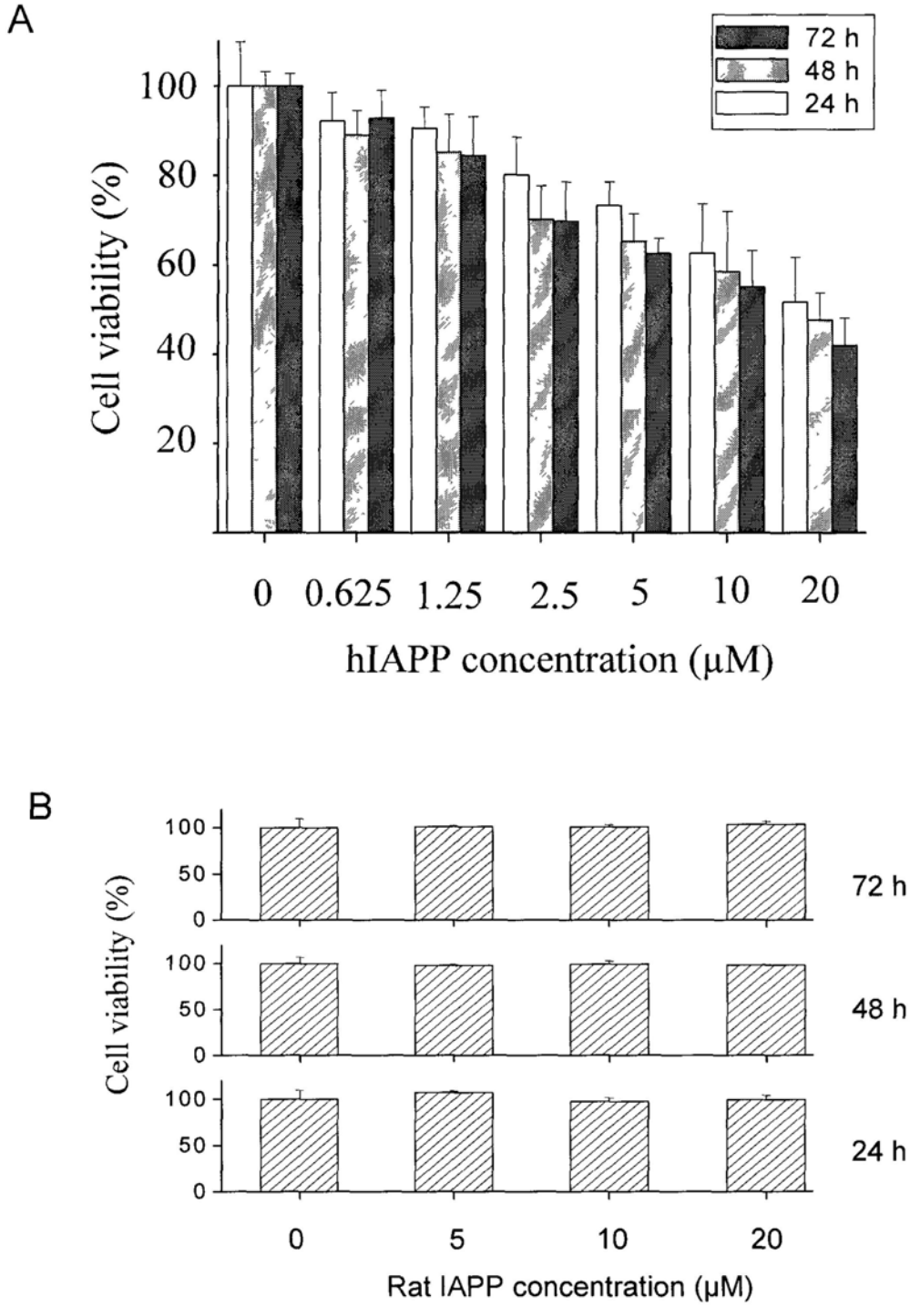

Fig. 3.1 Time- and dose-dependent effects of hIAPP (A) and rat IAPP (B) on growth of INS-1E cells. The cells were treated with 0-20 μM hIAPP or rat IAPP for 24 h, 48 h and 72 h and examined by MTT assay. The growth inhibitory of cells was expressed as percentage (%) of cell viability in treatment group relative to the control group. All data were obtained from three independent experiments and presented as the means ± SD.

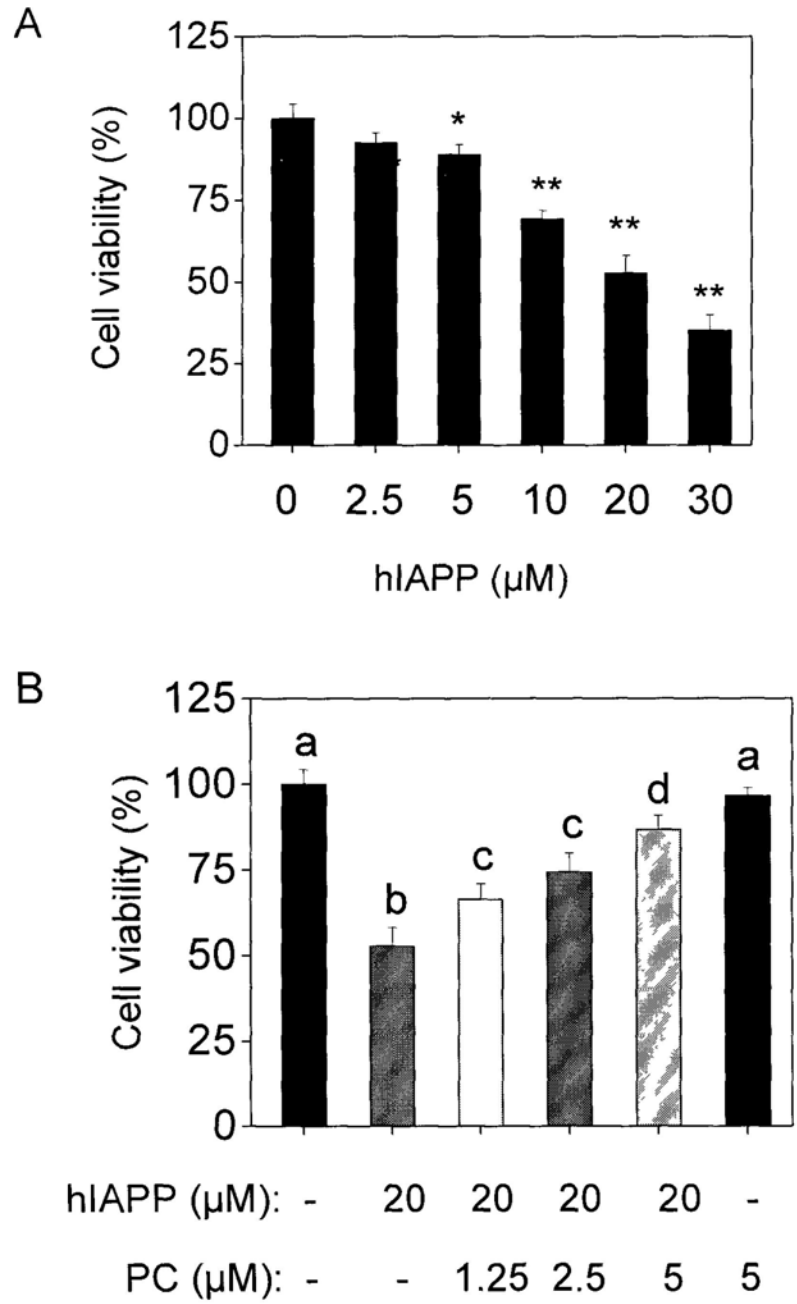

Fig. 3.2 (A) Growth inhibitory effects of hIAPP on INS-1E cells. The cells were treated with 0-30 μM hIAPP for 24 h and examined by MTT assay. The growth inhibition of cells was expressed as percentage (%) of cell viability in the treatment group relative to the control group. $*p < 0.05$, $**p < 0.01$ vs untreated controls. (B) PC prevented hIAPP-induced decrease in cell viability. Cells were pretreated with or without PC (2.5-5 μM) for 2 h and then cultured in the presence or absence of 20 μM hIAPP for 24 h. Cell viability was examined by MTT assay. Bars with different characters (a, b, c and d) are statistically different at $P<0.05$ level. All data were obtained from three independent experiments and presented as the means ± SD.

3.1.2 Evaluation of DNA synthesis

Cell proliferation was assessed by Brdu assay, which is a chemiluminescence immunoassay based on the measurement of BrdU incorporation during DNA synthesis. From the results of Brdu assay, we found that hIAPP dose-dependently inhibited the proliferation of INS-1E cell after 24-h exposure to hIAPP (**Fig. 3.3A**). As shown in **Fig. 3.3B**, 20 μM hIAPP inhibited proliferation of INS-1E cells by 42 % compared with the control cells after 24 h treatment. Similar to the MTT assay data, PC was able to dose-dependently prevent the hIAPP-induced decrease in INS-1E cell proliferation with maximal protective effect obtained at 5 μM PC. At concentrations of 1.25, 2.5 and 5 μM, PC increased the cell proliferation of hIAPP-treated cells to 60 %, 66 % and 78 %, respectively of the control cells. 5 μM of PC showed no inhibition on the cell proliferation of INS-1E cells.

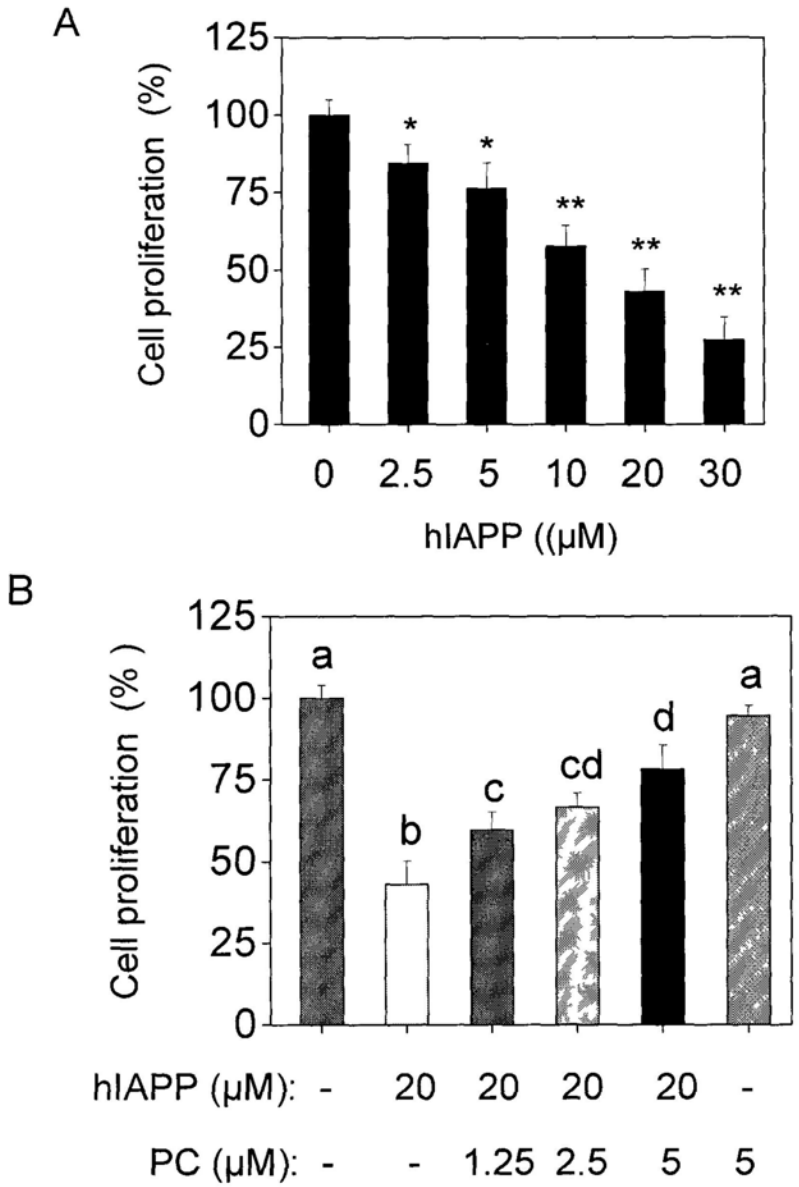

Fig. 3.3 (A) Antiproliferative effects of hIAPP on INS-1E cells. The cells were treated with 0-30 μM hIAPP for 24 h and examined by Brdu assay. The results were expressed as percentage (%) of cell proliferation in the treatment group relative to the control group. * $P < 0.05$, ** $P < 0.01$ vs untreated controls. (B) PC attenuated hIAPP-induced decrease in cell proliferation. Cells were pretreated with or without PC (2.5-5 μM) for 2 h and then cultured in the presence or absence of 20 μM hIAPP for 24 h. Cell proliferation was examined by Brdu assay. Bars with different characters (a, b, c and d) are statistically different at $P < 0.05$ level. All data were obtained from three independent experiments and presented as the means ± SD.

3.1.3 Evaluation of cytotoxicity

LDH is a cytoplasmic enzyme that is released from the cytoplasm upon cell lysis. Cell membrane damage leads to the release of cytoplasmic enzymes, and the measurement of LDH release is a well-accepted assay to estimate cell membrane integrity and quantify cell cytotoxicity. The results were represented as LDH release (%).

The results of LDH assay showed that hIAPP induced LDH release in INS-1E cells in a dose-dependent manner (**Fig. 3.4A**). The effect of 10 μM of hIAPP on the LDH release of INS-1E cells was not significant. LDH release was elevated to 141 % of control value after a 24-h exposure to 20 μM of hIAPP. The LDH release was significantly decreased by co-treatment with PC in a dose-dependent manner (**Fig. 3.4B**). At concentrations of 1.25, 2.5 and 5 μM, PC reduced the extent of LDH release to 125 %, 117 % and 105 %, respectively. 5 μM of PC alone did not show any cytotoxicity on INS-1E cells.

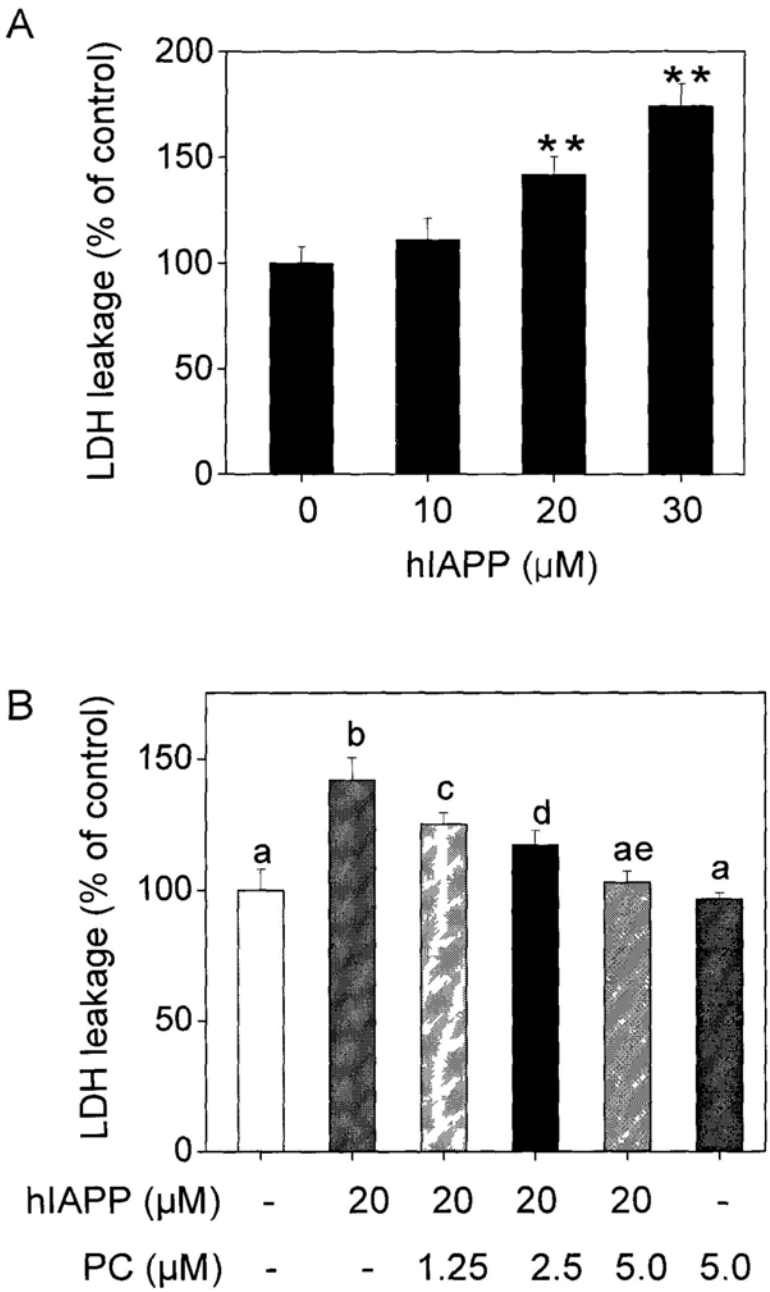

Fig. 3.4 (A) Cytotoxic effects of hIAPP on INS-1E cells. The integrity of the plasma membrane was measured by LDH released into the culture medium. The cells were treated with 0-30 μM hIAPP for 24 h and examined by LDH assay. The results were expressed as percentage (%) of LDH release in the treatment group relative to the control group * $P < 0.05$, ** $P < 0.01$ vs untreated controls. (B) PC inhibited hIAPP-induced LDH release in INS-1E cells. Cells were pretreated with or without PC (2.5-5 μM) for 2 h and then cultured in the presence or absence of 20 μM hIAPP for 24 h, and examined by LDH assay. Bars with different characters (a, b, c, d and e) are statistically different at $P<0.05$ level. All data were obtained from three independent experiments and presented as the means ± SD.

3.1.4 Evaluation of viable cell number

The above results were further corroborated when viable cells were counted in trypan blue exclusion assay. The trypan blue exclusion assay was based on the capability of viable cells to exclude the dye. Since viable INS-1E cells maintained membrane integrity, the cells did not allow trypan blue dye to pass through the cell membrane. Cells with damaged membrane appeared blue due to accumulation of dye and were counted as dead.

The results of trypan blue exclusion assay revealed that hIAPP dose-dependently reduced the viable cell numbers of INS-1E cell (**Fig. 3.5A**). Similar to the LDH release data, PC dose-dependently prevented the hIAPP-induced decrease in the number of viable INS-1E cells, with maximal protective effect obtained at 5 μM PC (**Fig. 3.5B**).

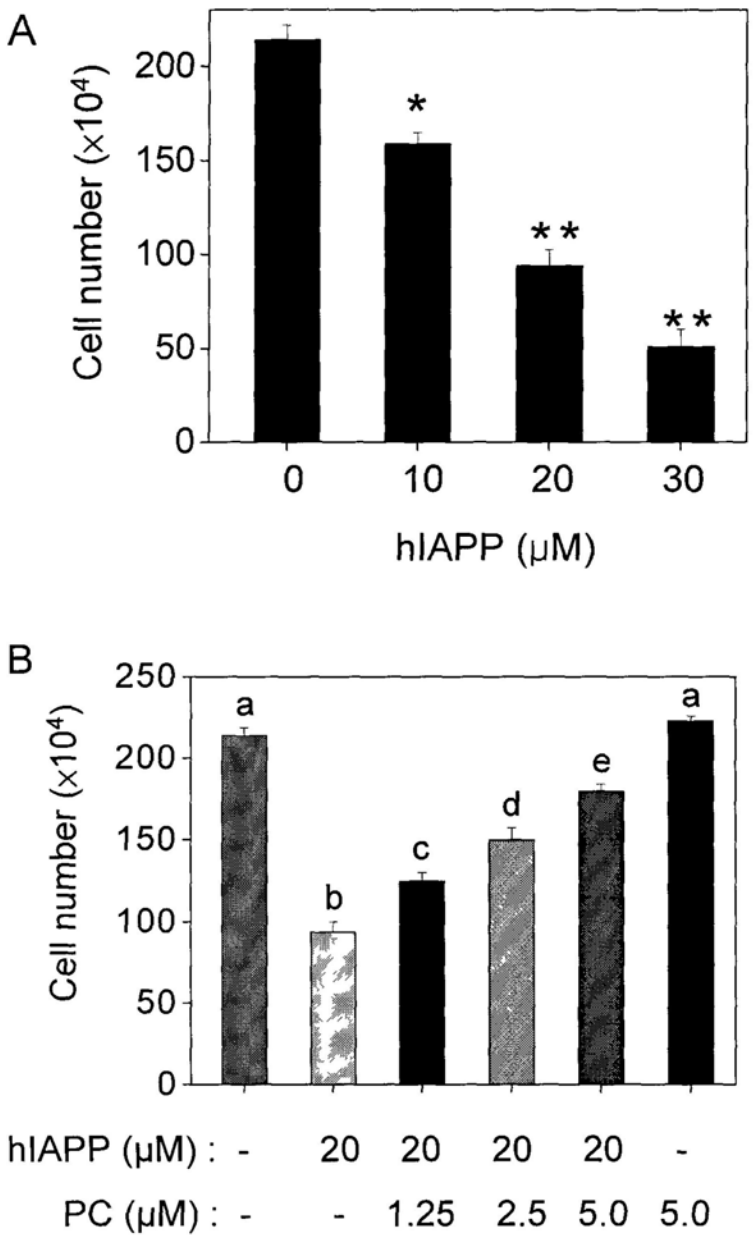

Fig. 3.5 (A) hIAPP induced decrease in the number of viable INS-1E cells. The cells were treated with 0~30 μM hIAPP for 24 h. Number of viable cells was evaluated by Trypan blue exclusion assay. * $P < 0.05$, ** $P < 0.01$ vs untreated controls. (B) PC prevented hIAPP-induced decrease in the number of viable INS-1E cells. Cells were pretreated with or without PC (2.5-5 μM) for 2 h and then cultured in the presence or absence of 20 μM hIAPP for 24 h, and examined by Trypan blue exclusion assay. Bars with different characters (a, b, c, d and e) are statistically different at $P<0.05$ level. All data were obtained from three independent experiments and presented as the means ± SD.

3.2 Evaluation of apoptotic morphological changes

Apoptosis occurs in several pathological situations and is characterized by morphological changes, including progressive cell shrinkage, membrane blebbing, condensation and fragmentation of nuclear chromatin, and formation of apoptotic body. To characterize cell death induced by hIAPP, INS-1E cells were examined by phase-contrast microscopy, DAPI staining and TUNEL assay.

To observe hIAPP-induced changes in cell morphology, INS-1E cells were examined by phase-contrast microscopy. As shown in **Fig. 3.6A**, cells treated with hIAPP for 24 h were seen to have detached from the dish, with cell rounding, irregularity in shape, reduction in cell numbers and loss of cell-to-cell contact. Moreover, hIAPP induced morphological changes in a dose-dependent manner. However, these changes in hIAPP-treated cells were attenuated by co-treatment with 5 μM PC (**Fig. 3.6B**). By contrast, control cells and cells treated with PC appeared healthy, with regularity in shape and well developed cell-to-cell contact.

In addition, cells were observed via fluorescence microscopy following staining with DAPI, which specifically binds the DNA of nuclei. After exposure to 20 μM hIAPP for 24 h, INS-1E cells exhibited typical apoptotic features such as chromatin condensation and condensed nuclear fragment, as indicated by the arrows in **Fig. 3.7** (upper panel). Co-treatment with 5 μM PC prevented these hIAPP

induced morphological alterations while control cells and PC-treated cells showed normal nuclei of ovum shape.

To confirm the morphological changes of apoptosis data, we treated INS-1E cells with hIAPP for 24 h, and the DNA fragmentation was detected by the in situ DNA labeling TUNEL assay, which is a sensitive indicator of apoptosis. As shown in **Fig. 3.7** (lower panel), in hIAPP-treated INS-1E cells, there was a significant increase in the number of TUNEL-positive nuclei, compared to normal cells. In the presence of PC, the number of TUNEL-positive nuclei was significantly reduced in hIAPP-treated INS-1E cells. The numbers of TUNEL-positive nuclei were not evident in control cells and PC-treated cells. The data from TUNEL assay also supported that PC protected INS-1E cells from hIAPP-induced apoptosis.

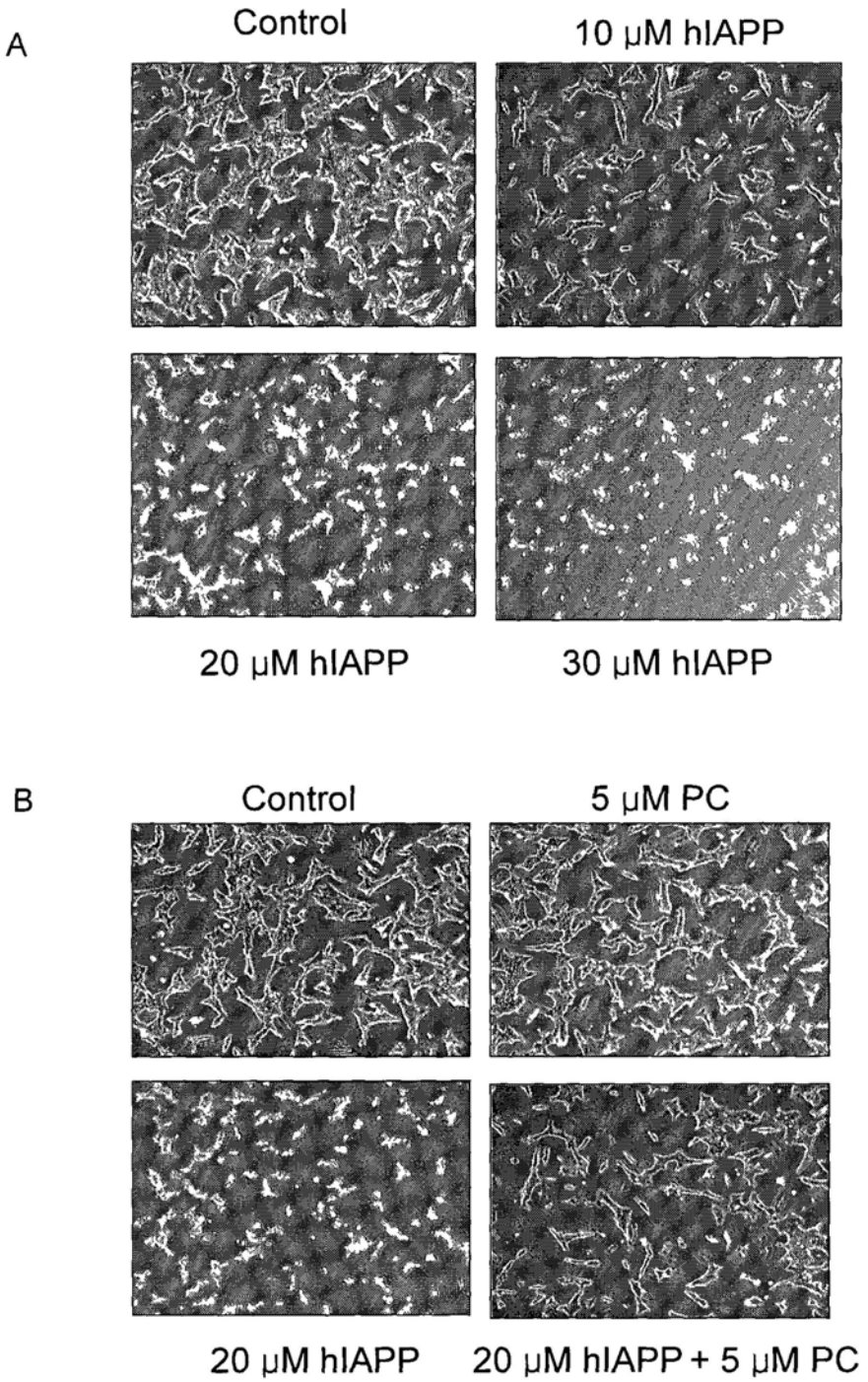

Fig. 3.6 Phase-contrast micrographs of INS-1E cells. (A) hIAPP induced morphology changes in INS-1E cells. The cells were treated with 0-30 μM hIAPP for 24 h, and observed by phase-contrasted microscopy (magnification, 100×). (B) PC prevented hIAPP-induced morphology changes in INS-1E cells. Cells were pretreated with or without 5 μM PC for 2 h and then cultured in the presence or absence of 20 μM hIAPP for 24 h, and observed by phase-contrast microscopy (magnification, 100×).

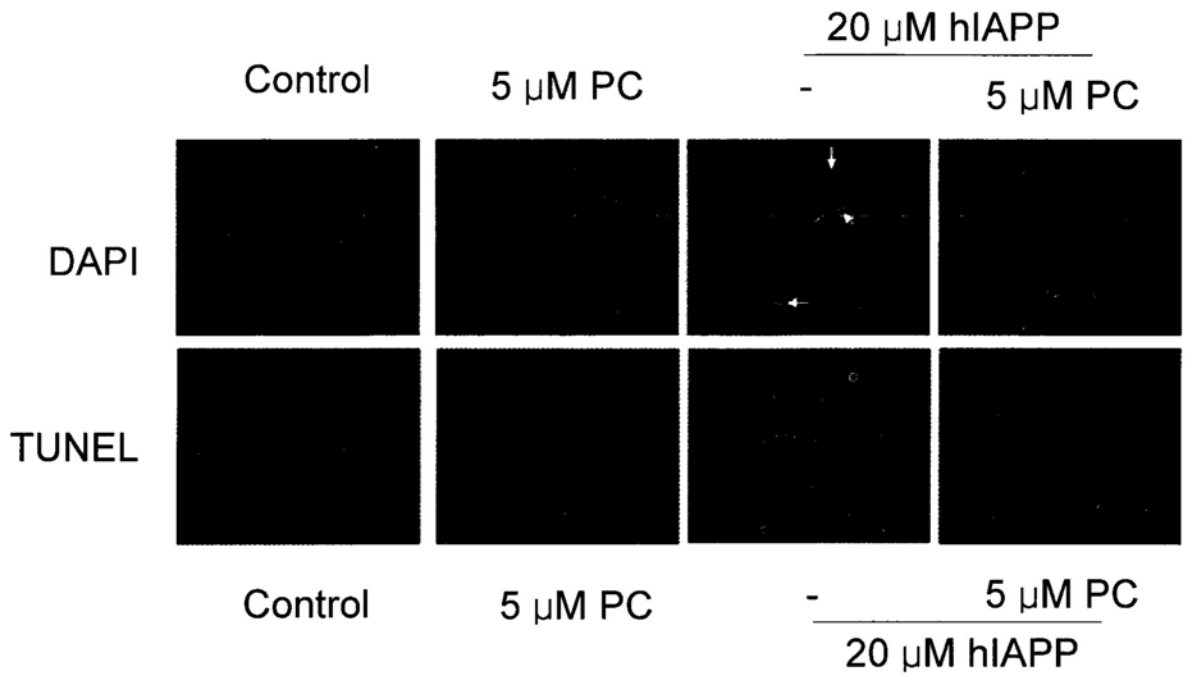

Fig. 3.7 Analysis of apoptotic morphology in INS-1E cells. (A) Evaluation of apoptosis in INS-1E cells was examined by DAPI staining (magnification, 600×). White arrows indicate condensed nuclei. Cells were pretreated with or without 5 μM PC for 2 h and then cultured in the presence or absence of 20 μM hIAPP for 24 h, and observed under fluorescence microscope after DAPI staining. (B) DNA fragmentation was detected by TUNEL assay (magnification, 600×). TUNEL-positive nuclei due to DNA fragmentation appeared as green areas. Cells were pretreated with or without 5 μM PC for 2 h and then cultured in the presence or absence of 20 μM hIAPP for 24 h, and examined by TUNEL assay. The images shown here are representative of three independent experiments with similar results.

3.3 Flow cytometric analysis of DNA content

To quantify the amount of cells undergoing apoptosis after treatment with hIAPP, INS-1E cells were stained with a nuclear stain (PI) and analyzed by flow cytometry. The amount of bound dye correlates with the DNA content in a given cell count. The apoptotic cells with fragmented DNA are shown as sub-G1 peak in DNA histogram.

INS-1E cells were treated with hIAPP (0, 10, 20 or 30 μM) for 24 h, and then examined by DNA-PI flow cytometry. The apoptotic cells, which had fragmented DNA shown as sub-G1 in DNA histogram, were significantly increased by hIAPP at dosage as low as 10 μM (**Fig. 3.8A**). The proportion of apoptotic cells were increased by hIAPP in a dose-dependent manner. For instance, the apoptotic cells were significantly increased by 38.53 % by hIAPP at the concentration of 20 μM (**Fig. 3.8B**). However, PC dose-dependently inhibited hIAPP-induced apoptosis in INS-1E cells. Co-treatment with PC (1.25, 2.5 and 5 μM) reduced the number of apoptotic cells to 27.14 %, 23.62 % and 13.45 %, respectively (**Fig. 3.9A** and **Fig. 3.9B**). Additionally, the percentage of apoptotic cells between the control group and the PC-treated group was not significantly different.

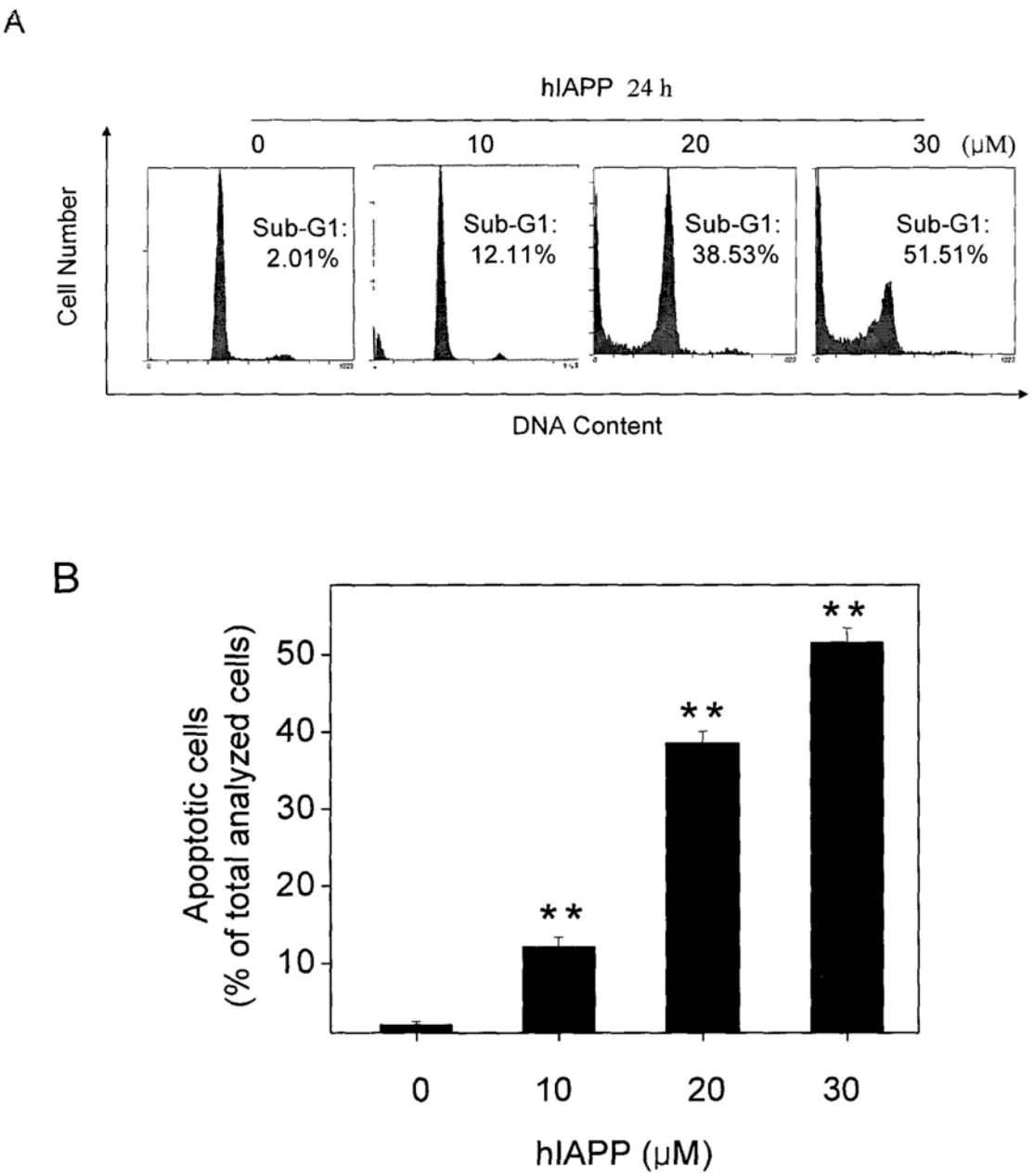

Fig. 3.8 (A) Representative DNA histograms showing the effect of hIAPP concentration on DNA fragmentation of INS-1E cells. The cells were incubated with hIAPP (0, 10, 20 or 30 μM) for 24 h, and then analyzed by flow cytometer after staining with propidium iodide. The cells with sub-G1 DNA content were calculated. (B) Numeric data showing the dose effect of hIAPP on DNA fragmentation in INS-1E cells. The cells were incubated with hIAPP (0, 10, 20 or 30 μM) for 24 h, and then analyzed by flow cytometer. The cells with sub-G1 DNA content were calculated, and their numbers are expressed as a percentage of total population. All data were obtained from three independent experiments and presented as the means ± SD. $^{**}P < 0.01$ vs untreated controls.

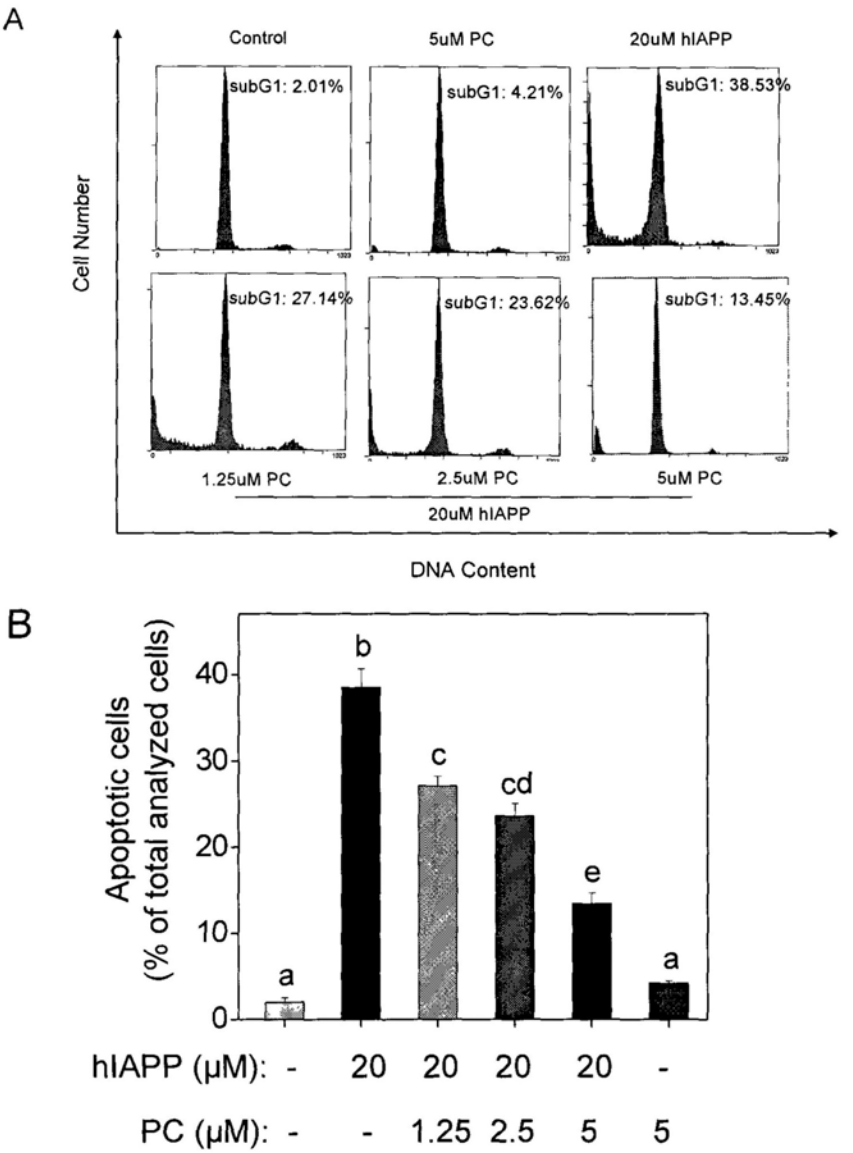

Fig. 3.9 (A) Effects of PC on DNA fragmentation of INS-1E cells subject to hIAPP exposure. Cells were pretreated with or without PC (2.5-5 μM) for 2 h and then cultured in the presence or absence of 20 μM hIAPP for 24 h, and analyzed by flow cytometer. The cells with sub-G1 DNA content were calculated. (B) Numeric data showing the effects of PC on DNA fragmentation of INS-1E cells subject to hIAPP exposure. Cells were pretreated with or without PC (1.25-5 μM) for 2 h and then cultured in the presence or absence of 20 μM hIAPP for 24 h, and analyzed by flow cytometer. The cells with sub-G1 DNA content were calculated, and their numbers are expressed as a percentage of total population. Bars with different characters (a, b, c, d and e) are statistically different at $P<0.05$ level. All data were represented as the means ± SD and the values were obtained from three separate experiments.

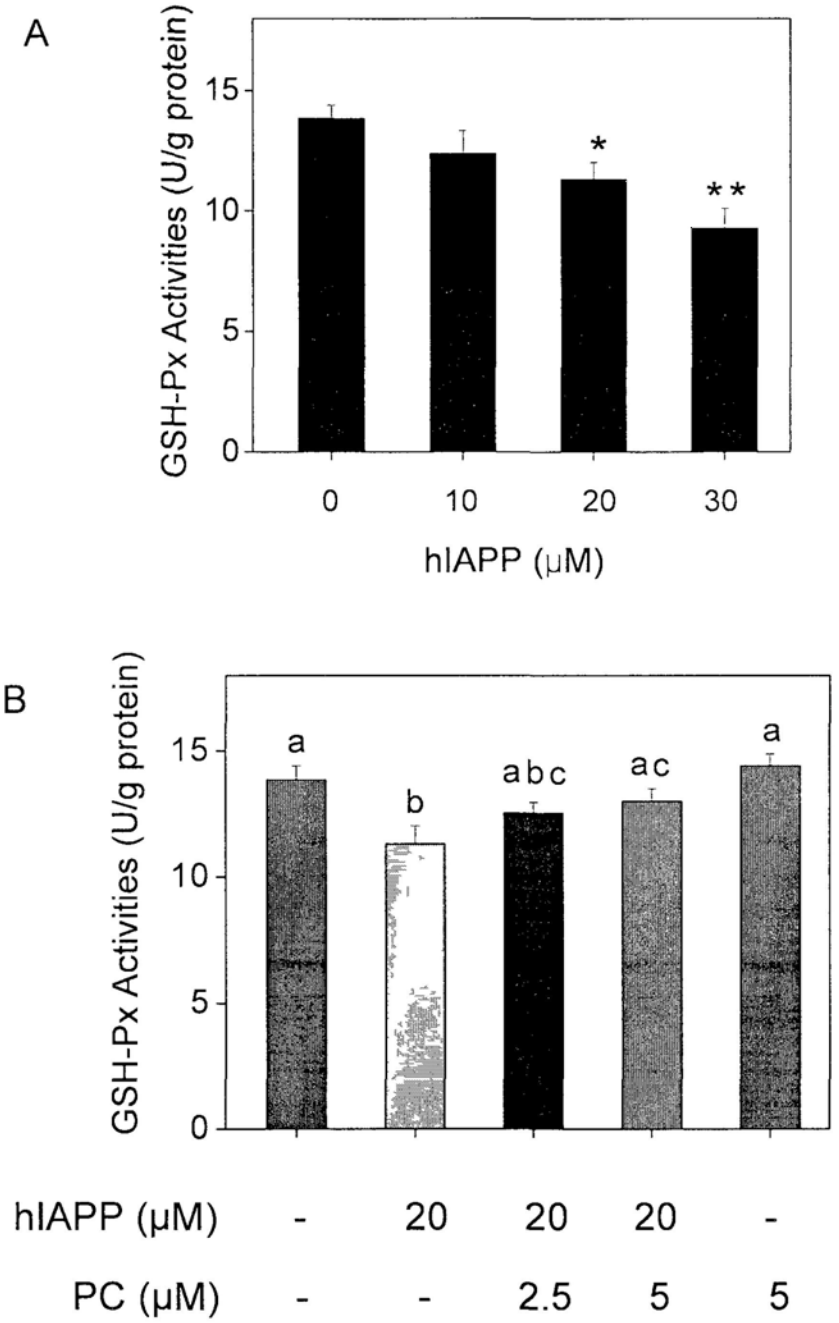

Fig.13. Evaluation of GSH-Px activities in INS-1E cells. (A) hIAPP treatment decreased GSH-Px activities in INS-1E cells. The cells were incubated with hIAPP (0, 10, 20 or 30 μM) for 24 h. All data are expressed as means ± SD of triplicates. $*P < 0.05$, $**P < 0.01$ vs untreated controls. (B) PC prevented hIAPP-induced decrease in GSH-Px activities in INS-1E cells. Cells were pretreated with or without PC (2.5-5 μM) for 2 h and then cultured in the presence or absence of 20 μM hIAPP for 24 h. All data are expressed as means ± SD of triplicates. Bars with different characters are statistically different at $P < 0.05$ level.

3.4 Evaluation of intracellular ROS

To further explore the biochemical basis contributing to the protective effects of PC on beta cell, hIAPP-induced free radical generation and free radical scavenging capacity of PC were examined in INS-1E cells. Intracellular ROS was detected by fluorescein-labeled dye, DCFH-DA. Treatment of cells with hIAPP resulted in dose-dependent increase in intracellular ROS as shown by increased fluorescence intensity (**Fig. 3.10A**). Treatment with 20 μM hIAPP for 24 h increased the ROS level to 179 % of control cells. At the concentrations of 2.5 and 5 μM, PC reduced intracellular ROS to 142 % and 135 %, respectively (**Fig. 3.10B**). These findings were further confirmed by fluorescence microscopy using DCF staining (**Fig. 3.10C**).

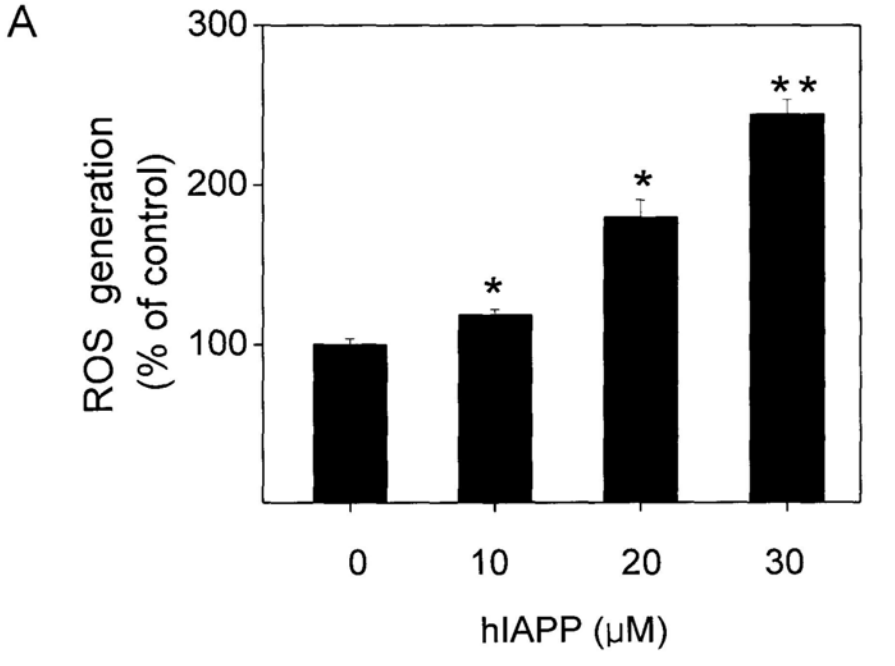
A
300
200
100
ROS generation
(% of control)
*
*
**
0
10
20
30
hIAPP (μM)

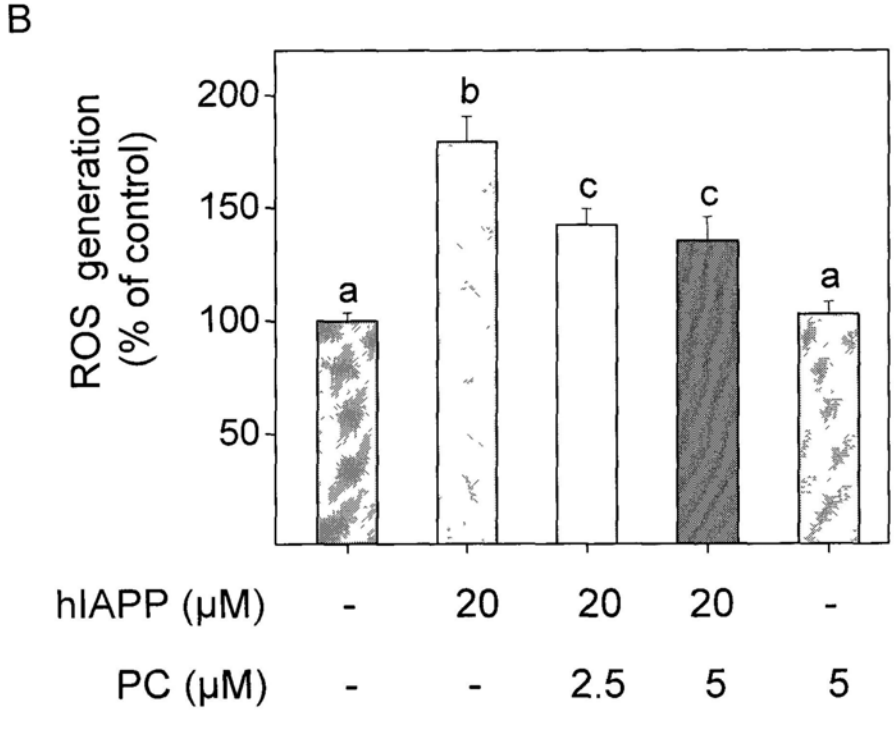
B
200
150
100
50
ROS generation
(% of control)
a
b
c
c
a
hIAPP (μM) - 20 20 20 -
PC (μM) - - 2.5 5 5

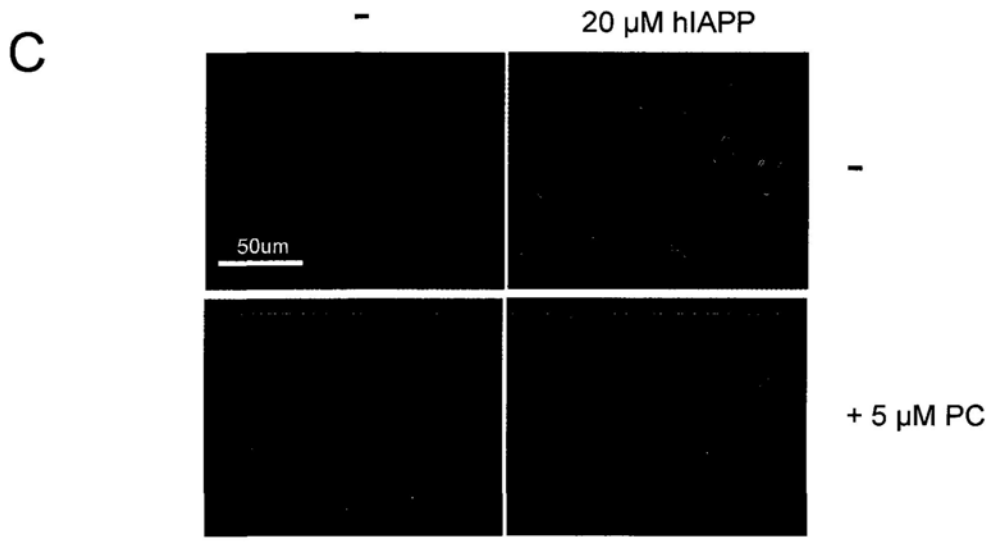

Fig. 3.10 Intracellular ROS generation in INS-1E cells. (A) hIAPP induced ROS overproduction in INS-1E cells. The cells were incubated with hIAPP (0, 10, 20 or 30 μM) for 24 h. Intracellular ROS was determined by measuring the fluorescence intensity of an oxidation-sensitive fluorescein DCFH-DA. All data are expressed as means ± SD of triplicates. $*P < 0.05$, $**P < 0.01$ vs untreated controls. (B) PC inhibited hIAPP-induced accumulation of ROS in INS-1E cells. Cells were pretreated with or without PC (2.5-5 μM) for 2 h and then cultured in the presence or absence of 20 μM hIAPP for 24 h. (C) Intracellular ROS level was examined by fluorescence microscopy (magnification, 200×). The cells were incubated with hIAPP (0, 10, 20 or 30 μM) for 24 h. After treatment, INS-1E cells were stained with DCFH-DA and imaged under a fluorescence microscope using ex/em of 495/525 nm. All data are expressed as means ± SD of triplicates. Bars with different characters (a, b and c) are statistically different at $P<0.05$ level.

3.5 Evaluation of the levels of O_2^- and •OH

As shown in **Fig. 3.11A**, hIAPP treatment even at the low dose of 10 μM for 24 h, significantly increased the levels of O_2^-, compared to the control group in a dose-dependent manner. At 20 μM of hIAPP treatment, cells showed a 144 % increase in levels of O_2^- compared to the control group. Interestingly, at the concentration of 2.5 and 5 μM, PC was able to reduce the levels of O_2^- to 131 % and 118 %, respectively (**Fig. 3.11B**).

Additionally, after 24 h treatment, hIAPP increased the levels of OH in INS-1E cells in a dose dependent manner (**Fig. 3.12A**). The levels of OH in the cells treated with 20 μM hIAPP increased significantly to 149 % compared with the control group. Co-treatment with 5 μM PC reduced the levels of O_2^- from 149 % to nearly 120 %. PC at 2.5 μM slightly suppressed the production of ·OH in the cells treated with 20 μM hIAPP, albeit short of significance (**Fig. 3.12B**).

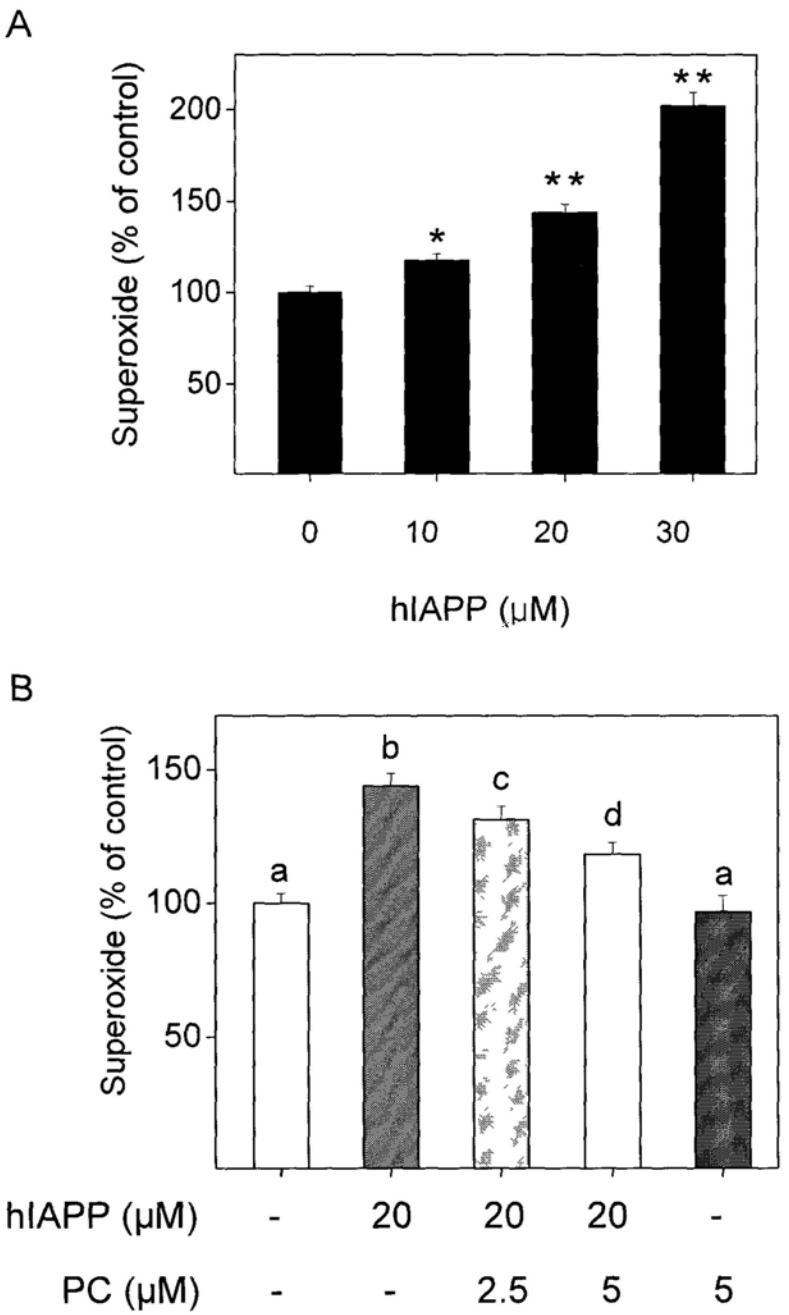

Fig. 3.11 Evaluation of superoxide levels in INS-1E cells. (A) hIAPP induced accumulation of superoxide in INS-1E cells. The cells were incubated with hIAPP (0, 10, 20 or 30 μM) for 24 h. All data are expressed as means ± SD in triplicates. * $P <$ 0.05, ** $P < 0.01$ versus untreated controls. (B) PC suppressed hIAPP-induced accumulation of superoxide in INS-1E cells. Cells were pretreated with or without PC (2.5-5 μM) for 2 h and then cultured in the presence or absence of 20 μM hIAPP for 24 h. All data are expressed as means ± SD in triplicates. Bars with different characters (a, b, c and d) indicate statistically different at $P <0.05$ level.

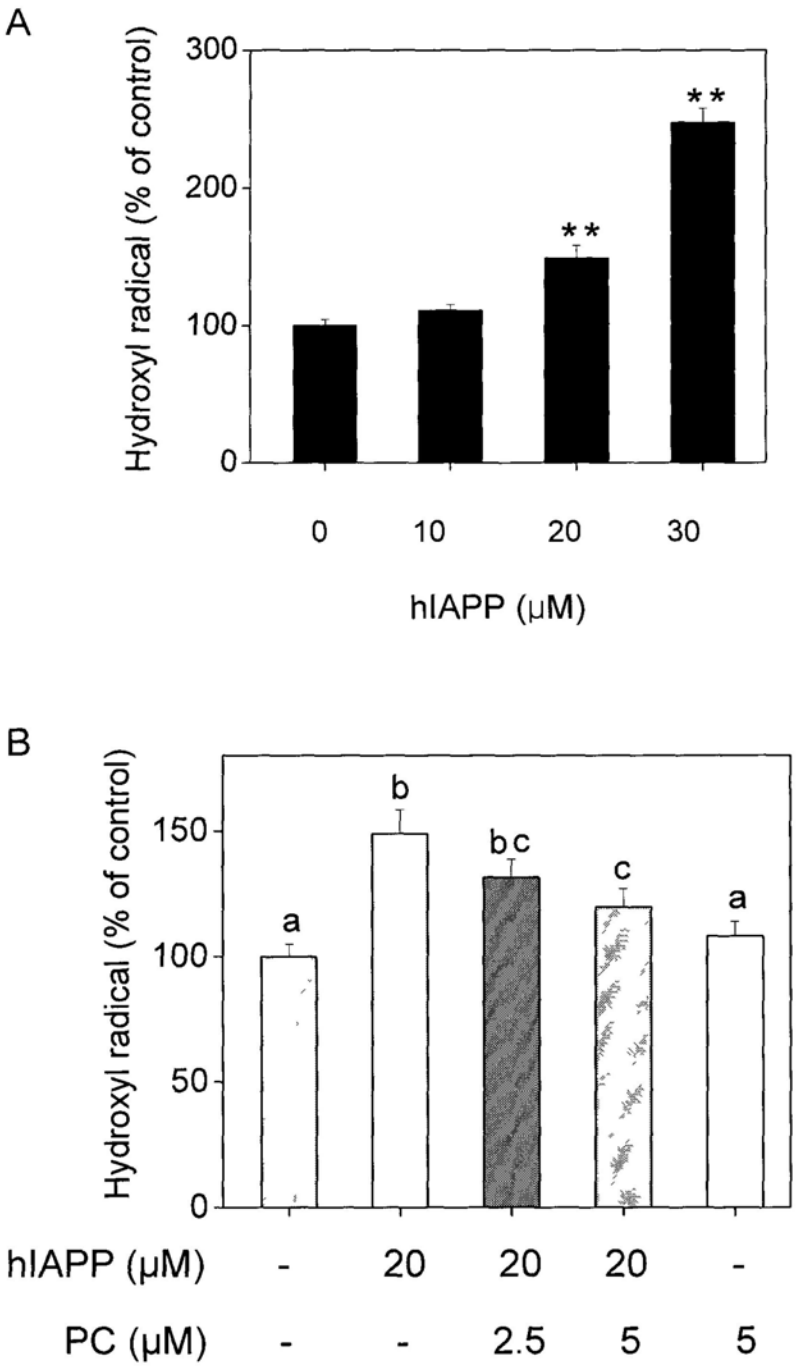

Fig. 3.12 Evaluation of hydroxyl radical levels in INS-1E cells. (A) hIAPP induced accumulation of hydroxyl radical in INS-1E cells. The cells were incubated with hIAPP (0, 10, 20 or 30 μM) for 24 h. All data are expressed as means ± SD in triplicates. $^{**}P < 0.01$ versus untreated controls. (B) PC suppressed hIAPP-induced accumulation of hydroxyl radical in INS-1E cells. Cells were pretreated with or without PC (2.5-5 μM) for 2 h and then cultured in the presence or absence of 20 μM hIAPP for 24 h. All data are expressed as means ± SD in triplicates. Bars with different characters (a, b and c) indicate statistically different at $P<0.05$ level.

3.6 Evaluation of antioxidant enzyme activities and content of MDA

After treatment with hIAPP for 24h, the INS-1E cells showed decrease in GSH-Px activity in a dose-dependent manner (**Fig. 3.13A**). At the concentration of 20 μM, hIAPP reduced GSH-Px activity by 18 % compared with the control group. Co-treatment with 5 μM PC significantly prevented the reduction of GSH-Px activity in hIAPP-treated cells. PC at the concentration of 2.5 μM failed to significantly attenuate the reduction of GSH-Px activity induced by hIAPP (**Fig. 3.13B**).

Additionally, treatment with hIAPP increased SOD activity in a dose-dependent manner in INS-1E cells (**Fig. 3.14A**). This activity increased by 29% in cells exposed to 20 μM hIAPP compared with the control cells. Co-treatment with 5 μM PC significantly prevented the increase in SOD activity although the reduction with 2.5 μM PC fell short of significance (**Fig. 3.14B**).

As shown in **Fig. 3.15A**, hIAPP dose-dependently increased the contents of MDA in INS-1E cells after 24-h treatment. The content of MDA was significantly increased by 35 % compared with the control group after treatment with 20 μM hIAPP. This was prevented by co-treatment with 5 μM PC (**Fig. 3.15B**). No effect on hIAPP-induced accumulation of MDA in cells was observed with 2.5 μM PC. Taken together, these results indicated that PC prevented hIAPP-induced changes in activities of antioxidant enzyme and level of MDA in INS-1E cells.

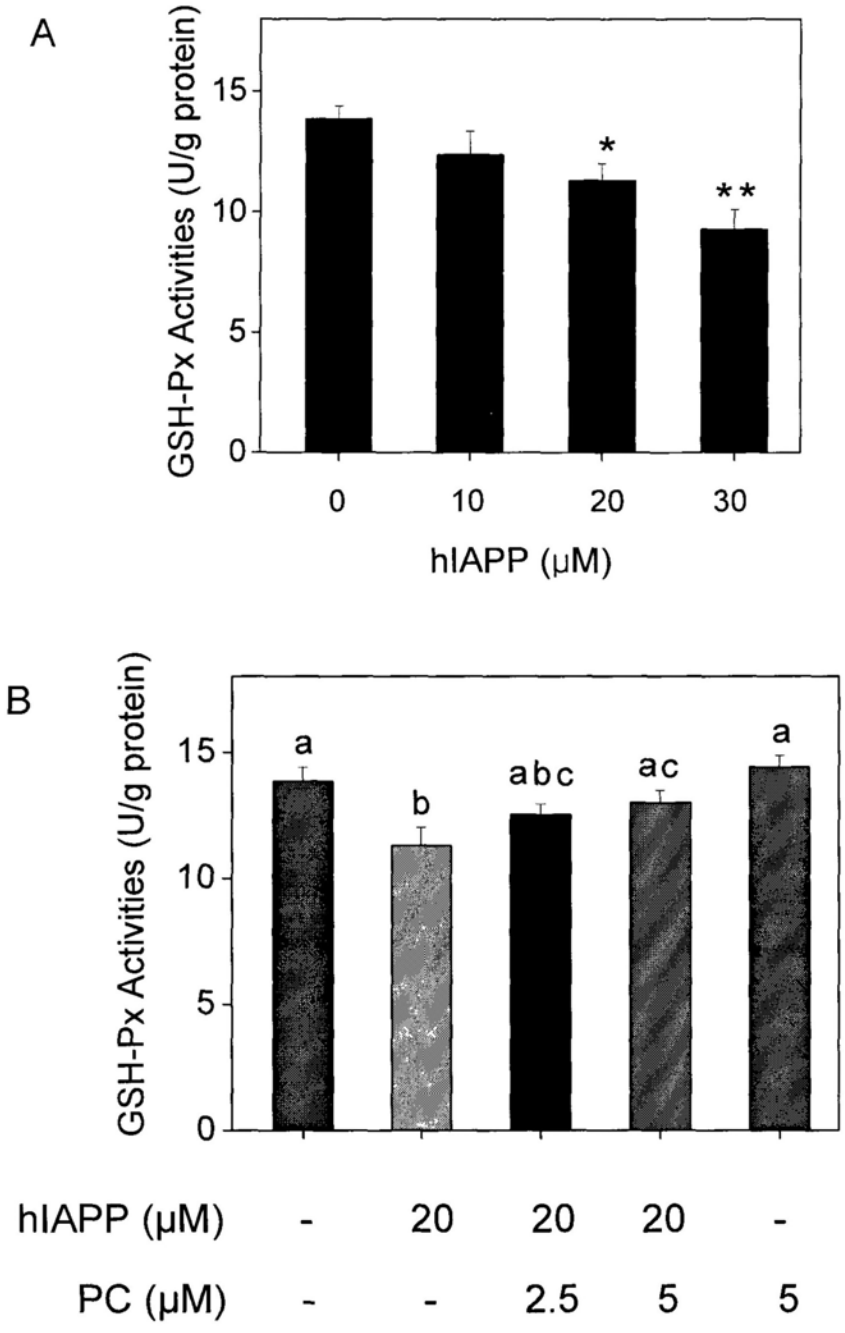

Fig. 3.13 Evaluation of GSH-Px activities in INS-1E cells. (A) hIAPP treatment decreased GSH-Px activities in INS-1E cells. The cells were incubated with hIAPP (0, 10, 20 or 30 μM) for 24 h. All data are expressed as means ± SD in triplicates. *P < 0.05, **P < 0.01 vs untreated controls. (B) PC prevented hIAPP-induced decrease in GSH-Px activities in INS-1E cells. Cells were pretreated with or without PC (2.5-5 μM) for 2 h and then cultured in the presence or absence of 20 μM hIAPP for 24 h. All data are expressed as means ± SD in triplicates. Bars with different characters (a, b and c) indicate statistically different at P <0.05 level.

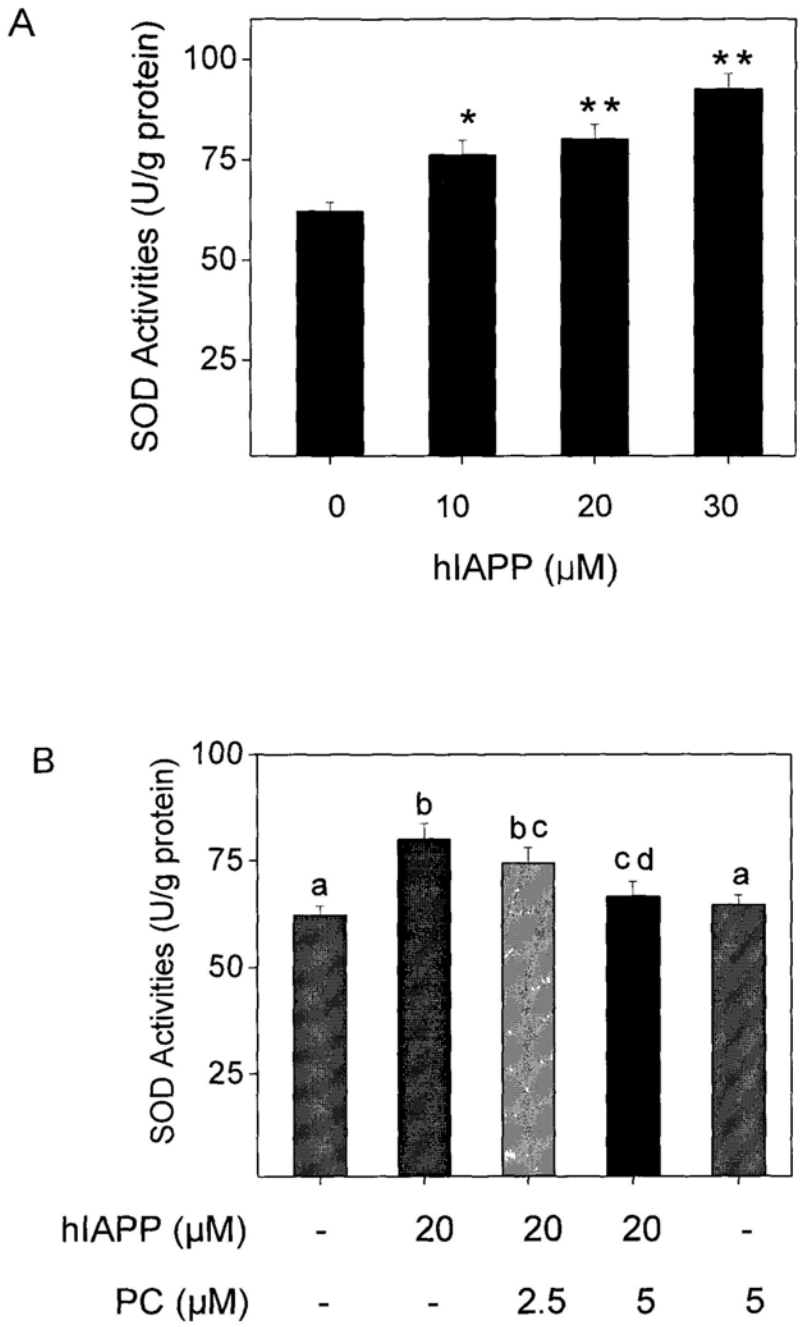

Fig. 3.14 Evaluation of SOD activities in INS-1E cells. (A) hIAPP treatment increased SOD activities in INS-1E cells. The cells were incubated with hIAPP (0, 10, 20 or 30 μM) for 24 h. All data are expressed as means ± SD in triplicates. $*P < 0.05$, $**P < 0.01$ vs untreated controls. (B) PC prevented hIAPP-induced increase in SOD activities in INS-1E cells. Cells were pretreated with or without PC (2.5-5 μM) for 2 h and then cultured in the presence or absence of 20 μM hIAPP for 24 h. All data are expressed as means ± SD in triplicates. Bars with different characters (a, b, c and d) indicate statistically different at $P<0.05$ level.

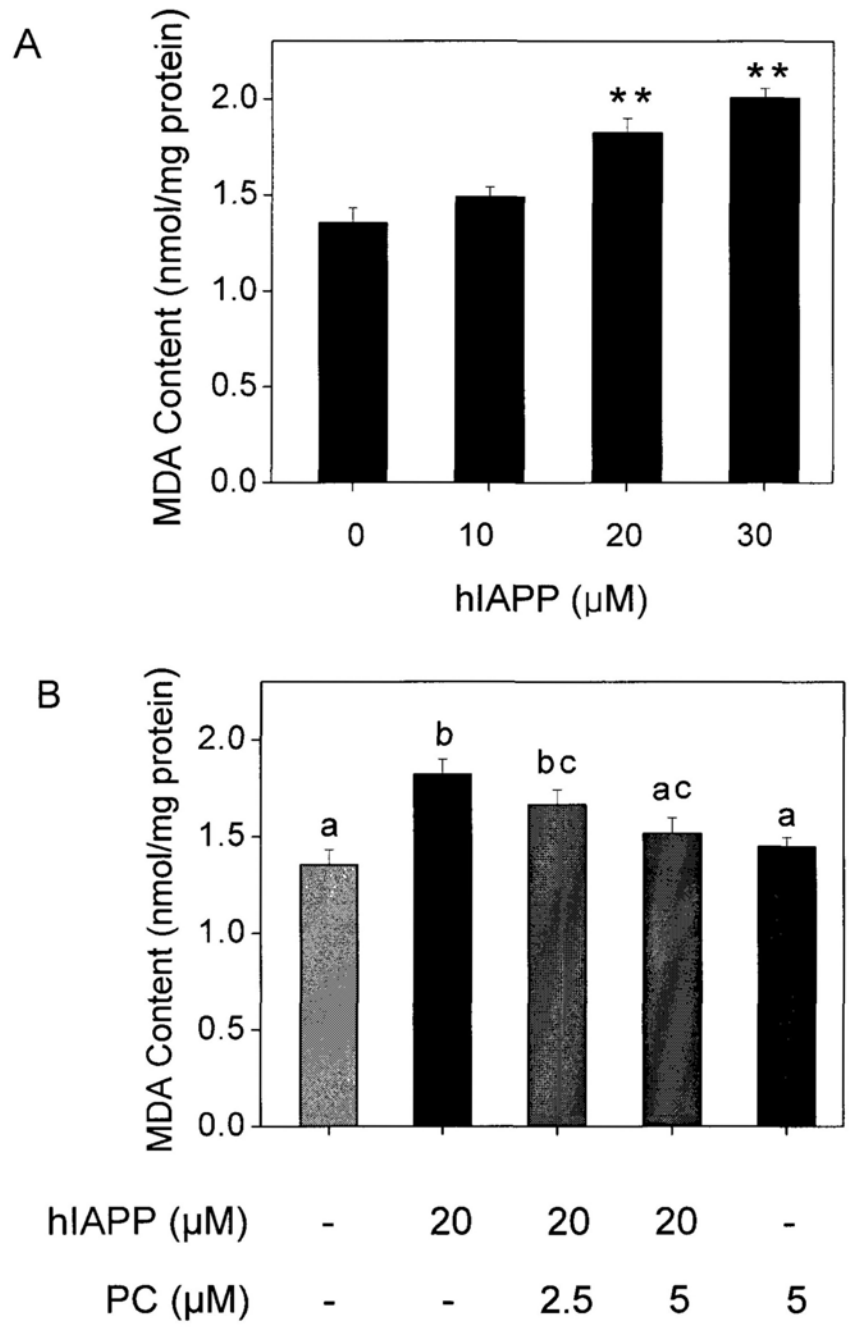

Fig. 3.15 Evaluation of MDA content in INS-1E cells. (A) hIAPP treatment induced accumulation of MDA content in INS-1E cells. The cells were incubated with hIAPP (0, 10, 20 or 30 μM) for 24 h. All data are expressed as means ± SD in triplicates. $^{**}P < 0.01$ vs untreated controls. (B) PC inhibited hIAPP-induced accumulation of MDA content in INS-1E cells. Cells were pretreated with or without PC (2.5-5 μM) for 2 h and then cultured in the presence or absence of 20 μM hIAPP for 24 h. All data are expressed as means ± SD in triplicates. Bars with different characters (a, b and c) indicate statistically different at $P<0.05$ level.

3.7 MAPK signaling pathways

It has been reported that oxidative stress can provoke activation of MAPKs of the c-Jun N-terminal kinase (JNK) and p38 families. MAPKs regulate cell death or cell survival, depending on cell types and the balance amongst the JNK, p38 and ERK status (Blair et al., 1999). In this context, MAPK pathways has been implicated in hIAPP-induced RINm5F pancreatic beta cells death (Rumora et al., 2002; Zhang et al., 2006).

In the present study, I examined the activation of these MAPKs in INS-1E cells at different time points after exposure to 20 μM hIAPP. From the results of Western blotting analysis, we found that hIAPP treatment induced differential activation and phosphorylation of JNK, p38 and ERK in INS1-E cells. **Fig. 3.16** shows that exposure of the cells to hIAPP resulted in activation of both JNK and p38, including total protein and phosphorylated forms. Treatment with hIAPP had no effect on level of total ERK, but increased phosphorylated ERK in INS-1E cells. Activation of MAPKs by hIAPP was observed as early as 2 h after hIAPP treatment, and peaked at approximately 8-12 h followed by decline thereafter.

To determine whether MAPKs are important for hIAPP-induced cell death, I examined the effects of specific inhibitors of MAPKs on hIAPP-induced cytotoxicity in INS-1E cell by MTT assay. As shown in **Fig. 3.17**, pretreatment of cells with

SP600125 (JNK inhibitor) and SB203580 (p38 inhibitor) partially prevented hIAPP-induced cytotoxicity. Contrarily, pretreatment of cells with U0126 (ERK inhibitor) showed no significant protection against hIAPP-induced cytotoxicity. These data indicated that activation of JNK and p38 is required for hIAPP-induced cell death, whereas activation of ERK did not play an important role in hIAPP-induced cytotoxicity.

To explore the role of MAPK kinases in the mechanism of protection of PC, I examined the effects of the PC on hIAPP-mediated MAPK signaling pathways. Based on the results of Western blotting, pretreatment of INS-1E cells with PC suppressed hIAPP-induced expression of total and phosphrylated JNK and p38 (**Fig. 3.18**). At the same time, pretreatment of INS-1E cells with PC also attenuated hIAPP-induced phosphorylation of ERK (**Fig. 3.18**). These results suggest that PC protect INS-1E cells from hIAPP-induced cell death at least partly through suppression of JNK and p38.

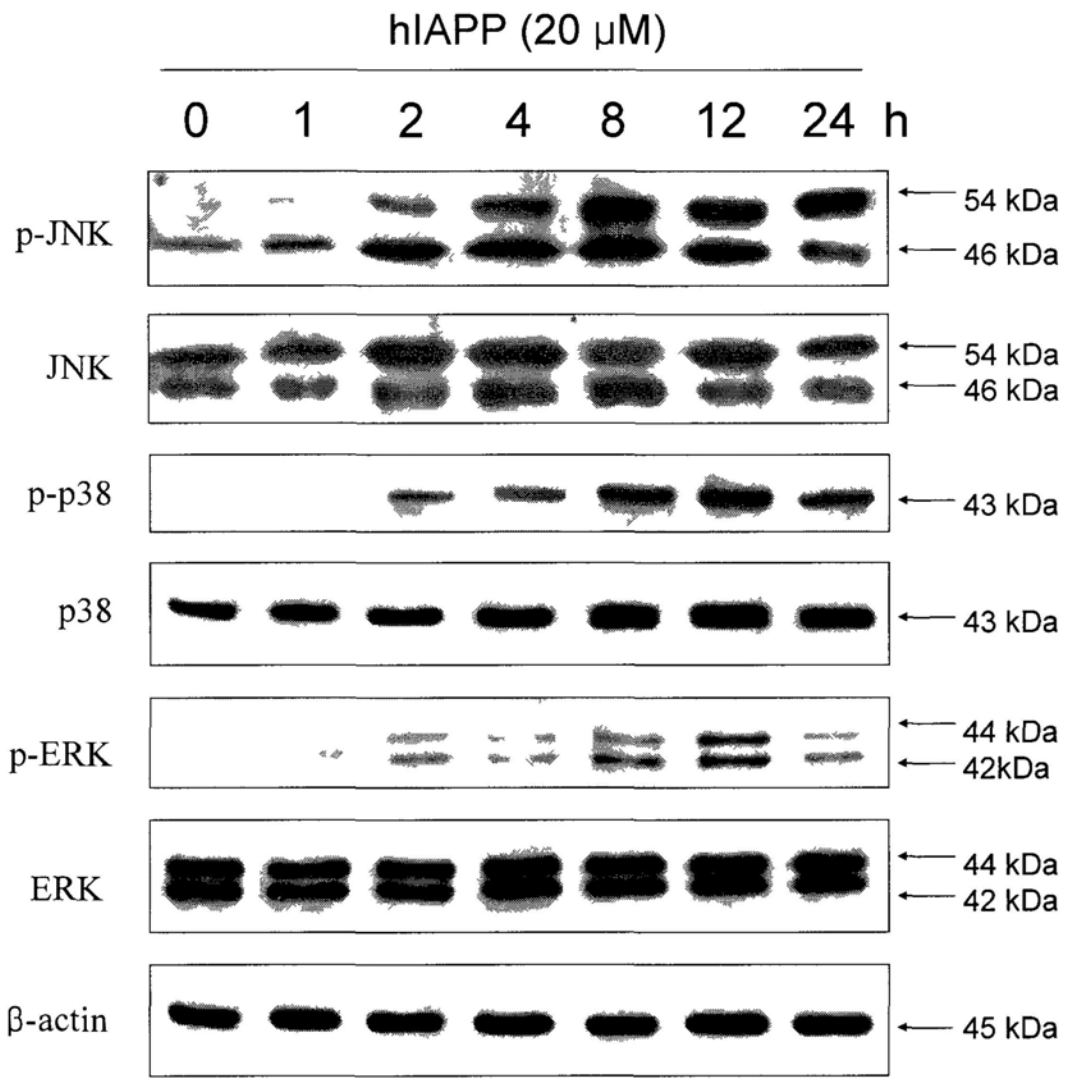

Fig. 3.16 The time-course analysis of activation of MAPKs in INS-1E cells subject to hIAPP exposure. Cells were treated with 20 μM hIAPP and harvested at various times. Cell lysates were subjected to Western blot analysis with the primary antibodies. Protein levels of phosphorylated JNK, total JNK, phosphorylated p38, total p38, phosphorylated ERK and total ERK were determined. Beta-actin was measured as internal control to normalize expression of other proteins. Data represent similar results from three independent experiments.

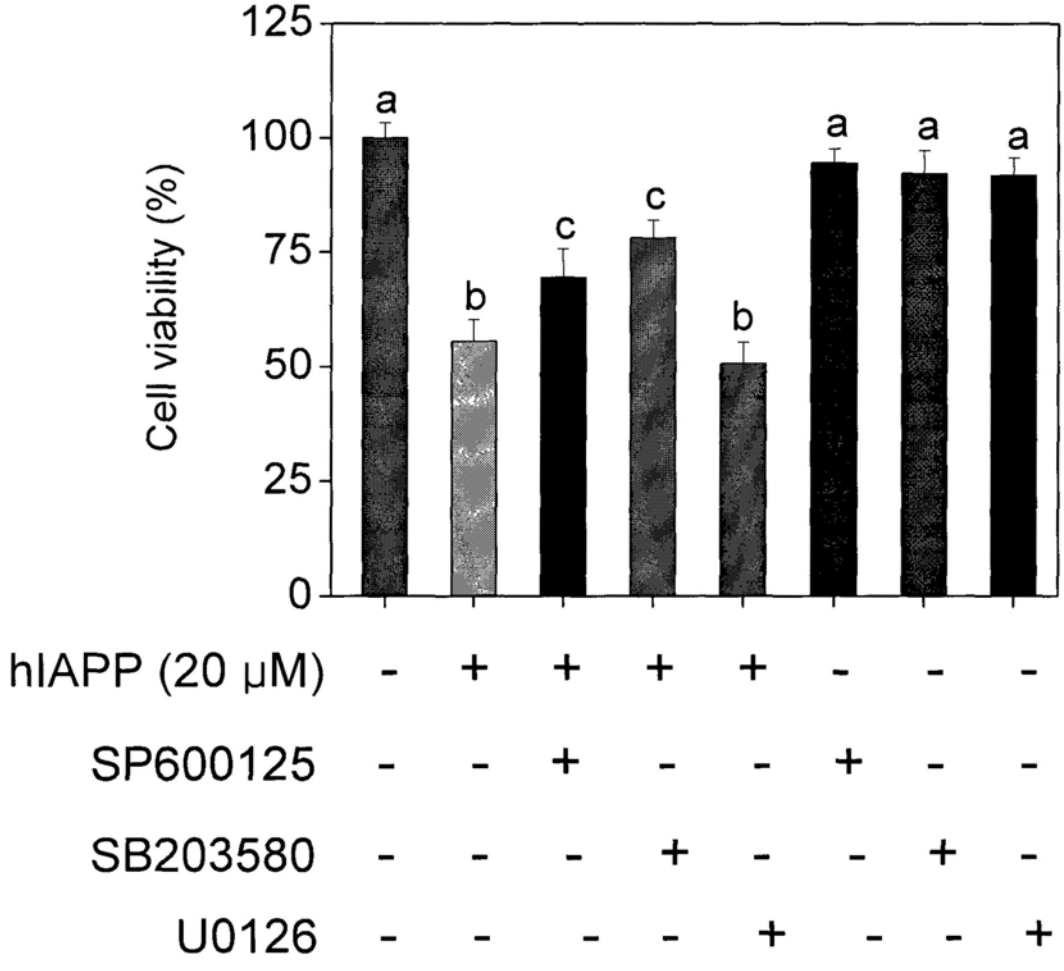

Fig. 3.17 Effect of MAPK inhibitors on cell viability of hIAPP-treated INS-1E cells. The cells were pretreated with specific inhibitors of MAPKs (JNK inhibitor SP600125 20 μM, p38 inhibitor SB203580 10 μM, ERK inhibitor U0126 20 μM) for 1 h and then incubated in the presence or absence of 20 μM hIAPP for 24 h. Cell viability was determined by MTT assay. All data are expressed as means ± SD of triplicates. Bars with different characters (a, b and c) indicate statistically different at $P<0.05$ level.

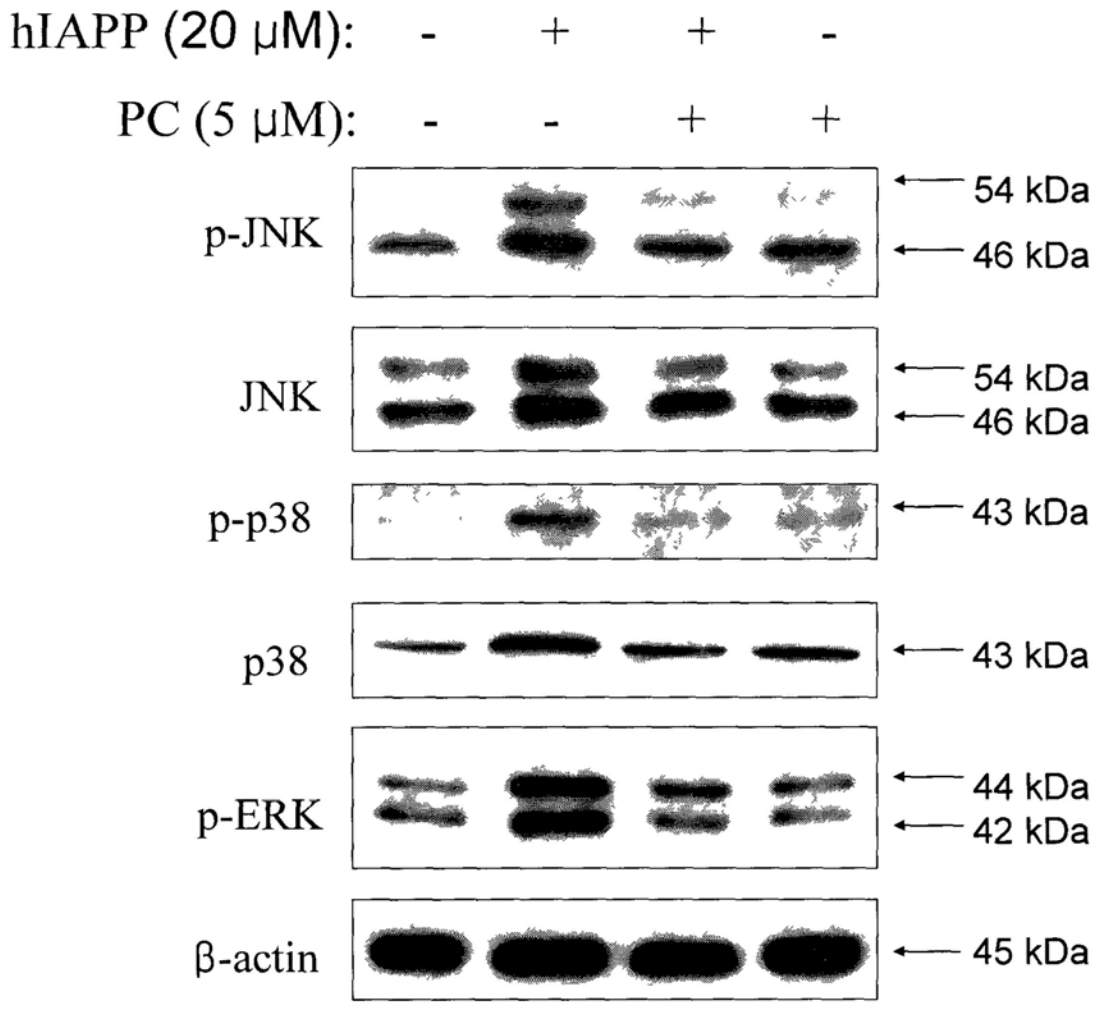

Fig. 3.18 PC blocked hIAPP-induced activation of MAPKs in INS-1E cells. Cells were pretreated with or without 5 μM PC for 2 h and then incubated with the presence or absence of 20 μM hIAPP for 12 h. Cell lysates were analyzed for protein levels of MAPKs by Western blotting using specific antibodies. Beta-actin was used as an internal control. Data represent similar results from three independent experiments.

3.8 Activation caspase cascade

Apoptosis occurs normally during development and throughout adulthood, and serves to eliminate unwanted, aged or potentially harmful cells. There are two major pathways for induction of apoptosis, the extrinsic and intrinsic apoptotic pathways. The extrinsic death receptor pathway is initiated by engagement of plasma membrane death receptors on the cells resulting in activation of the initiator caspases (e.g. caspase-8 and -10) (Nagata, 1997). The intrinsic pathway of apoptosis involves increased mitochondria permeability and release of pro-apoptotic molecules (death inducers) from the mitochondria into the cytosol to activate another initiator caspase, i.e. caspase-9 (Cory and Adams, 2002). Both the extrinsic and intrinsic apoptosis pathways terminate their signals through activation of downstream effector caspases (e.g. caspase-3, -6 and -7), causing DNA fragmentation and cellular disintegration (Kumar, 2007). Since poly(ADP-ribose) polymerase (PARP) is a substrate of effector caspases, its cleavage indicates activation of caspases during the cell death process.

To elucidate the molecular mechanisms of cell apoptosis triggered by hIAPP, we examined the activation of initiator and effector caspases in INS-1E cells. Based on the results of Western blot analysis, treatment of INS-1E cells with hIAPP caused activation of caspase-3, caspase-7, caspase-8, caspase-9, cleavage of PARP, and up-regulation of adaptor molecule apoptotic protease activating factor 1 (Apaf-1)

expression (**Fig. 3.19**), indicating activation of both intrinsic and extrinsic apoptotic pathways. The activation of caspases cascade induced by hIAPP was further confirmed by the time course analysis (**Fig. 3.20A** and **Fig. 3.20B**).

To determine whether the activation of caspases is essential for the apoptosis, the effect of z-VAD-fmk, a general caspase inhibitor, was examined. As shown in **Fig. 3.21A**, pretreatment with z-VAD-fmk attenuated the cleavage of PARP induced by hIAPP, indicating that hIAPP elicited caspase-dependent apoptosis in INS-1E cells.

To further evaluate the contribution of these caspases to hIAPP -induced cell death, I examined the effects of other caspase-specific inhibitors. INS-1E cells were pretreated with z-VAD-fmk, z-IETDfmk (caspase-8 inhibitor) and z-LEHD-fmk (caspase-9 inhibitor), and then incubated with hIAPP for 24 h. Firstly, morphology of treated cells was observed by phase-contrast microscopy. As shown in **Fig. 3.21B**, INS-1E cells treated with 20 μM hIAPP for 24 h showed reduction in cell numbers and loss of cell-to-cell contact. These morphological changes in hIAPP-treated cells were partially attenuated by co-treatment with these caspase inhibitors. By contrast, control cells and cells treated with caspase inhibitors appeared healthy. Furthermore, results of MTT assay revealed that pretreatment of cells with z-VAD-fmk, z-IETDfmk and z-LEHD-fmk partially prevented hIAPP-induced cytotoxicity (**Fig. 3.21C**). These data suggested that activation of caspase-8 and caspase-9 was

important for hIAPP-induced cell death in INS-1E cells.

To investigate the underlying mechanisms for protection of PC against hIAPP-induced apoptosis, I analyzed whether caspases and PARP were involved in this process. Activation of caspase-3 and PARP was first examined by Western blot analysis. As shown in **Fig. 3.22A**, hIAPP induced activation of caspase-3 in INS-1E cells after 24 h treatment as evidenced by decreased level of pro-caspase-3 (35 kDa) and appearance of cleaved caspase-3 (19 kDa). Co-treatment with PC markedly attenuated the activation of caspase-3. After 24 h treatment with hIAPP, INS-1E cell showed cleavage of PARP at 85 kDa and reduced level of total PARP (116 kDa). The activation of PARP was recovered by co-treatment with PC.

Caspase activation was also assessed by using specific fluorometric caspase activity assays. As shown in **Fig. 3.22B**, exposure of INS1-E cells to hIAPP resulted in significant increase in the activities of caspase-3, -8 and -9. Co-treatment with 5 μM PC reduced the caspase-3 activity from 200 % to 149 %. PC alone induced a slight increase in caspase-3 activity compared with the control, albeit insignificant. At the same time, treatment with 20 μM hIAPP for 24 h increased the caspase-8 activity to 185% of control cells. PC at the concentration of 5 μM decreased this value to 121 % of control cells. Additionally, at the concentration of 5 μM, PC reduced the caspase-9 activity from 174 % to 116 % in hIAPP-treated cells. PC alone

had no significant effects on activity of both caspase-8 and caspase-9.

Moreover, cleavage of PARP was confirmed by using PathScan® Cleaved PARP (Asp214) Sandwich ELISA Kit. As shown in **Fig. 3.22C**, after 24 h treatment with 20 μM hIAPP, cleavage of PARP was increased to 168 % of control cells. However, PC at the concentration of 5 μM was able to decrease this value to 109 % of control cells. PC alone induced a slight increase in cleavage of PARP compared with the control, albeit insignificant.

Taken together, our results suggest that the anti-apoptotic effects of PC involved suppression of the caspase-mediated pathway.

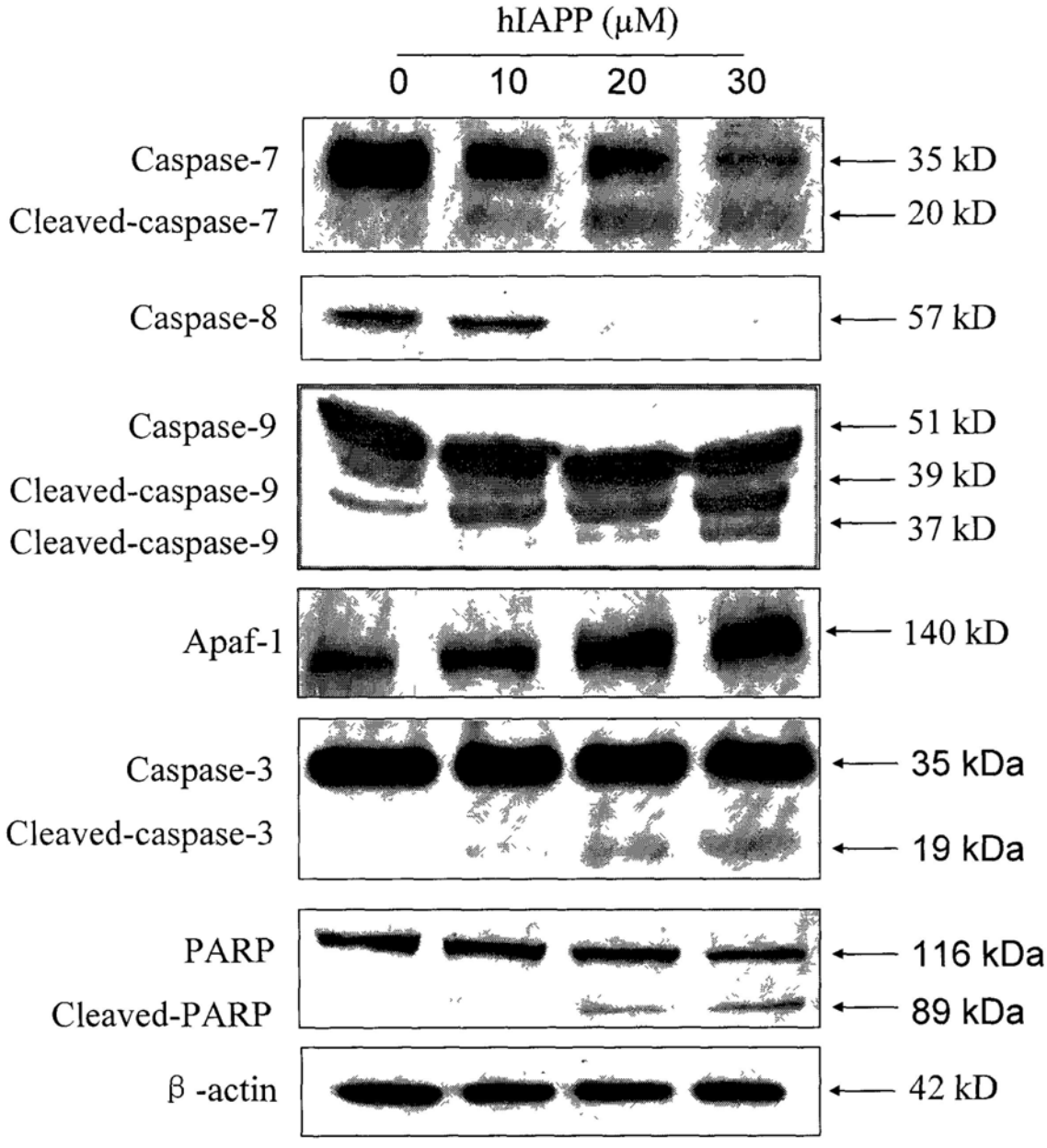

Fig. 3.19 Dose-dependent effect of hIAPP on caspase processing in INS-1E cells by Western blot analysis. The cells were incubated with hIAPP (0, 10, 20 or 30 μM) for 24 h. Cell lysates were subjected to Western blot analysis with specific antibodies. Protein levels of caspase-3, -7, -8, -9, Apaf-1 and PARP were determined. Beta-actin was measured as internal control to normalize expression of other proteins. This experiment was repeated twice with similar results.

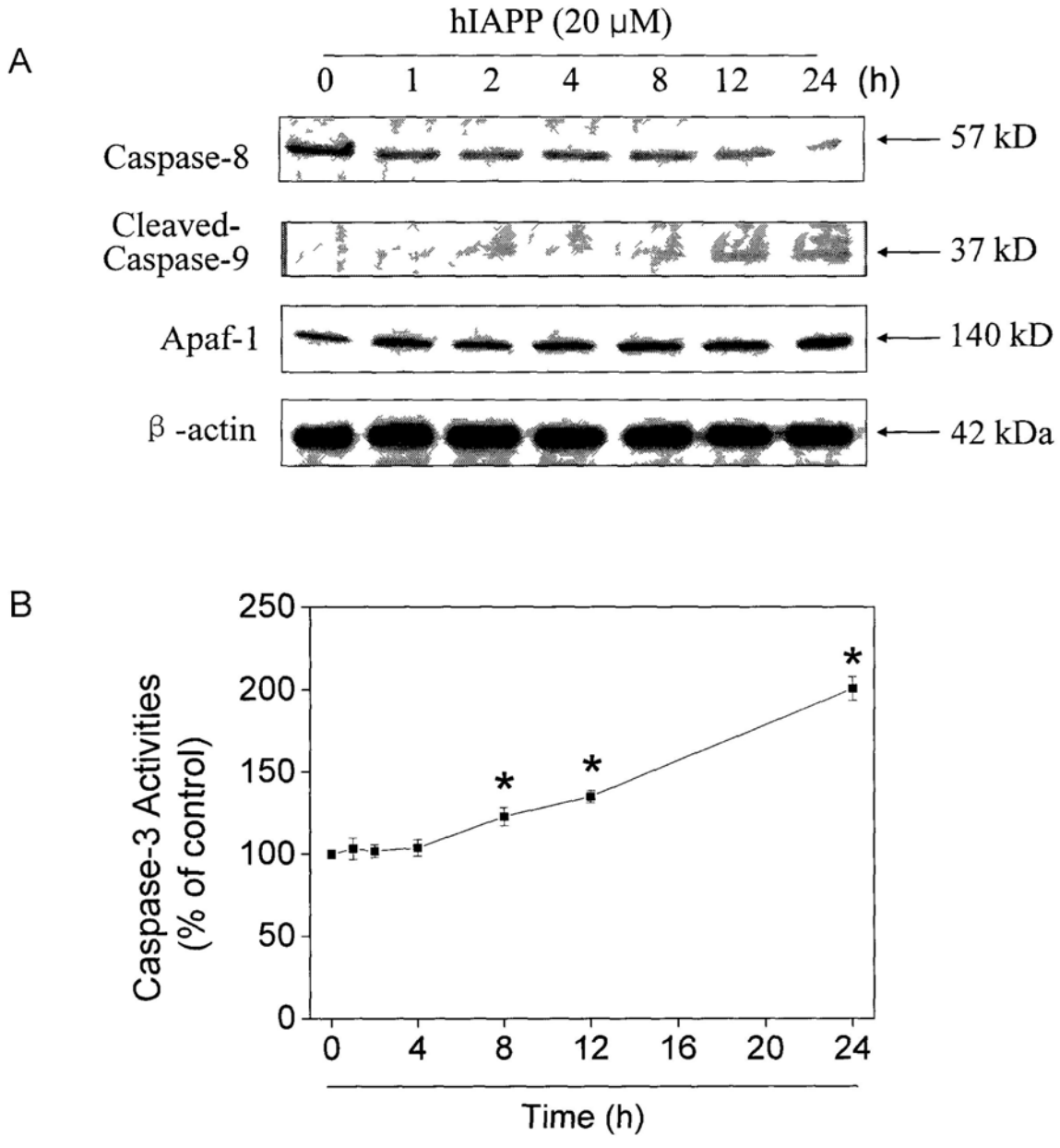

Fig. 3.20 Time-dependent effect of hIAPP on caspase processing in INS-1E cells. (A) Cells were treated with 20 μM hIAPP and harvested at the indicated time points. Cell lysates were subjected to Western blot analysis with specific antibodies. Protein levels of caspase-8, -9, and Apaf-1 were determined. Beta-actin was used as an internal control. (B) Cells were treated with 20 μM hIAPP and harvested at the indicated time points. Caspase activity was measured with whole cell extracts by a fluorometric method. Ac-DEVD-AMC was used as the substrate for caspase-3. Data are presented as means ± SD from three independent experiments, each performed in duplicate. Significant difference between the treatment and control groups was indicated by $P< 0.05$ (*).

A

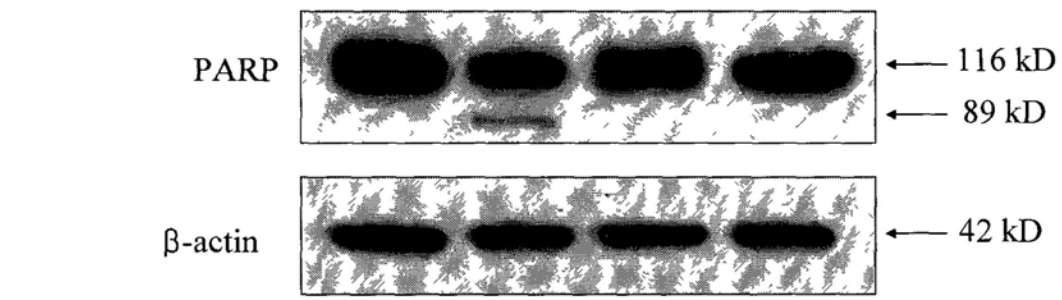
z-LEHD-fmk (40μM) - - + +
hIAPP (20μM) - + + -
PARP
116 kD
89 kD
β-actin
42 kD

B

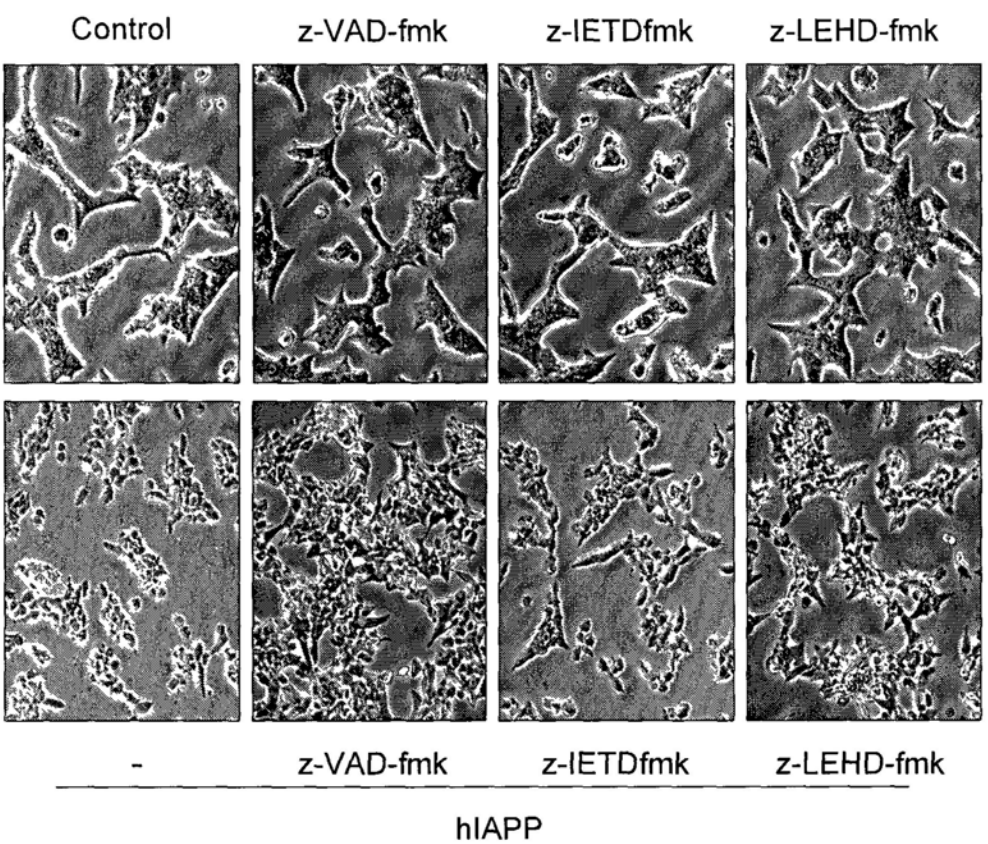
Control
z-VAD-fmk
z-IETDfmk
z-LEHD-fmk
-
z-VAD-fmk
z-IETDfmk
z-LEHD-fmk
hIAPP

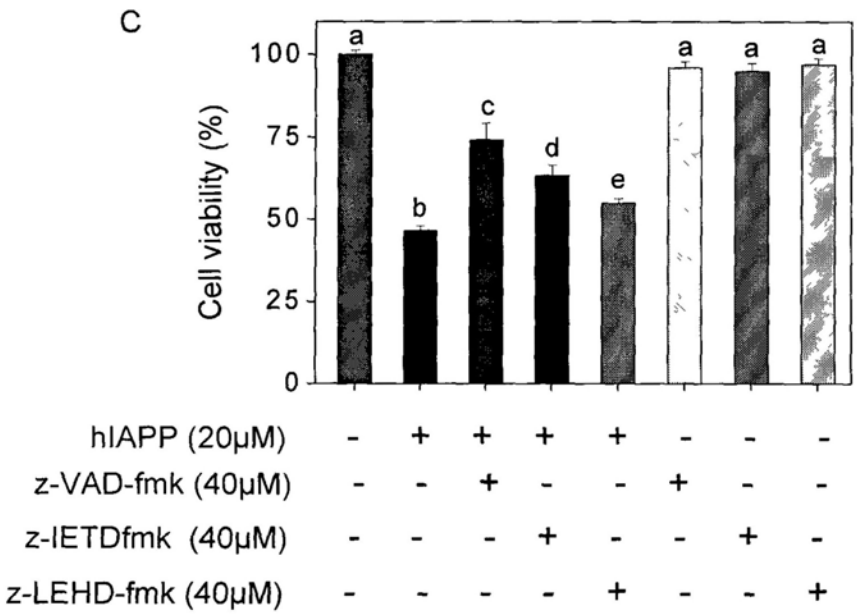

Fig. 3.21 Effect of caspase inhibitors on INS-1E cells subject to hIAPP exposure. (A) Effects of general caspase inhibitor on hIAPP-induced cleavage of PARP. The cells were pretreated with or without 40 μM of the general caspase inhibitor (z-VAD-fmk) for 1 h and then incubated in the presence or absence of 20 μM hIAPP for 24 h. Cell lysates were subjected to Western blot analysis. (B) Microscopic study of caspase inhibitors on INS-1E cells after hIAPP treatment. The cells were pretreated with or without specific inhibitors of caspase (general caspase inhibitor: 40 μM z-VAD-fmk, caspase-8 inhibitor: 40 μM z-IETDfmk, caspase-9 inhibitor: 40 μM z-LEHD-fmk) for 1 h and then incubated in the presence or absence of 20 μM hIAPP for 24 h. Morphology of treated cells was observed by phase-contrast microscopy (magnification, 100×). (C) Effects of caspase inhibitors on hIAPP-induced cytotoxicity. The cells were pretreated with or without specific inhibitors of caspase (general caspase inhibitor: 40 μM z-VAD-fmk, caspase-8 inhibitor: 40 μM z-IETDfmk, caspase-9 inhibitor: 40 μM z-LEHD-fmk) for 1 h and then incubated in the presence or absence of 20 μM hIAPP for 24 h. Cell viability was determined by MTT assay. All data are expressed as means ± SD of triplicates. Bars with different characters (a, b, c, d and e) indicate statistically different at $P<0.05$ level.

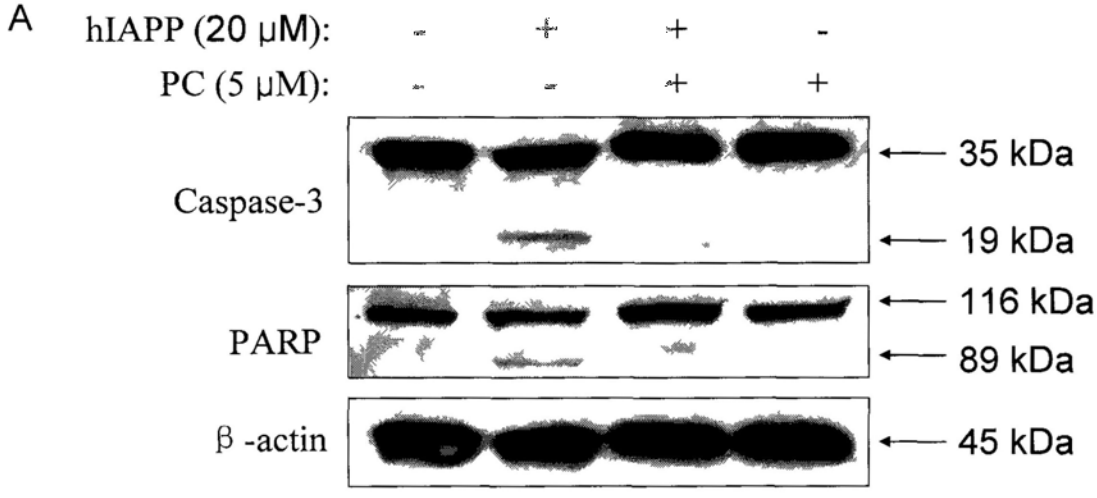
A
hIAPP (20 μM):
PC (5 μM):
Caspase-3
PARP
β -actin
35 kDa
19 kDa
116 kDa
89 kDa
45 kDa

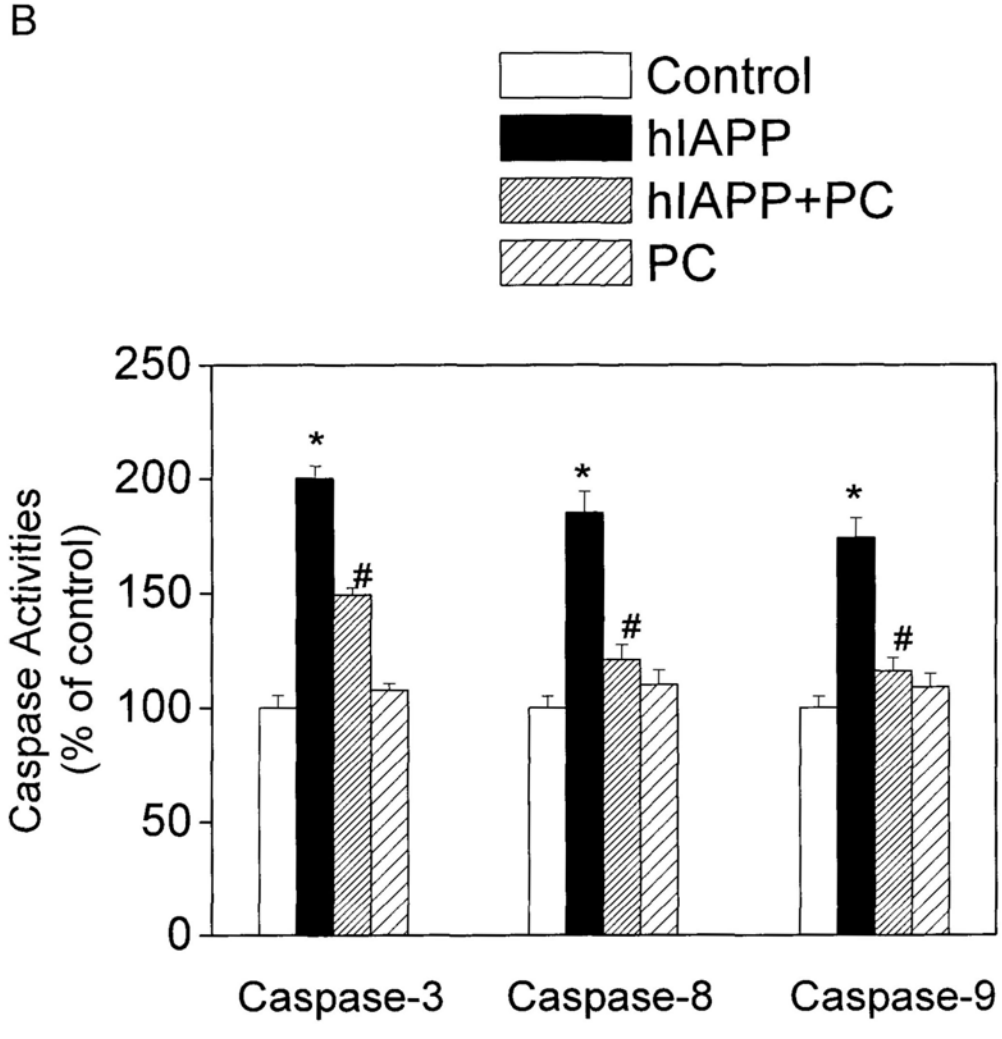
B
Control
hIAPP
hIAPP+PC
PC
Caspase Activities
(% of control)
250
200
150
100
50
0
*
#
Caspase-3
Caspase-8
Caspase-9

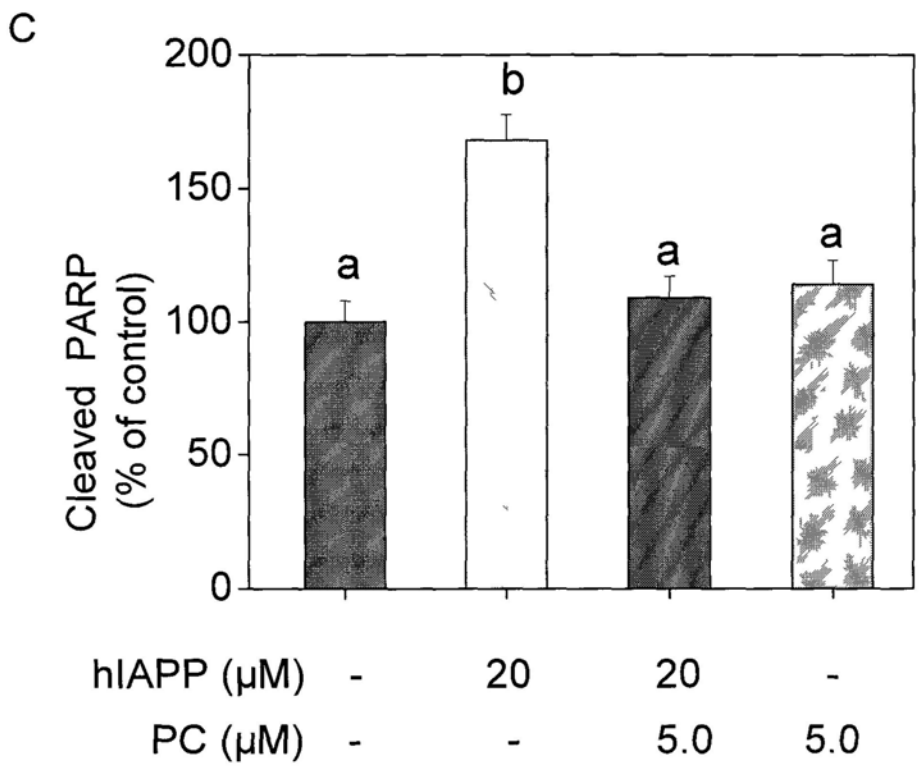

Fig. 3.22 PC suppressed hIAPP-induced activation of caspases and cleavage of PARP in INS-1E cells. (A) Representative immunoblots showing effects of PC on hIAPP-induced activation of caspases-3 and cleavage of PARP. Cells were pretreated with or without 5 μM PC for 2 h and then incubated with the presence or absence of 20 μM hIAPP for 24 h. Cell lysates were analyzed for protein levels of caspases-3 and PARP by Western blotting using specific antibodies. Beta-actin was used as an internal control. This experiment was repeated three times with similar results. (B) PC inhibited hIAPP-induced activation of caspases-3, -8 and 9. Cells were pretreated with or without 5 μM PC for 2 h and then incubated with the presence or absence of 20 μM hIAPP for 24 h. Caspase activity was measured with whole cell extracts by a fluorometric method. All data were obtained from three independent experiments and presented as the means ± SD. $*P < 0.05$ vs untreated controls. $\#P < 0.05$ vs cells treated with hIAPP. (C) PC prevented hIAPP-induced cleavage of PARP. The cells were pretreated with or without 5 μM PC for 2 h and then incubated in the presence or absence of 20 μM hIAPP for 24 h. The content of cleaved PARP in INS-1E cells was measured by a sandwich ELISA kit. All data were obtained from three independent experiments and presented as the means ± SD. Bars with different characters (a and b) indicate statistically different at $P < 0.05$ level.

3.9 Intracelluar ATP levels

Mitochondria are important for maintaining cell life by providing metabolic energy in the form of ATP. ATP depletion is regarded as an important characteristic of mitochondrial damage (Kroemer and Reed, 2000). Thus, I evaluated the effect of hIAPP on the ATP levels in INS-1E cells.

After 24-h treatment, hIAPP reduced intracellular ATP content in a dose-dependent manner in INS-1E cells (**Fig. 3.23A**), which indicated that the metabolic and energetic state of these cells was changed by hIAPP treatment. hIAPP at the concentration of 20 μM significantly decreased intracellular ATP levels to about 36 % of the untreated control level. However, PC was able to prevent hIAPP-induced depletion of intracellular ATP in INS-1E in a dose-dependent manner (**Fig. 3.23B**). At the concentration of 1.25, 2.5 and 5 μM, PC increased ATP levels to 45 %, 74 % and 82 %, respectively.

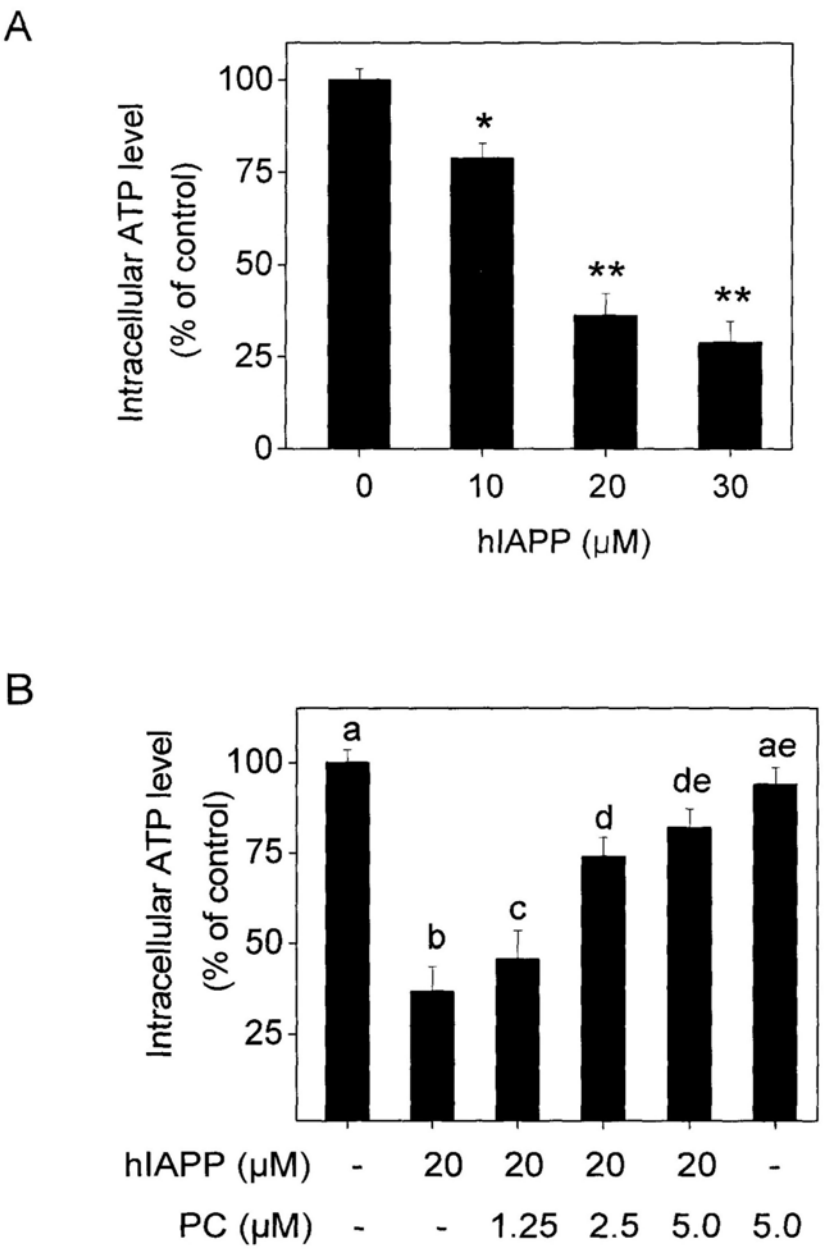

Fig. 3.23 Evaluation of intracellular ATP levels in INS-1E cells. (A) Intracellular ATP levels were depleted in INS-1E cells after hIAPP treatment. Cells were incubated with hIAPP (0, 10, 20 or 30 μM) for 24 h. The ATP content was examined using a bioluminescence somatic cell assay kit. All data are expressed as means ± SD from three independent experiments, each performed in duplicate. $*P < 0.05$, $**P < 0.01$ vs untreated controls. (B) PC prevented hIAPP-induced depletion of ATP. Cells were pretreated with or without PC (1.25-5 μM) for 2 h and then cultured in the presence or absence of 20 μM hIAPP for 24 h. All data are expressed as means ± SD from three independent experiments, each performed in duplicate. Bars with different characters (a, b, c, d and e) indicate statistically different at $P < 0.05$ level.

3.10 Mitochondrial mass

We further analyzed alterations in mitochondrial abundance in INS-1E cells after exposure to hIAPP. INS-1E cells were pretreated with PC and then incubated with hIAPP for 24 h. The treated cells were stained with MitoTracker Green FM, a mitochondrial specific fluorescent dye, and the mitochondrial mass was determined by flow cytometry analysis. It was found that hIAPP-induced mitochondrial mass reduction was dose-dependent (**Fig. 3.24A** and **Fig. 3.24B**). After incubation with 20 μM hIAPP for 24 h, the mitochondrial mass was decreased from 139 % to 113 %. However, at the concentration of 5 μM, PC was able to increase the mitochondrial mass from 113 % to 130 %.

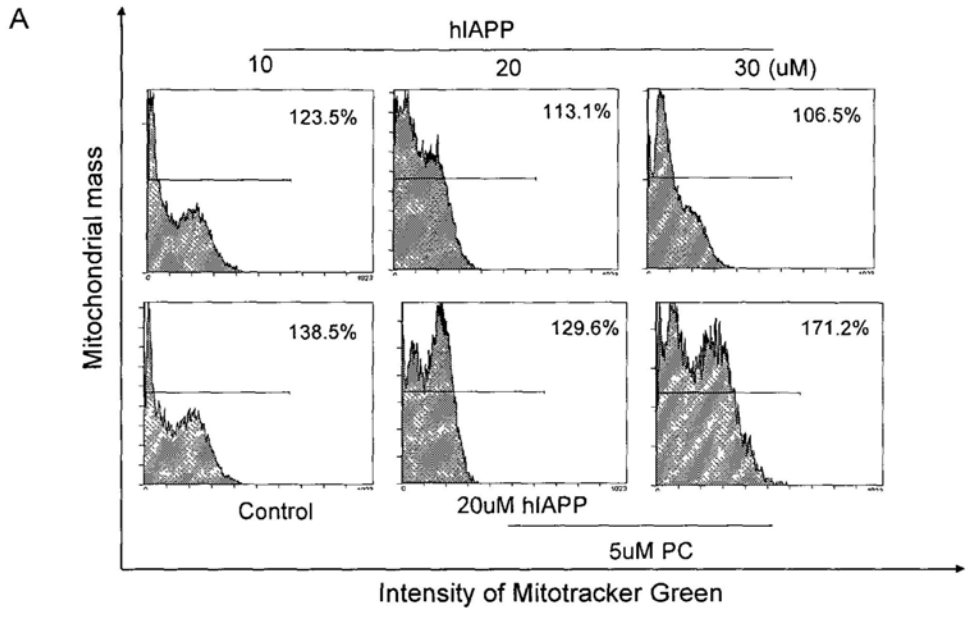

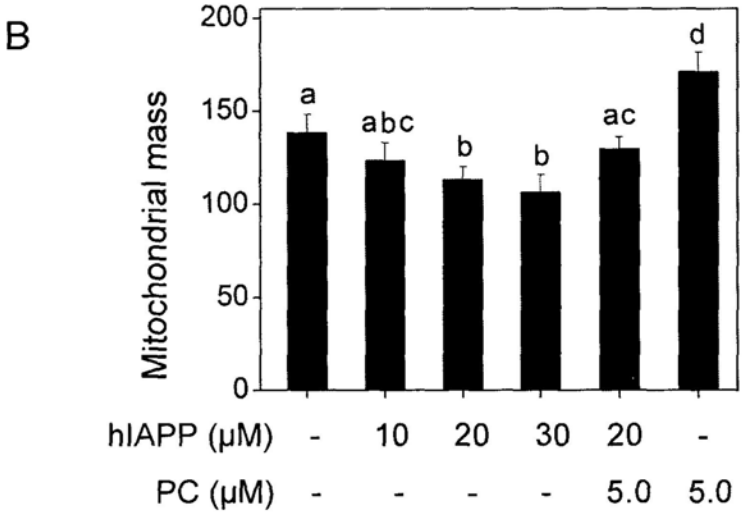

Fig. 3.24 Effect of PC on mitochondrial mass in INS-1 E cells subject to hIAPP exposure. (A) PC prevented hIAPP-induced mitochondrial mass reduction in INS-1 E cells. Cells were pretreated with or without 5 μM PC for 2 h and then cultured in the presence or absence of hIAPP at the indicated concentration for 24 h. mitochondrial mass was determined with fluorescent dye Mitotracker Green FM by flow cytometric analysis. (B) Numerical data showing the effect of PC hIAPP-induced mitochondrial mass reduction. Cells were pretreated with or without 5 μM PC for 2 h and then cultured in the presence or absence of hIAPP at the indicated concentration for 24 h. All data are expressed as means ± SD in triplicates. Bars with different characters (a, b, c and d) indicate statistically different at $P<0.05$ level.

3.11 Changes of mitochondrial morphology

To examine the mitochondrial morphology of INS-1E cells after hIAPP treatment, the cells were stained with MitoTracker Red CMXRos and DAPI, and then examined by differential internal reflection fluorescence microscopy for a time-course analysis.

As shown in **Fig. 3.25A**, in control cells, mitochondria appeared interconnected in a filamentous network and were abundant throughout the cytoplasm. In most of the viable cells, the nucleus was ovum-shaped. Within 4 h of hIAPP treatment, the cells displayed morphological landmarks of apoptosis-associated mitochondrial fragmentation with perinuclear redistribution of mitochondria. After incubation with hIAPP for 24 h, mitochondria became fragmented and scarce and the nucleus was condensed in INS-1E cells.

INS-1E cells were pretreated with PC and then incubated with hIAPP. As shown in **Fig. 3.25B**, PC prevented hIAPP-induced changes in mitochondrial morphology after treatment for 4 h. The protective effect of PC was obvious even at the 24 h time point.

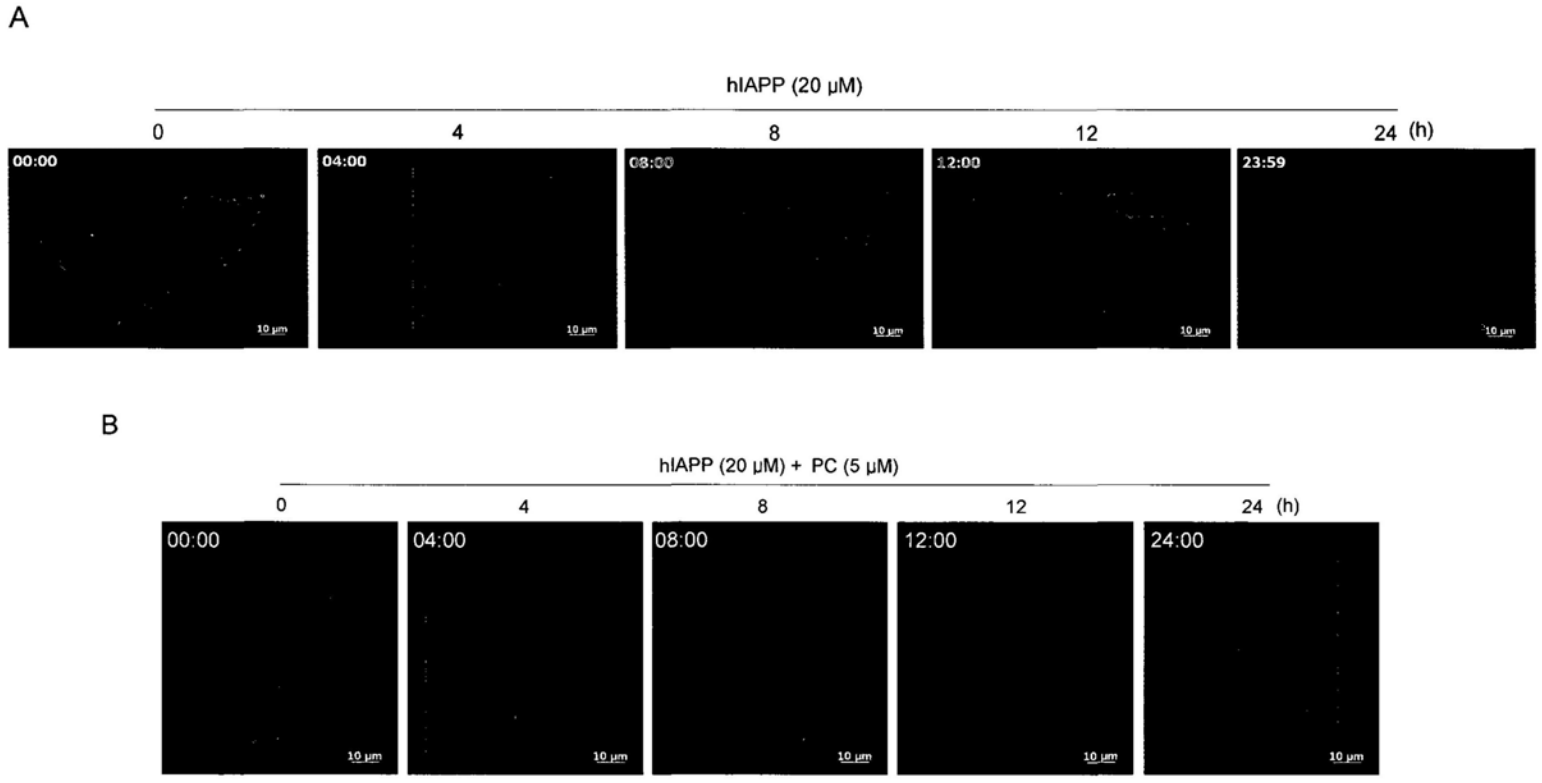

Fig. 3.25 Time-lapse living cell microscopy of INS-1E cells. (A) Real-time imaging of the same cells subject to hIAPP exposure. Cells were incubated with 20 μM hIAPP for the indicated time points. (B) Real-time imaging of the same cells treated with hIAPP in the presence of PC. Cells were pretreated with 5 μM PC for 2 h and then incubated with 20 μM hIAPP for the indicated time points. Cell morphology was captured by differential internal reflection fluorescence microscopy (red: mitochondria; blue: nucleuses). Scale bar: 10 mm. The images shown here are representative of three independent experiments with similar results.

3.12 Mitochondria membrane potential

Mitochondria act as a point of integration for apoptotic signals originating from both the extrinsic and intrinsic apoptosis pathways. Depletion of mitochondrial membrane potential ($\Delta\Psi m$) is associated with activation of caspases and initiation of apoptotic cascades (Kroemer and Reed, 2000).

I examined the status of mitochondria in INS-1E cells exposed to hIAPP using JC-1 flow cytometric analysis. As shown in **Fig. 3.26A** and **Fig. 3.26B**, after 24 h treatment, hIAPP induced a dose-dependent increase in depletion of $\Delta\Psi m$ in INS-1E cells, as evidenced by the shift of fluorescence from red to green. The depletion of $\Delta\Psi m$ was further confirmed by time-course analysis (**Fig. 3.27A** and **Fig. 3.27B**). Loss of $\Delta\Psi m$ occurred significantly as early as 2 h after hIAPP treatment, and continued to decline with prolonged hIAPP treatment. On the other hand, the administration of PC significantly prevented this depolarization of $\Delta\Psi m$ in a dose-dependent manner (**Fig. 3.28A** and **Fig. 3.28B**). For instance, the percentage of INS-1E cells with depolarized mitochondria was 46.25 % after exposure to 20 μM of hIAPP for 24 h. At concentrations of 2.5 and 5 μM, PC reduced the values to 18.33 % and 11.91 %, respectively.

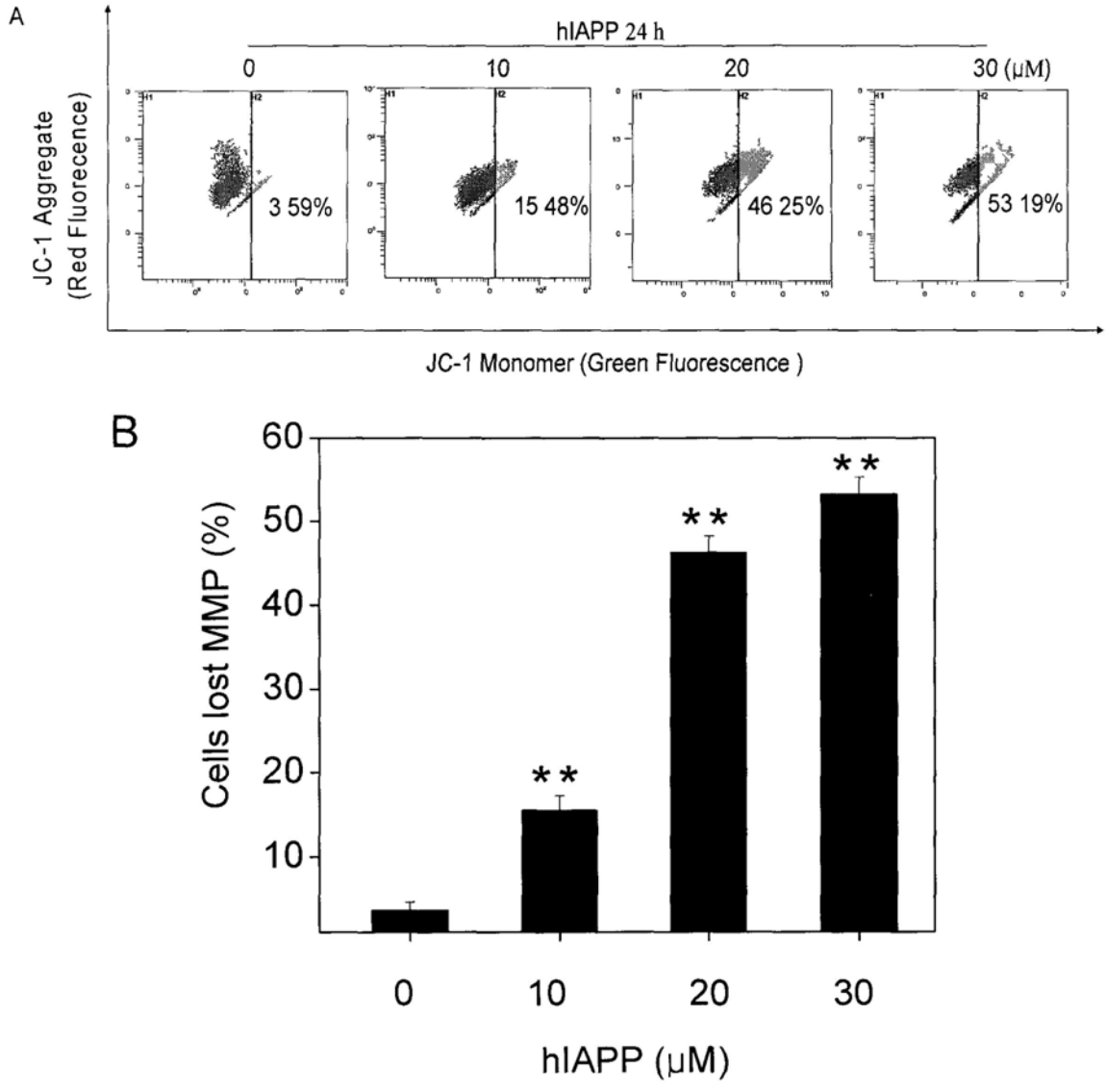

Fig. 3.26 (A) Representative histograms showing the dose-dependent effect of hIAPP on mitochondrial membrane potential ($\Delta\Psi m$) in INS-1E cells. Cells were incubated with hIAPP (0, 10, 20 or 30 μM) for 24 h. The treated cells were stained with the JC-1 dye and subjected to flow cytometric analysis. The number in the right region of each dot plot represents the percentage of cells that emit green fluorescence due to the depletion of $\Delta\Psi m$. (B) Numeric data showing dose-dependent effect of hIAPP on $\Delta\Psi m$ in INS-1E cells. Cells were incubated with hIAPP (0, 10, 20 or 30 μM) for 24 h. The treated cells were stained with the JC-1 dye and subjected to flow cytometric analysis. All data are expressed as means ± SD from three independent experiments, each performed in duplicate. $^{**}P < 0.01$ vs untreated controls.

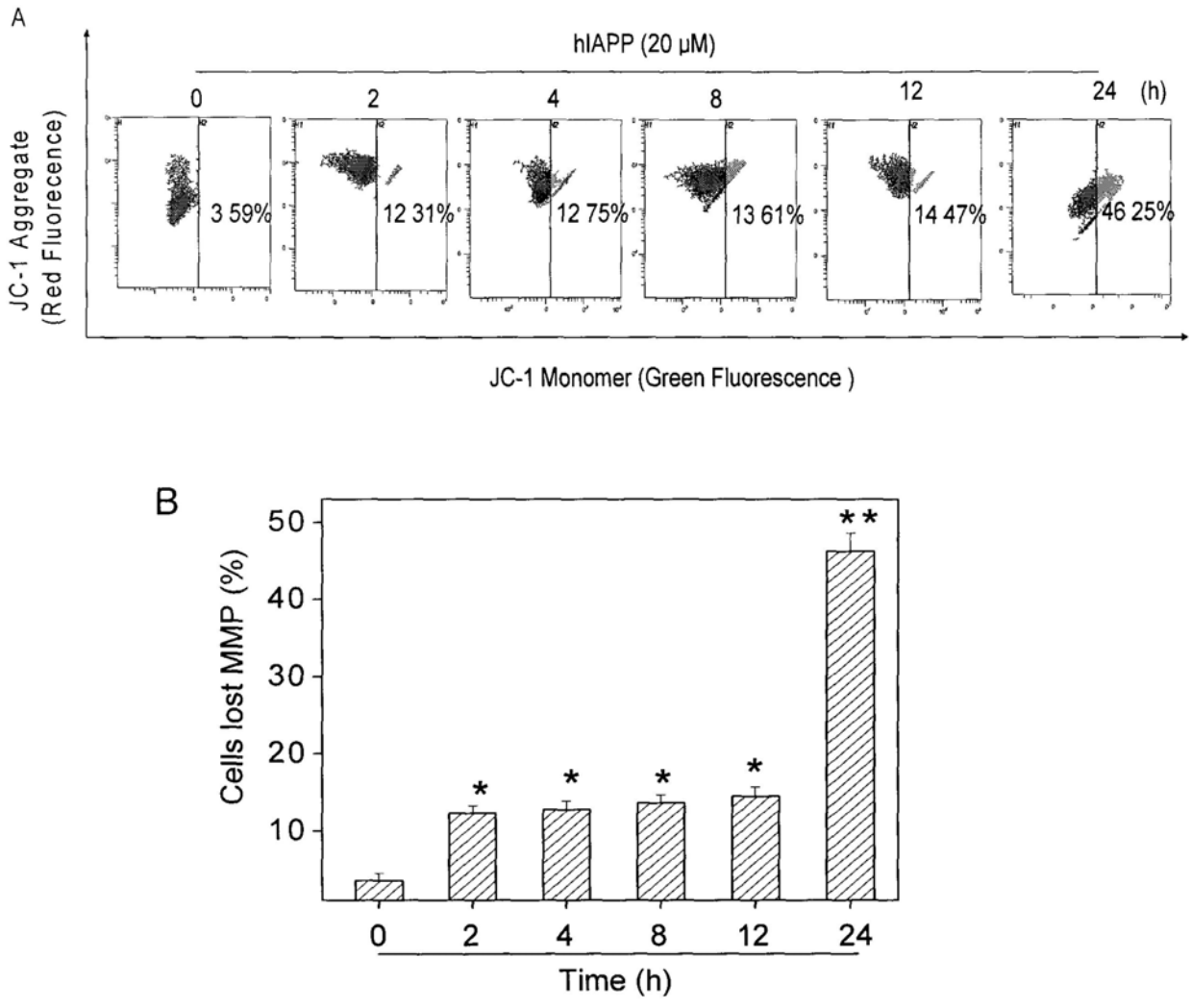

Fig. 3.27 (A) Representative histograms showing the time-dependent effect of hIAPP on mitochondrial membrane potential ($\Delta\Psi m$) in INS-1E cells. Cells were incubated with 20 μM hIAPP for the indicated time points. The treated cells were stained with the JC-1 dye and subjected to flow cytometric analysis. The number in the right region of each dot plot represents the percentage of cells that emit green fluorescence due to the depletion of $\Delta\Psi m$. (B) Numeric data showing the time-dependent effect of hIAPP on $\Delta\Psi m$ in INS-1E cells. Cells were incubated with 20 μM hIAPP for the indicated time points. The treated cells were stained with the JC-1 dye and subjected to flow cytometric analysis. All data are expressed as means ± SD of from three independent experiments, each performed in duplicate. $^{*}P < 0.05$, $^{**}P < 0.01$ vs untreated controls.

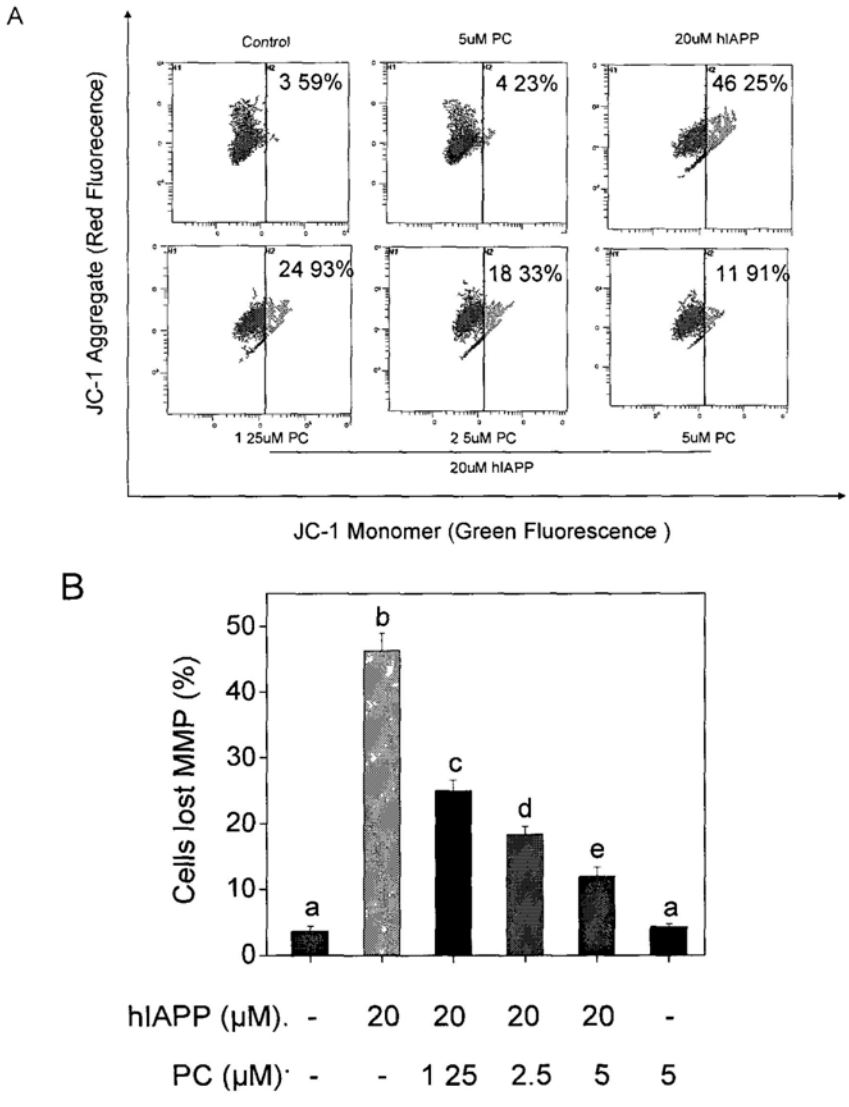

Fig. 3.28 (A) Representative histograms showing the effect of PC on mitochondrial membrane potential (ΔΨm) in INS-1E cells subject to hIAPP exposure. Cells were pretreated with or without PC (1.25-5 μM) for 2 h and then cultured in the presence or absence of 20 μM hIAPP for 24 h. The treated cells were stained with the JC-1 dye and subjected to flow cytometric analysis. The number in the right region of each dot plot represents the percentage of cells that emit green fluorescence due to the depletion of ΔΨm. (B) Numeric data showing effect of PC on mitochondrial membrane potential (ΔΨm) in INS-1E cells subject to hIAPP exposure. Cells were pretreated with or without PC (1.25-5 μM) for 2 h and then cultured in the presence or absence of 20 μM hIAPP for 24 h. The treated cells were stained with the JC-1 dye and subjected to flow cytometric analysis. All data are expressed as means ± SD from three independent experiments, each performed in duplicate. Bars with different characters (a, b, c, d and e) indicate statistically different at $P < 0.05$ level.

3.13 Release of mitochondrial apoptogenic factors

When mitochondrial-membrane integrity is compromised, the mitochondrial apoptogenic factors such as cytochrome c and AIF may be released into the cytosol. To investigate whether the mitochondrial release of cytochrome c and AIF was involved in the apoptotic process induced by hIAPP, mitochondrial and cytosolic fractions were prepared from INS-1E cells after 24-h treatment with hIAPP. The cytosolic and mitochondrial fractions were obtained by fractionating the cell lysate through specific lysis, mechanical disruption of cells and differential centrifugation. Specific antibody against cytochrome c and AIF was used to detect the relative amount of cytochrome c in both fractions. The results of Western blot analysis revealed that the levels of Cytochrome c and AIF in the cytosolic fraction were increased significantly upon hIAPP treatment (**Fig. 3.29A**), indicating that hIAPP treatment promoted the release of cytochrome c and AIF from the mitochondria to the cytosol.

INS-1E cells were pretreated with PC and then incubated with hIAPP for 24 h. Interestingly, hIAPP-induced release of cytochrome c and AIF was blocked by PC treatment (**Fig. 3.29B**). These results suggested that PC exerted protective effects against hIAPP-induced apoptosis by inhibiting release of apoptogenic factors.

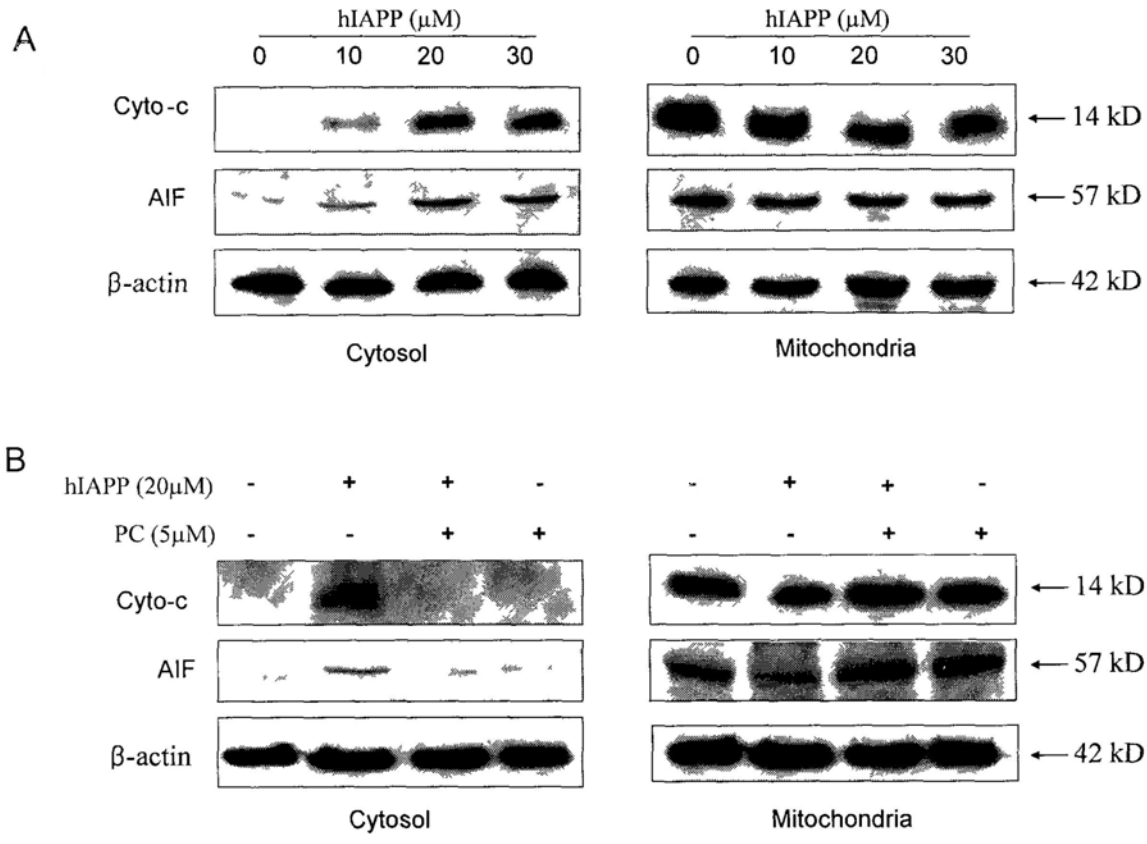

Fig. 3.29 Immunoblots showing the expression of cytochrome c (Cyto-c) and apoptosis inducing factor (AIF) in INS-1E cells. (A) hIAPP induced release of Cyto-c and AIF from mitochondria into cytosol. Cells were incubated with hIAPP (0, 10, 20 or 30 μM) for 24 h. The treated cells were separated into cytosolic and mitochondrial fractions. Cell lysates were subjected to Western blot analysis. (B) PC inhibited hIAPP-induced release of Cyto-c and AIF from mitochondria into cytosol. Cells were pretreated with or without 5 μM PC for 2 h and then cultured in the presence or absence of 20 μM hIAPP for 24 h. The treated cells were separated into cytosolic and mitochondrial fractions. Cell lysates were analyzed for protein levels of Cyto-c and AIF by Western blot analysis. Beta-actin was used as an internal control. This experiment was repeated three times with similar results.

3.14 Role of MPT pores

Collapse of $\Delta\Psi m$ is thought to result from opening of MPT pore during the initiation phase of apoptosis. Our results indicated that hIAPP induced loss of $\Delta\Psi m$ in INS-1E cells and this prompts us to explore the possible involvement of MPT pores in the action of hIAPP.

In this study, MPT pore opening was measured by loss of mitochondrial calcein-AM fluorescence. **Fig. 3.30A** showed that mitochondrial calcein-AM fluorescence remained unchanged after 24-h hIAPP treatment, which indicated that hIAPP had no effect on MPT pores in INS-1E cells. To further identify whether apoptosis triggered by hIAPP was associated with the opening the MPT pore, the effects of cyclosporin A (CsA), a well known inhibitor of MPT pore, on hIAPP-induced apoptosis was examined. After 24 h treatment, it was found that CsA failed to prevent the loss of $\Delta\Psi m$ (**Fig. 3.30B**), release of cytochrome c and AIF (**Fig. 3.30C**), and activation of caspase-3 (**Fig. 3.30D**) induced by hIAPP. These results indicated that hIAPP-induced apoptotic cell death and the release of these apoptogenic factors were mediated through mechanisms independent of MPT pore.

A

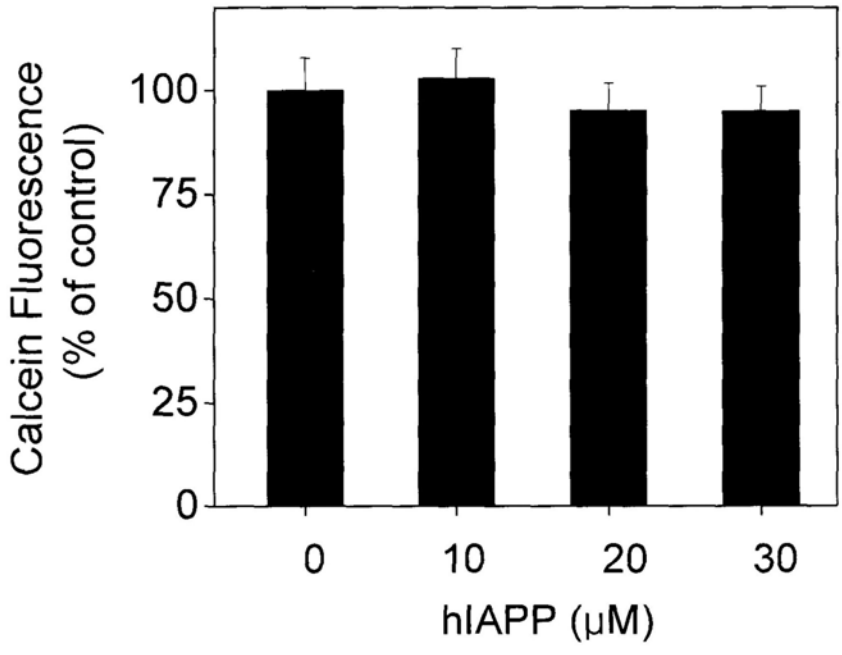
Calcein Fluorescence
(% of control)
100
75
50
25
0
0
10
20
30
hIAPP (μM)

B

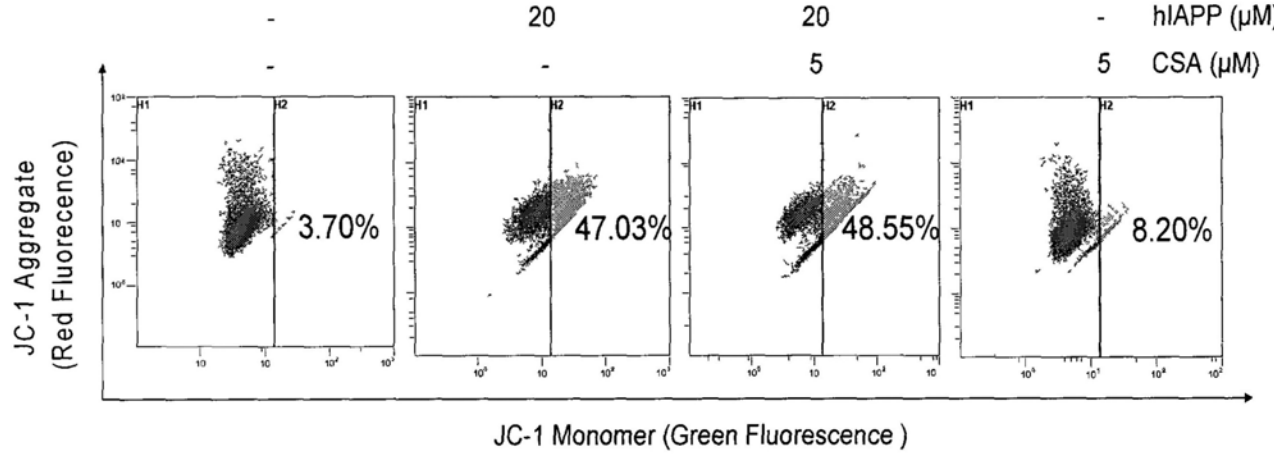
- 20 20 - hIAPP (μM)
- - 5 5 CSA (μM)
3.70%
47.03%
48.55%
8.20%
JC-1 Aggregate
(Red Fluorecence)
JC-1 Monomer (Green Fluorescence)

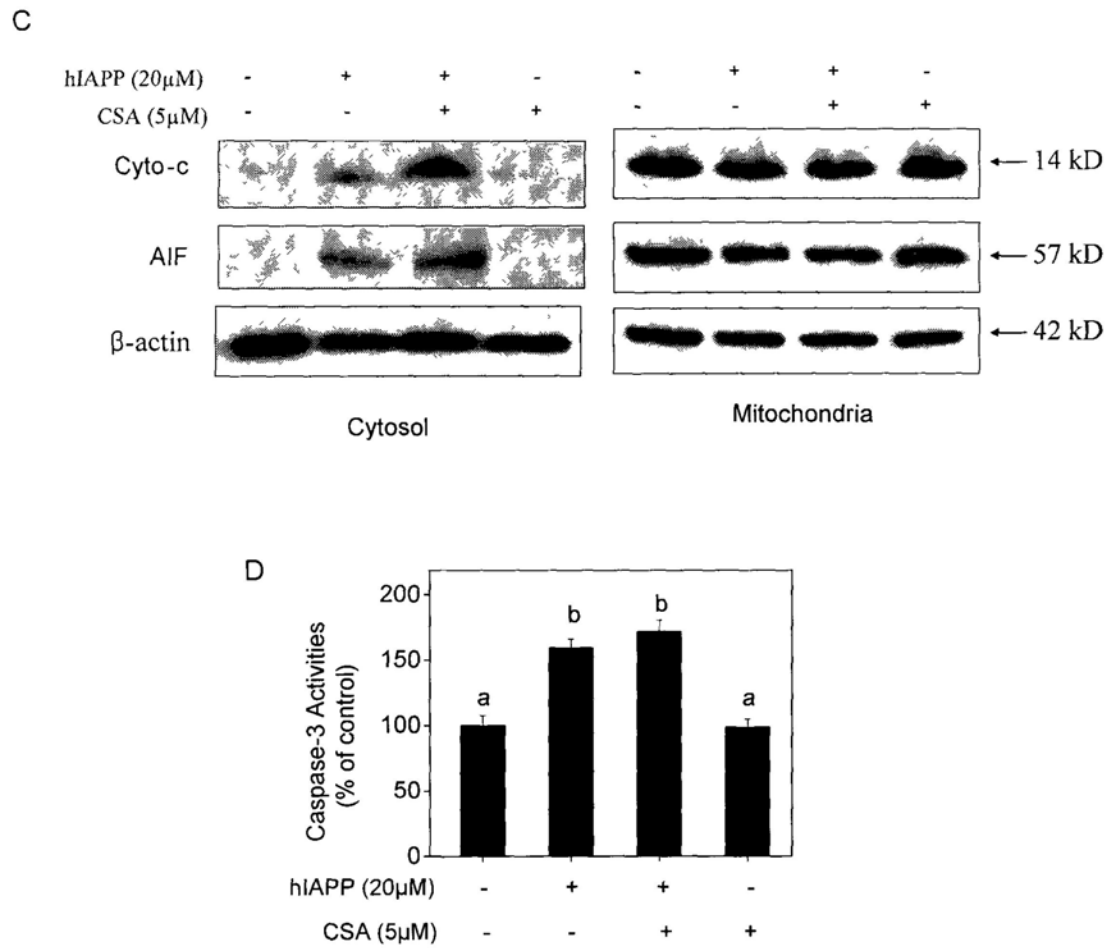

Fig. 3.30 The role of mitochondrial permeability transition (MPT) pore in hIAPP-induced apoptosis in INS-1E cells. (A) Effects of hIAPP on MPT pore of INS-1E cells. Cells were incubated with hIAPP (0, 10, 20 or 30 μM) for 24 h. The opening of MPT pores was examined using the MitoProbe™ Transition Pore Assay Kit. The effects of MPT pore inhibitor Cyclosporin A (CsA) on the mitochondrial membrane potential depletion (B), Cyto-c and AIF release (C), and caspase-3 activation (D) induced by hIAPP. The cells were pretreated with or without 5 μM CsA for 1 h and then incubated in the presence or absence of 20 μM hIAPP for 24 h. The treated cells were subjected to detection of mitochondrial membrane potential, Cyto-c and AIF release, and caspase-3 activity. Values expressed are means ± SD in triplicates. All data represent similar results from three independent experiments. Bars with different characters (a and b) indicate statistically different at $P < 0.05$ level.

3.15 Involvement of Bcl-2 family member expression

Bcl-2 family members are central mediators of the mitochondrial apoptotic pathway, comprising of both anti-apoptotic and pro-apoptotic proteins. The balance between these proteins is important for maintaining the integrity of mitochondrial membrane and regulating release of mitochondrial apoptogenic factors (Green and Kroemer, 2004). In my previous experiments, I demonstrated depletion of $\Delta\Psi m$, and release of cytochrome c and AIF from mitochondria in INS-1E cells treated with hIAPP. Thus, I went on to study the expression of Bcl-2 family proteins under hIAPP treatment by Western blot analysis.

As shown in **Fig. 3.31**, hIAPP treatment decreased the expression of pro-survival Bcl-2 family proteins, such as Bcl-2 and Mcl-1, and moderately increased the expression of pro-apoptosis Bcl-2 family proteins, such as Bax, Bad and PUMA. At the same time, hIAPP treatment did not affect the expression levels of Bcl-xl. The effects of hIAPP treatment on the expression levels of Bcl-2 family proteins were further confirmed by the time-course analysis (**Fig. 3.32**). The expression of Bax and Bad protein were detected as early as 1 h after hIAPP treatment. The levels of Bcl-2 and tBid expression were decreased after 24-h treatment with hIAPP.

Participation of mitochondria in the apoptotic process induced by hIAPP was further demonstrated by the cleavage of Bid protein. Bid, a BH3-only member, serves the unique function of interconnecting the extrinsic death receptors to the mitochondrial amplification loop of the intrinsic pathway (Zha et al., 2000). It is

generally accepted that activation of caspase-8/10 leads to cleavage of Bid, which will cooperate with Bax to trigger the release of cytochrome c, and thereby induce downstream mitochondria-mediated apoptotic events (Kluck et al., 1999). As shown in **Fig. 3.33**, pretreatment of the cells with z-IETD-FMK (caspase 8 inhibitor) and z-VADFMK (pan-caspase inhibitor) partially attenuated cleavage of Bid (tBid) induced by hIAPP, suggesting that cleavage of Bid was due to activation of caspase-8. These data indicated that the Bid-mediated crosstalk between extrinsic and intrinsic pathway was involved in the apoptosis induced by hIAPP in INS-1E cells, and the cleavage of Bid by hIAPP may contribute to release of cytochrome c.

To further examine the molecular mechanisms of protection of PC, we examined the effects of PC on the expression of Bcl-2 family proteins in the hIAPP-treated cells. Based on the results of western blotting, PC effectively prevented hIAPP-induced decreased expression of Bcl-2 protein. The up-regulation of Bax and Bad protein expression in hIAPP-treated INS-1E cells was also restored by co-treatment with PC (**Fig. 3.34**).

3.16 Formation of hIAPP oligomer

In order to test the ability of PC to inhibit the oligomerization of synthesized hIAPP, Dot blot analysis was performed using the anti-oligomer antibody to detect the oligomer formation. 20μM hIAPP or 20μM rIAPP was incubated with or without PC (1.25-5 μM) for 24 h before oligomer dection. As shown in **Fig. 3.35**, the amount of hIAPP oligomer in the sample with hIAPP was greater than that with hIAPP plus PC. I used rIAPP as a negative control and found that the amount of hIAPP oligomer in

the sample with rIAPP was smaller than the one with hIAPP. Although there are some detectable oligomer in rIAPP sample, which may in part be due to reaction background of enhanced chemiluminescence reagent in the process of this assay. Compared with the sample with hIAPP, the amount of hIAPP oligomer in the sample with PC was also smaller. These data suggested that PC was able to partly inhibit formation of hIAPP oligomer.

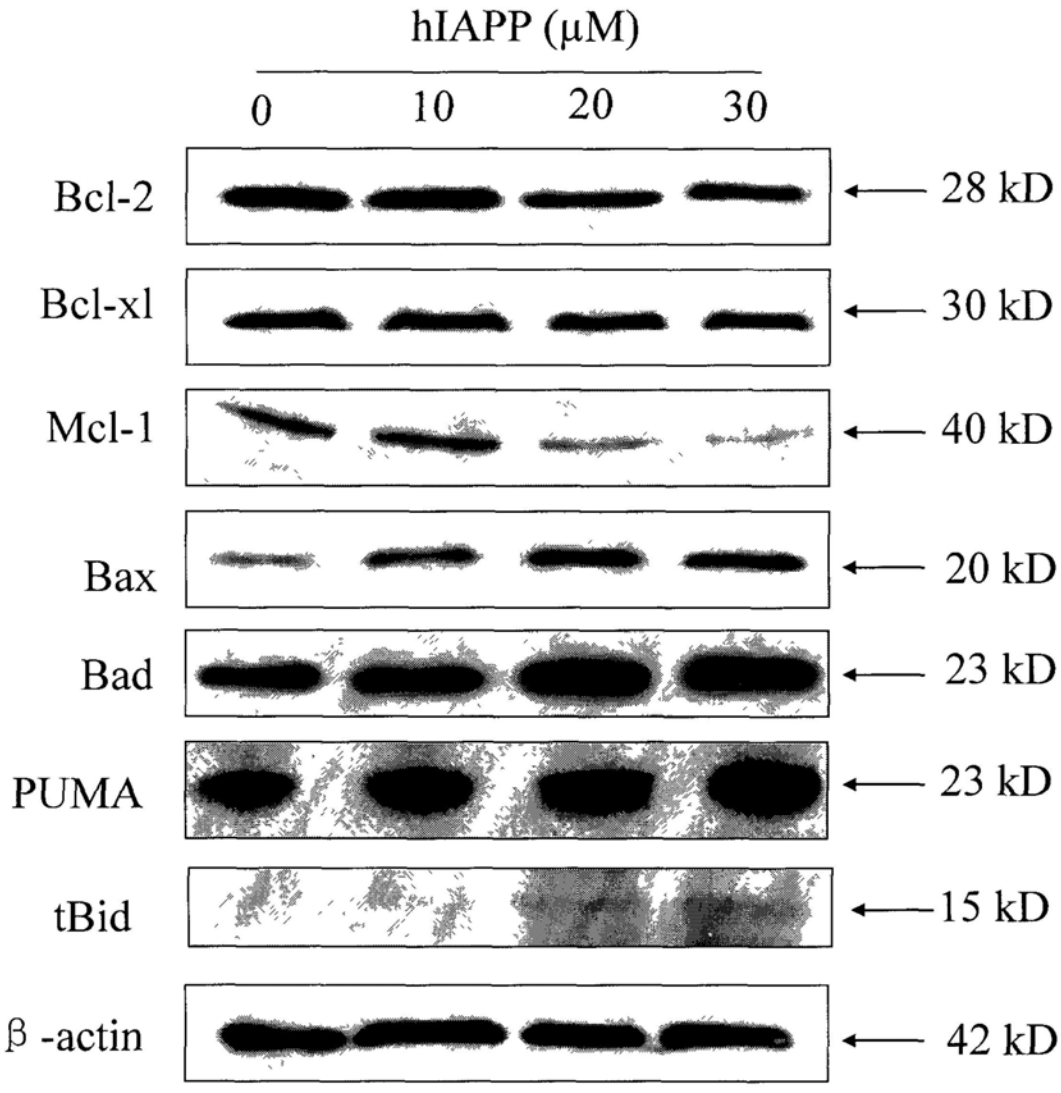

Fig. 3.31 Representative immunoblots showing the dose-dependent effect of hIAPP on Bcl-2 family members expression in INS-1E cells. Cells were incubated with hIAPP (0, 10, 20 or 30 μM) for 24 h. Cell lysates were subjected to Western blot analysis with specific antibodies. Protein levels of Bcl-2, Bcl-xl, Mcl-1, Bax, Bad, PUMA and tBid were determined. Beta-actin was measured as internal control to normalize expression of other proteins. This experiment was repeated three times with similar results.

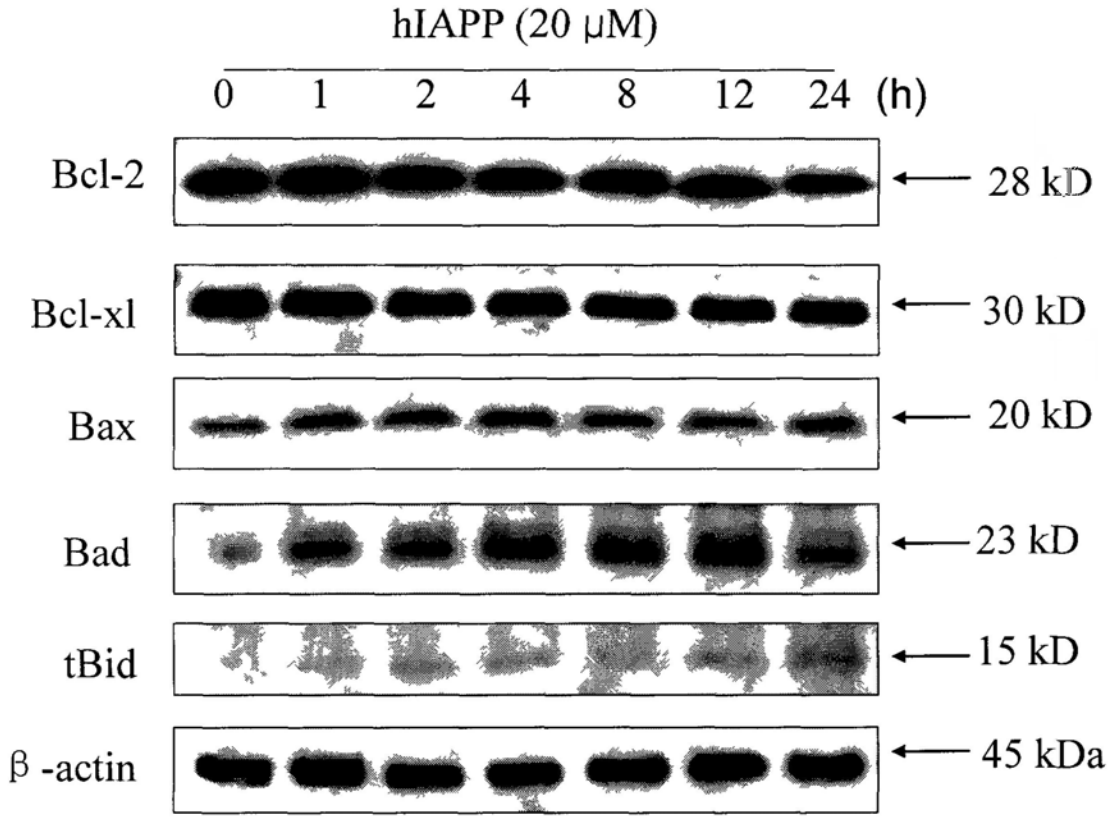

Fig. 3.32 Representative immunoblots showing the time-dependent effect of hIAPP on Bcl-2 family members expression in INS-1E cells. Cells were incubated with 20 μM hIAPP and harvested at various times. Cell lysates were subjected to Western blot analysis with specific antibodies. Protein levels of Bcl-2, Bcl-xl, Bax, Bad, and tBid were determined. Beta-actin was measured as internal control to normalize expression of other proteins. Data represent similar results from three independent experiments.

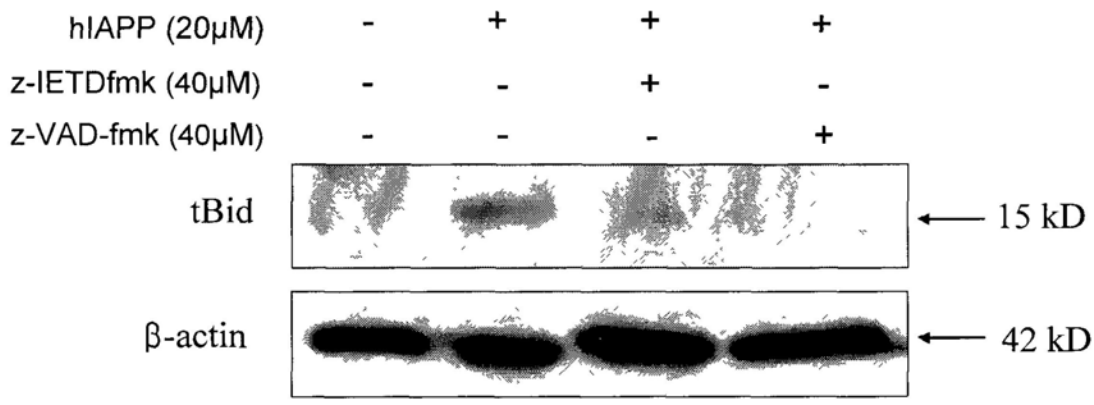

Fig. 3.33 Representative immunoblots showing effects of caspase inhibitors on the processing of Bid induced by hIAPP. Cells were pre-treated with or without 40 μM z-IETDfmk (caspase-8 inhibitor) and 40 μM z-VAD-fmk (general caspase inhibitor) for 1 h, and then incubated with the presence or absence of 20 μM hIAPP for 24 h. Cell lysates were analyzed for protein levels of tBid by Western blot analysis using specific antibodies. Beta-actin was measured as internal control to normalize expression of other proteins. Data represent similar results from three independent experiments.

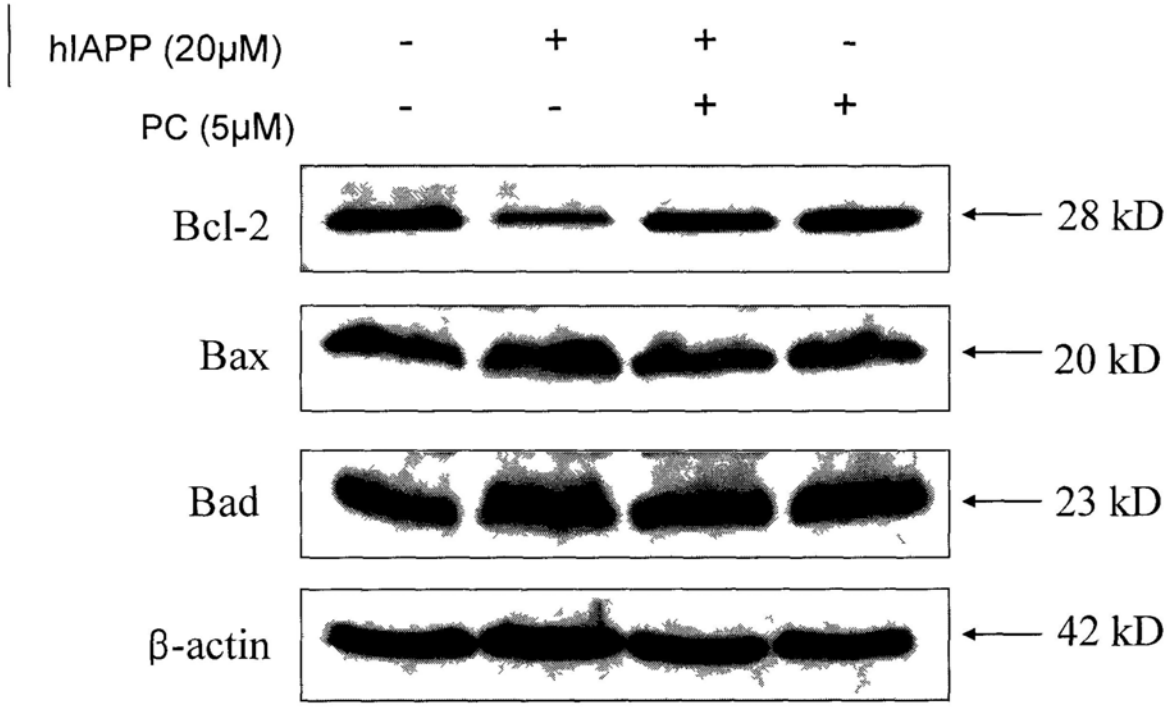

Fig. 3.34 PC prevented hIAPP-induced changes of expression of Bcl-2 family proteins in INS-1E cells by Western blot analysis. Cells were pretreated with or without 5 μM PC for 2 h and then incubated with the presence or absence of 20 μM hIAPP for 24 h. Cell lysates were analyzed for protein levels of Bcl-2, Bcl, Bax and Bad by Western blot analysis using specific antibodies. Beta-actin was measured as internal control to normalize expression of other proteins Data represent similar results from three independent experiments.

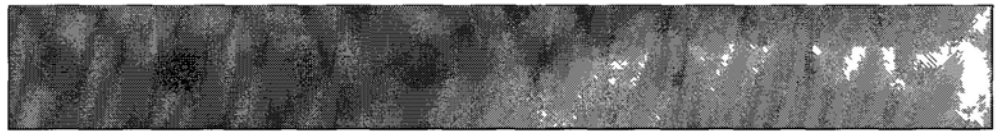

rIAPP (μM)	20	-	-	-	-	-	-	-
hIAPP (μM)	-	20	20	20	20	-	-	-
PC (μM)	-	-	1 25	2.5	5	1.25	2 5	5

Fig. 3.35 PC prevented oligomer formation induced by hIAPP in vitro. 20μM human or rat amylin was incubated with or without PC (1.25-5 μM) at 37 °C for 24 h. Dot blot analysis was applied using the anti-oligomer antibody to detect the oligomer formation after incubation. Data represent similar results from three independent experiments.

Chapter 4: Discussion

In this thesis, I demonstrated for the first time that mitochondria participated in the apoptosis induced by hIAPP in INS-1E pancreatic beta cells. Our results showed that hIAPP induced INS-1E cells apoptosis with involvement of oxidative stress, mitochondrial dysfunction and activation of JNK and p38, which was markedly attenuated by co-administration of PC, a natural product from blue-green algae that is widely used as food supplement.

4.1 Cytotoxic effect of hIAPP on beta cells

In *in vitro* and *in vivo* experiments, hIAPP tends to self-assemble to form beta-sheet-containing aggregates that are cytotoxic to pancreatic beta cells (Haataja et al., 2008; Lorenzo et al., 1994). A target region between positions of 20 and 29 is thought to be responsible for amyloid fibril formation by the human peptide. By contrast, rat amylin, which has a different amino acid sequence in the amyloidogenic molecular segment, does not aggregate to form fibrils and exhibits no cytotoxicity (Westermark et al., 1990).

Cellular damage inevitably results in loss of its ability to maintain and provide energy for metabolic cell function and growth. Thus, metabolic activity can be assayed to reflect cell viability. MTT assay is a colorimetric assay for the measurements of cell growth and metabolic activity. In the present study, MTT assay was first used to determine the effects of hIAPP on the growth of INS-1E pancreatic beta cells. I found that exposure of INS-1E cells to hIAPP resulted in time- and dose-dependent decrease in cell viability (**Fig. 3.1A**). As a negative control, rat IAPP

showed no cytotoxicity on INS-1E cells at various doses and time (**Fig. 3.1B**). Brdu incorporation assay was also performed to examine the effect of hIAPP on DNA synthesis of INS-1E cells. The results showed that hIAPP dose-dependently inhibited the proliferation of INS-1E cell after 24-h treatment (**Fig. 3.3A**). On the other hand, pretreatment with PC dose-dependently prevented the reduction in cell viability and proliferation of INS-1E cells (**Fig. 3.2B** and **Fig. 3.3B**).

The *in vitro* cytotoxicity of hIAPP was also determined by the release of cytosolic enzyme LDH into cell culture medium as a marker of membrane integrity. The results of LDH assay showed that hIAPP dose-dependently induced LDH release from INS-1E cells (**Fig. 3.4A**). However, the LDH release was significantly decreased by co-treatment with PC in a dose-dependent manner (**Fig. 3.4B**). These results are further confirmed by a trypan blue exclusion assay. Using this assay, I found that hIAPP dose-dependently reduced the viable cell numbers (**Fig. 3.5A**). Similar to the LDH release data, PC prevented the hIAPP-induced decrease in the number of viable cells in a dose-dependent manner (**Fig. 3.5B**).

4.2 Induction of apoptosis by hIAPP

Apoptosis is a highly regulated death process that plays an essential role in the maintenance of homeostasis in multicellular organisms. It is well known that cells undergoing apoptosis exhibit cell shrinkage, membrane blebbing, nuclear chromatin condensation, DNA fragmentation, and formation of apoptotic body (Darzynkiewicz et al., 1997; Raff, 1998). A number of studies revealed that the predominant mode of cell death induced by hIAPP in pancreatic beta cells is apoptosis (Butler et al., 2003;

Zhang et al., 2006; Zhang et al., 2003).

To identify cell death induced by hIAPP, INS-1E cells were first examined by phase-contrast microscopy. Under microscopic observation, INS-1E cells exposed to hIAPP exhibited cell shrinkage, reduction in cell volume, irregularity in shape, and finally, the cells detached from the dish (**Fig. 3.6A**). Additionally, chromosomal condensation and formation of apoptotic bodies were observed in the hIAPP-treated cells stained with DAPI. Moreover, DNA fragmentation is known to be generated in the nucleus during apoptosis, and the nicks in DNA molecules can be examined by TUNEL assay. As evidenced by the increase of positively stained cells in TUNEL assay, the presence of cells with characteristic DNA fragmentation increased on exposure to hIAPP (**Fig. 3.7**). However, these morphological features of apoptosis induced by hIAPP were significantly restored by co-treatment with PC (**Fig. 3.6A** and **Fig. 3.7**).

To further confirm the occurrence of apoptosis in hIAPP-treated cells, cells were stained with a nuclear stain (PI) and analyzed by flow cytometry. During apoptosis, chromosomal DNA can be degraded into small fragments (50 to 200 kb), then later into nucleosomal units of DNA fragments (Nagata, 2000). Therefore, cells undergoing apoptosis will appear as discrete peak called sub-G1 peak, indicating the presence of hypodiploid nucleosomes in the DNA histogram (Fischer and Schulze-Osthoff, 2005). By contrast, necrosis does not trigger extensive DNA degradation comparable to that of apoptosis. The products of degradation of necrosis are heterogenous in size and fail to form discrete peaks on the DNA histogram

(Darzynkiewicz et al., 1997). Therefore, the appearance of discrete sub-G1 peaks may serve as an evidence of occurrence of apoptosis. By the flow cytometry analysis, sub-G1 population appeared after 24 h of hIAPP incubation. The proportion of apoptotic cells were increased by hIAPP in a dose-dependent manner (**Fig. 3.8**). However, PC dose-dependently inhibited hIAPP-induced apoptosis in INS-1E cells (**Fig. 3.9**).

Taken together, our results confirmed that the cytotoxicity of hIAPP on INS-1E cells occurred mainly through induction of apoptosis, and cotreatment with PC prevented hIAPP-induced cytotoxicity toward INS-1E cells through inhibition of apoptosis.

4.3 Involvement of oxidative stress

Oxidative stress is a general term used to describe the potential biological damage in a cell, tissue or organ, caused by free radicals. Oxidative stress is associated with a number of pathological conditions, such as inflammation, carcinogenesis, aging, diabetes and associated complications (Halliwell et al., 1992; Uemura et al., 2001). Oxidative stress plays an important role in the pathophysiology of diabetes. Prolonged exposure to hyperglycemia causes nonenzymatic glycation of proteins through Maillard's reaction, and the resulting products, such as Schiff base and Amadori products, can lead to the production of ROS. Other circulating factors that are elevated in diabetes, such as free fatty acids and leptin, also contribute to increased ROS generation. The overproduction of ROS can cause cellular damage through modification and disruption of nucleic acids, phospholipids and proteins.

Due to very low levels of antioxidant enzyme expression, pancreatic islets are very sensitive to ROS-induced damage. Excessive reactive oxygen species may lead to further reduction in insulin secretion and contribute to progression of diabetes (Robertson et al., 2003; Tanaka et al., 2002; Xiong et al., 2006). Therefore, attenuation of oxidative stress is an important strategy to reduce the risk of diabetes-associated pathological damage.

ROS are highly reactive molecules which are formed by one or two electron reduction of O_2 (Czarna and Jarmuszkiewicz, 2006; Suh et al., 1999). They include singlet oxygen, non-radical hydrogen peroxide (H_2O_2) and radicals such as hydroxyl radical (HO•), superoxide anion (O_2•−). O_2•$^-$ is the primary ROS and can further transform to secondary ROS, such as HO•, hydrogen peroxide or singlet oxygen in living systems (Valko et al., 2007). ROS are generated as by-products of normal cellular metabolism. Under physiological conditions, ROS are scavenged by cellular antioxidant defense systems. Imbalance between ROS production and cellular defense mechanisms can result in overproduction of ROS.

ROS has been implicated in the initiation of apoptosis contributing to cell death signaling (Czarna and Jarmuszkiewicz, 2006). Several lines of evidence suggest that hIAPP-induced cell death was accompanied by ROS production in RINm5F cells (Janciauskiene and Ahren, 2000; Konarkowska et al., 2005). Other studies have shown that antioxidants, such as NAC and GSH, were able to scavenge ROS and rescued RINm5F cells from hIAPP toxicity (Konarkowska et al., 2005). Consistent with these studies, we also showed that hIAPP significantly induced generation of

intracellular ROS in INS-1E cells after 24-h treatment (**Fig. 3.10A**).

The superoxide anion is a well-recognized free radical species which is continuously generated during several cellular processes, including the microsomal and mitochondrial electron transport systems. It is the initial free radical formed from the mitochondrial electron transport systems. Mitochondria generate energy using electron chain reactions, reducing oxygen to water. Some of the electrons escaping from the chain reaction of mitochondria directly react with oxygen and result in generation of superoxide anion ? especially in situation where oxygen is insufficient. Additionally, superoxide is considered the "primary" ROS, which can interact with other molecules to generate "secondary" ROS. Thus, superoxide plays an important role in the formation of other ROS. Superoxide can be converted rapidly to H_2O_2 by SOD, while most of H_2O_2 are then further degraded to H_2O by the enzymes, catalase and GPX (Valko et al., 2005).

Hydroxyl radical, the most reactive free radical, can be generated from superoxide anion and hydrogen peroxide in the presence of metal ions such as iron or copper. The hydroxyl radical has a high reactivity and reacts with polypeptides, proteins, lipids and DNA (especially thiamine and guanosine). Thus, hydroxyl radical and its subsequent radicals are considered as the most harmful ROS being primarily responsible for the oxidative injury of biomolecules in living organisms.

In this thesis, I have shown that the levels of superoxide anion and hydroxyl radical were markedly up-regulated by hIAPP in a dose-dependent manner in INS-1E cells (**Fig. 3.11A** and **Fig. 3.12A**). Furthermore, pretreatment with PC inhibited the

hIAPP-induced overproduction of ROS and accumulation of superoxide anions and hydroxyl radicals (**Fig. 3.10B, Fig. 3.11B** and **Fig. 3.12B**) accompanied by recovery in cell viability. These findings suggest that PC is capable of scavenging free radicals and effectively protect INS-1 E cells against oxidative stress induced by hIAPP.

Oxidative stress occurs when free radical production exceeds antioxidant defence systems, when upon oxidative damage to cellular components follows. In order to prevent or repair oxidative damage, the cells develop both enzymatic and non-enzymatic systems. The enzymatic defense systems are conducted by SOD, GSH-PX and catalase (CAT). These antioxidant enzymes metabolize either free radicals or reactive oxygen intermediates to non-radical products, thereby exert defensive effects against oxidative damage. For example, SOD can catalyze the conversion of superoxide anions into H_2O_2 and oxygen, and then maintain a very low steady-state intracellular superoxide. H_2O_2 can be effectively converted to H_2O and molecular oxygen by CAT and/or GSH-PX.

The elimination of H_2O_2 is critical for attenuating oxidative stress, and the combined action of CAT and GSH-Px provides a repair mechanism for oxidized membrane components. When cells are under oxidative stress, these antioxidative enzymes are induced as an adaptive response. Besides enzymatic defense systems, the non-enzymatic mechanisms can also protect the cells from damages caused by oxidative stress. The non-enzymatic defense systems are antioxidant molecules such as glutathione (GSH) and ascorbate. GSH-Px utilizes reduced GSH as the hydrogen donor (Laybutt et al., 2002).

GSH-Px is a primary antioxidant enzyme responsible for detoxification of intracellular free radicals. Overexpression of GSH-Px can protect against ROS-induced apoptosis in many types of cells, while knockout of GSH-Px is particularly at risk for ROS-induced damage (Gouaze et al., 2001; Jaeschke et al., 1999). Decrease in cellular GSH-Px concentration was associated with cell damage and GSH-Px depletion enhanced the susceptibility of cells to stress-induced cell death (Chang et al., 2002). In agreement with previous reports of reduction in GSH-Px activity in neuronal cells exposed to beta-amyloid peptide (Wang et al., 2005), I found that hIAPP significantly decreased the GSH-Px activity in INS-1E cells (**Fig. 3.13A**), suggesting that hIAPP might damage these antioxidant enzymes.

It has been reported that beta-amyloid caused direct increase in activity of SOD in rat pheochromocytoma PC12 cells (Xiao et al., 2000). Consistent with these findings, I also demonstrated that hIAPP treatment induced increased SOD activity of INS-1E cells (**Fig. 3.14A**). This may indicate a stress response of the cells to hIAPP toxicity probably due to overproduction of ROS. Interestingly, co-treatment with PC prevented these changes in activities of GSH-Px and SOD and attenuated the cellular toxicity of hIAPP. Taken together, these findings suggest that PC might protect INS-1E cells against hIAPP through an antioxidant pathway.

Due to their reactive properties, overproduction of ROS can damage cell structures, leading to DNA degradation, lipid peroxidation and protein changes (Valko et al., 2007). Lipid peroxidation is one of the major outcomes of ROS-mediated cell damage, resulting in disrupted organization of the membrane.

These include changes in fluidity and permeability, inhibition of metabolic processes, and alterations of ion transport (Jia and Misra, 2007; Nigam and Schewe, 2000). Lipid peroxidation also causes damage to mitochondria resulting in further ROS generation. Importantly, lipid peroxides degrade to reactive aldehyde products, such as malondialdehyde (MDA), 4-hydroxynonenal and acrolein. These aldehydes then covalently bind to proteins through reaction with thiol groups and lead to alteration of protein function. As an end product of lipid peroxidation, MDA can alter the structure and function of the cell membrane and block cellular metabolism resulting in cytotoxicity. Thus, formation of MDA is a biomarker of lipid peroxidation which reflects cellular damage caused by ROS.

In this thesis, I showed that hIAPP not only elicited ROS overproduction, but also resulted in accumulation of MDA in INS-1E cells (**Fig. 3.15A**). In keeping with other findings, PC effectively inhibited the production of ROS and accumulation of MDA in hIAPP-treated cells (**Fig. 3.10B** and **Fig. 3.15B**).

4.4 Activation of MAPK pathways

MAPKs, mainly comprising of JNK, p38 and ERK, are implicated in various cellular processes, including cell proliferation, differentiation and apoptosis. MAPKs can be activated by a variety of stimuli including growth factors, hormones, mitogens, and stress factors (Raman et al., 2007; Razidlo et al., 2004). Additionally, oxidative stress is a key modulator of MAPK signaling cascades (Wada and Penninger, 2004). Activation of MAPKs may play a pathogentic role in progression of diabetes (Evans et al., 2002) by influencing survival and apoptotic signaling pathways in pancreatic

beta cells (Briaud et al., 2003; Simon et al., 2008). However, the divergent biological outcome of MAPK activation is dependent on the different stimuli and cell type.

JNK and p38 MAPK are involved in cell apoptosis and can be activated by stress stimuli, including cytokines, UV irradiation, toxic compounds, heat shock and oxidative stress (Nakano et al., 2006; Raman et al., 2007). In pancreatic beta cells, cytokine induced activation of JNK and p38 MAPK (Ammendrup et al., 2000; Larsen et al., 1998). Additionally, inhibition of JNK activation protected beta cells against IL-1 beta-induced apoptosis (Ammendrup et al., 2000; Bonny et al., 2001) and human islets against destruction mediated by IL-1beta and IFN-γ (Aikin et al., 2004). Conversely, JNK and p38 kinase have been reported to be associated with cell proliferation and anti-apoptosis (Nemoto et al., 1998; Wisdom et al., 1999). p38 is usually activated by stress stimuli, which can result in apoptosis in some cellular models. While activation of p38 was required for apoptosis induced by ischemia, cadmium and trophic factor withdrawal, SB203580, a p38 kinase inhibitor, was unable to prevent apoptosis induced by UV and S-nitrosoglutathione. Thus, the role of JNK and p38 activation remains controversial since it they can play a dual role either as an activator of apoptosis or survival pathways.

The link between these two kinases and hIAPP has been observed in RINm5F pancreatic beta cells with activation of JNK and p38 kinase in hIAPP-induced cell death (Rumora et al., 2002; Zhang et al., 2006). In agreement with these results, I found that hIAPP triggered the activation of JNK and p38 kinase in INS-1E cells (**Fig. 3.16**). Using the MTT assay, I found that inhibition of JNK and p38 activity by their

specific inhibitors attenuated cell death induced by hIAPP (**Fig. 3.17**), indicating the pro-apoptosis functions of JNK and p38 in the presence of hIAPP. Interestingly, PC could prevent the activation of JNK and p38 in hIAPP-treated INS-1E cells (**Fig. 3.18**), supporting the notion that the beta-cell protective effects of PC were at least partly mediated by suppressing the activation of JNK and p38.

In contrast to JNK and p38, ERK pathway is predominantly activated by mitogens or growth factors, and is associated with differentiation, proliferation and survival in many mammalian cells, including beta cells. Previous study showed that ERK mediated the pro-survival functions in primary pancreatic beta cells treated with IL1-beta (Hammar et al., 2004). Conversely, other study showed that activation of ERK contributed to IL-1 beta-induced apoptosis in primary rat pancreatic beta cells (Pavlovic et al., 2000). Even in the same cell type, the function of ERK can differ depending on cellular insults. For instance, hydrogen peroxide-induced apoptosis was inhibited by an ERK inhibitor in SH-SY5Y human neuroblastoma cells, while cadmium caused no change in ERK activation in the same cell line (Kim, 2005). Activation of ERK was also reported in hippocampal slices after beta-amyloid exposure (Dineley et al., 2001) and its inhibition could protect neurons from oxidative stress (Murray et al., 1998), which suggest the pro-death functions of ERK. Thus, the role of ERK activation is complex in the mediation of distinct cellular responses in different cell types.

In this context, my results are in line with previous reports that ERK activation does not contribute to hIAPP-induced apoptosis in RINm5F cells (Rumora et al., 2002;

Zhang et al., 2006), although phosphorylation of ERK was observed in the INS-1E cells treated with hIAPP. The final decision whether a cell will undergo apoptosis or survival may depend on the duration of activation and the balance of activity between the JNK, p38, ERK and possibly other pathways (Xia et al., 1995). When INS-1E cells was pretreated with a specific inhibitor of ERK upstream kinase (U0126), significant reduction of cell viability was not observed in hIAPP-treated cells (**Fig. 3.17**), which indicated that activation of ERK did not play an important role in hIAPP-induced apoptosis in INS-1E cells. Interestingly, cotreatment with PC prevented the activation of ERK in hIAPP-treated cells (**Fig. 3.18**), which may be due to the blocking of oxidative stress triggered by hIAPP.

4.5 Activation of caspase cascade

Apoptosis may occur via death receptor-mediated (extrinsic) and mitochondria-mediated (intrinsic) pathway. The former pathway involves activation of death receptors, caspase-8/-10, and subsequent activation of caspase-3. The mitochondrial pathway is regulated by Bcl-2 family members, which control the release of apoptogenic factors from the mitochondria into cytosol, such as cytochrome c, AIF and endonuclease G (Jourdain and Martinou, 2009).

Caspases, a family of aspartate-specific cysteine proteases, are known to play important roles in regulating apoptosis induced by different stimuli through cleavage of various specific substrates. Currently, more than 15 caspase family members are known to be activated by apoptotic signals. The caspase family includes the initiator caspases such as caspase -8, -9 and -10, and the effector caspases such as caspase-3,

-6 and -7 (Orrenius et al., 2007).

Among them, caspase-9 is the leading caspase in the intrinsic mitochondrial pathway; whereas caspase-8 is regarded as the key initiator of the death receptor-mediated apoptosis (Kumar, 2007). Previous works indicated that pancreatic beta cell apoptosis induced by hIAPP involved activation of caspase-8 in RINm5F cells (Zhang et al., 2008; Zhang et al., 2003). In agreement with these results, I demonstrated that hIAPP triggered the activation of caspase-8 in INS-1E cells (**Fig. 3.19**). Interestingly, I also found that activation of caspase-9 was evoked by hIAPP (**Fig. 3.19**), indicating that the mitochondria-dependent pathway was also implicated. The use of selective inhibitors of caspase-8 and caspase-9 confirmed that activation of caspase-8 and caspase-9 both contributed to hIAPP-induced apoptotic cell death (**Fig. 3.21B** and **Fig. 3.21C**). These initiator caspases then caused activation of effector capsase-7, capsase-3 and cleavage of PARP in INS-1E cells. Moreover, hIAPP-induced activation of caspase-8 and caspase-9 was attenuated by co-treatment with PC (**Fig. 3.22B**), suggesting that the protective effects of PC involve the suppression of both extrinsic and intrinsic apoptotic pathways.

Caspase-3 has been identified as a key mediator of apoptosis in mammalian cells (Putt et al., 2006). Activation of caspase-3 has been consistently observed in RINm5F cells after exposure to hIAPP (Zhang et al., 2003). In agreement with these findings, I showed that hIAPP induced activation of caspase-3 in a different pancreatic beta cell line INS-1E (**Fig. 3.19** and **Fig. 3.20B**), and hence triggered apoptosis. The activation of caspase-3 leads to the cleavage of specific substrates such

as Lamin A/C and PARP. PARP is a DNA repair protein that can be activated by DNA strand breaks (Schreiber et al., 2006). The cleavage of full-length PARP (116 kDa) to cleaved PARP (89 kDa) serves as a marker of apoptosis. In this study, hIAPP treatment caused cleavage of PARP in INS-1E cells (**Fig. 3.19**).

To further determine whether activation of caspase is required for hIAPP -induced cell apoptosis, the effects of general caspase inhibitors (z-VAD-fmk) were examined. Based on the results of Western blot analysis, I found that inhibition of caspase activation by general caspase inhibitor partially prevented hIAPP-induced cleavage of PARP (**Fig. 3.21A**). These findings indicated that hIAPP-induced caspase-dependent apoptosis in INS-1E cells. Furthermore, the results of MTT assay revealed that pretreatment of cells with z-VAD-fmk partially prevented hIAPP-induced cytotoxicity (**Fig. 3.21C**), suggesting that caspase activation was important for hIAPP-induced cell death in INS-1E cells.

To investigate the underlying mechanisms for protection of PC against hIAPP-induced apoptosis, I analyzed whether caspases and PARP were involved in this process. Using the Western blot analysis, caspase activity assay and Cleaved PARP Sandwich ELISA assay, PC treatment blocked the activation of caspase-3 and cleavage of PARP caused by hIAPP in INS-1E cells (**Fig.3.22**). Taken together, these results indicate that PC protected INS1-E cells against hIAPP-induced cytotoxicity through suppression of caspase-mediated apoptosis.

4.6 Involvement of mitochondrial dysfunction

Mitochondria play a central role in regulating apoptosis. Maintenance of $\Delta\Psi m$

is important for cell survival due to its implication in ATP synthesis and maintenance of oxidative phosphorylation (Bolt et al., 2001; Mingatto et al., 2002). Under normal physiological condition, the inner mitochondrial membrane is nearly impermeable to all ions to allow the build up of proton gradient necessary for oxidative phosphorylation (Kroemer et al., 1998). Therefore, the maintenance of the proton gradient within the mitochondria is an indicator of normal mitochondrial functions. Although a temporary loss of $\Delta\Psi m$ may occasionally occur in normal conditions, a permanent dissipation of $\Delta\Psi m$ is usually accompanied by cell apoptosis. Once the intrinsic apoptotic pathway is initiated, the mitochondrial membrane is perforated and the $\Delta\Psi m$ can no longer be maintained. Therefore, depletion of $\Delta\Psi m$ is a good indicator of mitochondrion-mediated cell apoptosis.

In this thesis, I used JC-1 flow cytometric analysis to detect the status of $\Delta\Psi m$ of INS-1E cells exposed to hIAPP. The loss of $\Delta\Psi m$ induces release of apoptogenic factors, such as cytochrome c and AIF from the mitochondrial inner space to cytosol. Once in the cytosol, cytochrome c binds to Apaf-1 in the presence of dATP and activates caspase-9, which, in turn, activates executioner caspase-3 and downstream cleavage of PARP, which eventually leads to cell apoptosis (Kroemer and Reed, 2000).

The activation of caspase-9 is a strong indicator of the elicitation of the mitochondrion-mediated apoptotic pathway. Caspase-9 is activated by the cytosolic complex called apoptosome which composes of Apaf-1, cyto c and dATP molecules. The apoptosome will recruit and activate caspase-9, which performs the subsequent

cleavage of apoptotic substrates (Shi, 2006). In this circumstance, the release of cyto c from depolarized mitochondria into the cytosol is critical for apoptosome formation. As a mobile electron carrier, cytochrome c binds electrostatically to negatively charged surfaces of respiratory complexes at the outer face of the inner membrane, and can freely shuttle among each complex. Thus, it is normally restricted to the intermembrane space because of the integrity of the mitochondrial membrane (Kannt et al., 1998). During the execution of apoptosis, disruption of mitochondrial membrane integrity will lead to release of apoptogenic factors such as cyto c into the cytosol. Therefore, the release of mitochondrial cyto c to the cytosol is a key event for execution of the intrinsic apoptotic pathway.

In the present study, during the apoptotic process induced by hIAPP, involvement of caspase-9 was further confirmed by cyto c release and loss of $\Delta\Psi m$. Based on the results of JC-1 flow cytometric analysis, hIAPP treatment induced a dose- and time-dependent depletion of $\Delta\Psi m$ in INS-1E cells (**Fig. 3.26** and **Fig. 3.27**). The loss of $\Delta\Psi m$ was accompanied by the release of mitochondrial cyto c into the cytosol (**Fig. 3.29A**), indicating the possible formation of apoptosome and thus activation of caspase-9. Interestingly, PC was able to prevent hIAPP-induced depletion of $\Delta\Psi m$ and release of mitochondrial cyto c into cytosol (**Fig. 3.28** and **Fig. 3.29B**).

AIF is a mitochondrial intermembrane protein with a dual-function that deals with events of life and death. In healthy cells, as a flavoprotein, AIF is confined to mitochondria where it exerts a vital function in bioenergetic and redox metabolism

(Modjtahedi et al., 2006). In apoptotic conditions, AIF is released from mitochondria during mitochondrial outer membrane permeabilization. AIF translocates first to the cytosol and then the nucleus, where it participates in chromatin condensation and large-scale DNA fragmentation, leading to cell death (Susin et al., 1999). In contrast to cyto c, AIF mediates the apoptotic cell death through a caspase-independent pathway (Krantic et al., 2007). In my experiments, AIF was released from mitochodria into cytosol in INS-1E cells after hIAPP treatment. Furthermore, I found that the general caspase inhibitor z-VAD-fmk failed to completely prevent hIAPP-induced apoptosis, which may be partly attributed to the occurrence of AIF-mediated caspase-independent apoptosis. Moreover, hIAPP-induced AIF release was effectively prevented by co-treatment with PC.

Mitochondria are the most important cellular organelles, which produce ATP by a process of oxidative phosphorylation in physiological conditions. Thus, ATP content is an indicator of mitochondrial function. It has been proposed that ATP is necessary for the execution of several steps in the apoptotic program (Eguchi et al., 1997). For instance, ATP is required for apoptosome complex formation which accelerates processing of pro-caspase-9, chromatin condensation and apoptotic body formation (Leung et al., 2007; Liu et al., 1996). Additionally, PARP can deplete cellular ATP due to its attempt to repair damaged DNA when activation of PARP is excessive. In the present study, we observed a decrease of ATP level after 24 h of incubation with the hIAPP and this effect was dose-dependent (**Fig. 3.23**). It is noteworthy that the reduction of ATP levels was accompanied by release of

cytochrome c, activation of PARP and apoptotic body formation. Therefore, the depletion of cellular ATP induced by hIAPP, may be in part due to release of cytochrome c and activation of PARP during the execution of apoptosis in INS-1E cells. However, hIAPP-induced ATP depletion was restored by co-treatment with PC. Taken together, these findings support our hypothesis that the mitochondria play a central role in the apoptotic process triggered by hIAPP. Moreover, PC was able to attenuate hIAPP-induced mitochondrial dysfunction in INS-1E cell.

4.7 Role of MPT pores

Mitochondria play an important role in cell death when their membrane permeability is increased. Mitochondria possess two discrete membrane systems, including an outer membrane which facilitates communication with the cytosol and an inner membrane involved in protein import, ion transport and energy production. The outer membrane permeabilization is regulated by Bcl-2 family members, which control the release of proteins from the mitochondrial intermembrane spaces. Activation of these mitochondrial proteins can result in cell apoptosis. Inner membrane permeabilization can be regulated by the mitochondrial permeability transition (MPT), which is activated by oxidative stress and calcium, and leads to bioenergetic failure and necrosis.

The mitochondrial permeability transition is an abrupt increase of permeability of the mitochondrial inner membrane to solutes with a molecular mass of less than 1.5 kDa. The MPT is mediated by a protein complex, the so-called mitochondrial permeability transition pore (MPT pore). MPT pore consists of the

voltage-dependent anion channel (VDAC: outer membrane channel), the adenine nucleotide translocator (ANT: inner membrane channel), cyclophilin D (Cyp D), and other molecule(s) (Crompton, 2003). A role of Cyp D in the MPT is supported by inhibition of the MPT by cyclosporine A, which is a specific inhibitor of the cyclophilin family.

The role of the MPT in apoptosis remains controversial. While some forms of apoptosis can be inhibited by CsA and the MPT pore ligands bongkrekic acid (Crompton, 2003; Green and Kroemer, 2004), other reported the lack of inihibition of apoptosis by CsA (Newmeyer and Ferguson-Miller, 2003) In other studies, the CsA-sensitive MPT was found to promote the complete release of cytochrome c during apoptosis (Crompton, 2003). Other researchers have shown that $\Delta\psi$ followed cytochrome c release in some types of apoptosis, indicating that the MPT was not always the cause of cytochrome c release and cell death.

MPT pore opening results in unequal distribution of ions in the inner membrane of mitochondria, swelling of the mitochondrial matrix, mitochondrial uncoupling, rupture of the mitochondrial outer membrane, and uncoupling of oxidative phosphorylation. After induction of MPT, small solutes equilibrate across the mitochondrial inner membrane. The high concentration of protein in the matrix then exerts a colloid osmotic pressure that drives the swelling of the inner membrane-matrix compartment. Swelling of inner membrane results in the rupture of the outer membrane and release of apoptogenic factors, such as cytochrome c, apoptosis inducer factor (AIF), second mitochondria-derived activator of

caspases/direct IAP binding protein (Smac/Diablo) and endonuclease G, from the intermembrane space into the cytosol.

The molecular mechanisms mediating release of cytochrome c remain elusive. There are at least two hypotheses to explain release of cytochrome c from mitochondria into cytosol. One involves the opening of an inner mitochondrial membrane channel, the so-called MPT pore, and another is independent of MPT pore opening (Kumarswamy and Chandna, 2009). The mechanism of mitochondrial AIF release remains unclear. There is some evidence indicating that release of AIF was independent of MPT pore opening. In the present study, after 24-h hIAPP treatment, release of cytochrome c and AIF was observed, but MPT pores were not opened. CsA is thought to be a specific inhibitor of MPT pore opening, as it interacts with cyclophilin D, part of the MPT pore, and thus prevents the release of proapoptotic factors. Our results showed that CsA was not able to prevent hIAPP-induced loss of $\Delta\Psi m$, release of cytochrome c and AIF, as well as activation of caspase-3 (**Fig. 3.30A** and **Fig. 3.30B**). These findings clearly indicate that hIAPP-induced apoptosis occurred independently of the MPT pore, and the release of cytochrome c and AIF was not due to the opening of conventional MPT pore.

4.8 Regulation of Bcl-2 family proteins

Another mechanism of cyto c release involves mitochondrial outer membrane permeabilization mediated by Bcl-2 family members. Pro-apoptotic members, including Bax and Bak, can oligomerize in mitochondrial outer membrane and form transmembrane channels, promote cell death by releasing cytochrome c and

other apoptogenic factors from the mitochondria. In contrast, anti-apoptotic members, including Bcl-2 and Bcl-XL, interact with the pro-apoptotic proteins, thereby maintain the integrity of mitochondrial outer membrane and prevent cyto c release. The BH3-only members such as Bim, PUMA and Bid antagonize and inactivate the anti-apoptotic members (Kroemer and Reed, 2000). Our results showed that hIAPP treatment up-regulated the expression of pro-apoptotic Bcl-2 family members and BH3-only proteins, and at the same time, down-regulated the expression of anti-apoptotic Bcl-2 family members (**Fig. 3.31** and **Fig. 3.32**). The regulation of Bcl-2 family proteins expression by hIAPP may be necessary to facilitate the release of mitochondrial cytochrome c. Interestingly, we demonstrated that hIAPP-induced changes in expression of Bcl-2 family proteins were restored by co-treatment with PC (**Fig. 3.34**). The BH3-only protein Bid is a specific substrate of caspase-8 in the Fas signaling pathway (Li et al., 1998). Once Bid is cleaved by caspase-8, the cleaved C-terminal Bid (tBid) translocates to the mitochondria to trigger cytochrome c release independent of the classic type of MPT pore mechanism. In addition, tBid is able to activate Bax to form oligomerization in mitochondrial membranes. We observed that exposure of INS-1E cells to hIAPP resulted in cleavage of Bid. Furthermore, cleaved Bid induced by hIAPP was attenuated by pretreatment with caspase 8 inhibitor z-IETD-FMK and pan-caspase inhibitor z-VAD-FMK, indicating that caspase 8 was responsible for Bid cleavage in hIAPP-treated cells (**Fig. 3.33**). These findings suggest that Bid-mediated cross-talk between extrinsic and intrinsic apoptotic pathways was implicated in the apoptotic process triggered by hIAPP, and the

cleavage of Bid by hIAPP may contribute to release of cytochrome c.

4.9 Protective effects of PC

Type 2 diabetes is characterised by islet amyloid deposits derived from hIAPP in the majority of patients, which is associated with islet beta cells loss. hIAPP has the propensity to aggregate from monomers into oligomers, fibrils, and mature amyloid deposits. Recent studies have suggested that the small hIAPP oligomers, rather than the amyloid fibrils, are responsible for beta cell cytotoxicity. Experimental studies which showed that cell death occurred in the absence of mature amyloid fibrils suggested that oligomers of hIAPP rather than fibrils were the main culprits for cell death (Ritzel et al., 2007). Preparations of hIAPP containing predominantly mature fibrils in beta sheet conformation exhibited low toxicity on RINm5F beta cells. By contrast, preparations containing fewer fibrils predominantly in the initial random coil state had high toxicity on RINm5F beta cells (Konarkowska et al., 2006). Other researchers have demonstrated activation of multiple apoptotic pathways by treatment with fresh soluble synthetic hIAPP. The residue 20-29 of hIAPP is particularly important for formation of oligomers. The amino-acid sequence of rat IAPP differs from hIAPP so that rat IAPP is not predisposed to aggregate into oligomers (Zraika et al., 2010). Taken together, prevention of islet oligomerization may be an effective therapeutic approach to reduce beta cells loss in type 2 diabetes.

Oligomer formation can be detected by high-resolution microscopy techniques, such as scanning tunnelling electron microscopy and atomic-force microscopy. Conformation-dependent antibodies have been developed to recognise

oligomers but not monomers or fibrils of several amyloidogenic proteins. A11 antibody was used to ensure its specificity and evaluate its reactivity kinetics. It was shown to detect soluble oligomers formed by hIAPP (Kayed and Glabe, 2006; Kayed et al., 2003). Interestingly, it has been shown that A11 antibody also binds natively folded proteins that display anti-aggregation activity, such as heat shock proteins and α-synuclein fibrils (Zraika et al., 2010). However, there is no report that A11 antibody has some cross reactivity with rIAPP.

In the present study, Dot blot assay was carried out to examine whether PC could interfere with aggregation of hIAPP. rIAPP was used as a negative control, and A11 antibody was used to detect the hIAPP oligomer in this assay. I found that PC partly prevented formation of oligomers induced by hIAPP. Throughout the study, before application to cells, lyophilized hIAPP was dissolved in HFIP which was then removed by evaporation under N_2. This process ensured that the monomer status of hIAPP. All hIAPP solutions applied to cultured cells were freshly prepared. In the culture media, hIAPP was likely to aggregate to oligomers and finally form amyloid fibrils. When PC was added to the medium, it was able to prevent formation of hIAPP oligomers and fibrils.

Amyloid β peptide (Aβ) and islet amyloid polypeptide (IAPP) are peptides of similar size, which are found in the amyloid deposits associated with Alzheimer's disease (AD) and type 2 diabetes mellitus, respectively. Aβ could induce oxidative stress and cause neuronal death. Oxidative stress and Aβ are linked to each other. Aβ can induce oxidative stress and acts as pro-oxidants, which in turn increase Aβ

production. Accordingly, Aβ may initiate generation of hydrogen peroxide at micromolar concentrations and reduce antioxidant defense systems. The consequent increase in oxidative stress may up-regulate expression of Aβ precursor protein with increased formation of Aβ peptides. It has been suggested that hydrogen peroxide was generated during the early stages of Aβ aggregation, while mature Aβ fibrils lacked the ability to generate hydrogen peroxide. Since oxidative stress can increase Aβ production, the presence of hydrogen peroxide may set up a potentially catastrophic positive feedback mechanism whereby Aβ oligomers stimulate their own production. Since amyloidogenic proteins share the ability to form oligomeric and fibrillar aggregates with common structures, a common mechanism has been proposed for cytotoxicity of Aβ and human IAPP (Paola et al., 2000; Tabner et al., 2005; Tamagno et al., 2006).

The association between oxidative stress and amyloid fibril formation has been extensively investigated in AD, but has not been pursued with the same intensity for islet amyloid in type 2 diabetes. A limited number of studies showed that oxidative stress was linked to hIAPP-induced pancreatic beta cell death. Further, in autopsy tissue from Japanese patients with type 2 diabetes, examination of islets containing amyloid revealed increased oxidative stress. Recent study showed that oxidative stress might feed back to exacerbate amyloid formation, thus contributing to beta cell apoptosis (Sakuraba et al., 2002; Zraika et al., 2009). Previous report suggested that ROS might cause unfolding of the tightly folded native amylin and accelerate accumulation of IAPP, resulting in even more rapid free radical

polymerization in the islets (Hayden et al., 2005). Therefore, attenuation of oxidative stress might provide a solution to prevent aggregation of hIAPP, and thus protect islet beta cells.

Since oxidative stress plays a key role in Aβ-mediated neurotoxicity, various experimental approaches to examine the protective effects of antioxidants have emerged. Numerous free-radical scavengers have been shown to protect neurons from Aβ-induced neurotoxicity, such as Ginkgo-Biloba extract, green tea polyphenol EGCG, genistein and nicotine (Longpre et al., 2006; Zhao, 2009). Furthermore, antioxidant treatment inhibited progression of human IAPP-induced apoptosis (Konarkowska et al., 2005). PC is a natural product purified from *Spirulina platensis* that is widely used as food supplement. Experimental studies have revealed that PC exerted ROS scavenging effects with a potent antioxidant capacity (Romay et al., 2003). The present study demonstrated that PC protected islet beta cells from hIAPP-induced apoptosis, which may be due to its capability to interfere with aggregation of hIAPP. These protective effects may be due to the ability of PC to scavenge ROSand thus prevent formation of hIAPP oligomer/fibril. The molecular weight of PC is about 35 kDa. Currently, there are no reports on whether PC can enter the cells or not. Results of my study cannot clarify whether PC exerted an intracellular effect but it is plausible that its protective effect might be due to its ability to inhibit extracelluar formation of hIAPP oligomer. In this regard, PC has no cytotoxicity and has been used as a food additive in some countries. My experimental studies suggest that PC may be used as food supplement to reduce beta cell death in type 2 diabetes,

although more preclinical and clinical studies will be needed. Given the common mechanisms shared by Aβ and amylin, it is possible that PC can also be used in the prevention and treatment of other forms of amyloid-associated human disease, such as Alzheimer's disease.

4.10 Summary

It is well known that misfolded hIAPP in the pancreatic islets is associated with loss of insulin-secreting beta cells in type 2 diabetic patients (Kahn et al., 1999). Mitochondrial dysfunction is a possible mechanism for impaired insulin secretion and cell apoptosis in pancreatic beta cells. However, the role of mitochondria in cytotoxicity attributed to hIAPP has not been elucidated.

Several lines of evidence support that hIAPP-induced cytotoxicity is mediated by the generation of ROS. PC is a well known antioxidant purified from *Spirulina* that is widely used as food supplement. Currently, little is known about the effects of PC on beta cells in the presence of hIAPP.

Against this background, I have produced original and unique data in the investigation of the role of mitochondria in hIAPP-induced apoptosis which can be attenuated by cotreatment with PC. In my experiments, I used a stable INS-1E rat cell line which was established from a radiation-induced rat insulinoma (Asfari et al., 1992). These cells showed typical features of primary islet beta cells with insulin secretion responses to various secretagogues. Using INS-1E cells as a model, I showed that hIAPP inhibited the growth of INS-1E cells, and induced cell death with apoptotic characteristics, as evidenced by chromatin condensation, DNA

fragmentation, appearance of Sub-G1 peak and PARP cleavage. This was accompanied by increased intracellular ROS, MDA, changes in activities of SOD and GSH-Px enzymes, as well as activation of MAPKs such as JNK and p38. These changes were significantly prevented by co-treatment with PC. Further mechanistic studies revealed that PC protected INS-1E cells from hIAPP-induced apoptosis through attenuating oxidative stress and modulating JNK and p38 signaling pathways.

Further molecular analysis showed that hIAPP-induced apoptosis was mediated by a cascade of caspases, including initiator caspase-8 of the extrinsic pathway and caspase-9 of the intrinsic pathway of apoptosis. These initiator caspases then activated effector caspase-3 and caspase-7. Moreover, hIAPP-induced apoptosis was associated with disruption of mitochondrial function, as evidenced by ATP depletion, reduction of mitochondrial mass, mitochondrial fragmentation and loss of $\Delta\Psi m$. Moreover, up-regulated expression of pro-apoptotic Bcl-2 family members, down-regulated expression of anti-apoptotic Bcl-2 family members, and release of cytochrome c and AIF from mitochondria into cytosol also contributed to hIAPP induced apoptosis. These results indicated the important role of mitochondria in these apoptotic processes which were attenuated by co-treatment with PC. However, administration of CsA did not prevent hIAPP-induced $\Delta\Psi m$ collapse, cytochrome c and AIF release and caspase-3 activation, indicating that MPT pore was not involved in hIAPP-induced apoptotic cell death.

In conclusion, based on results from this thesis, I proposed a comprehensive mechanism for the cytotoxicity of hIAPP on INS-1E cells, as depicted in **Fig. 4.1**.

These findings highlight the role of mitochondria in hIAPP-induced apoptosis. Thus, in insulin resistant subjects especially those with preserved beta cell function, measures to reduce hyperamylinemia may preserve beta cell function and prevent onset of diabetes. Results from my thesis also suggest that PC may possess such therapeutic potential while other compounds which can reduce oxidative stress or attenuate apoptotic signals are also be potential targets.

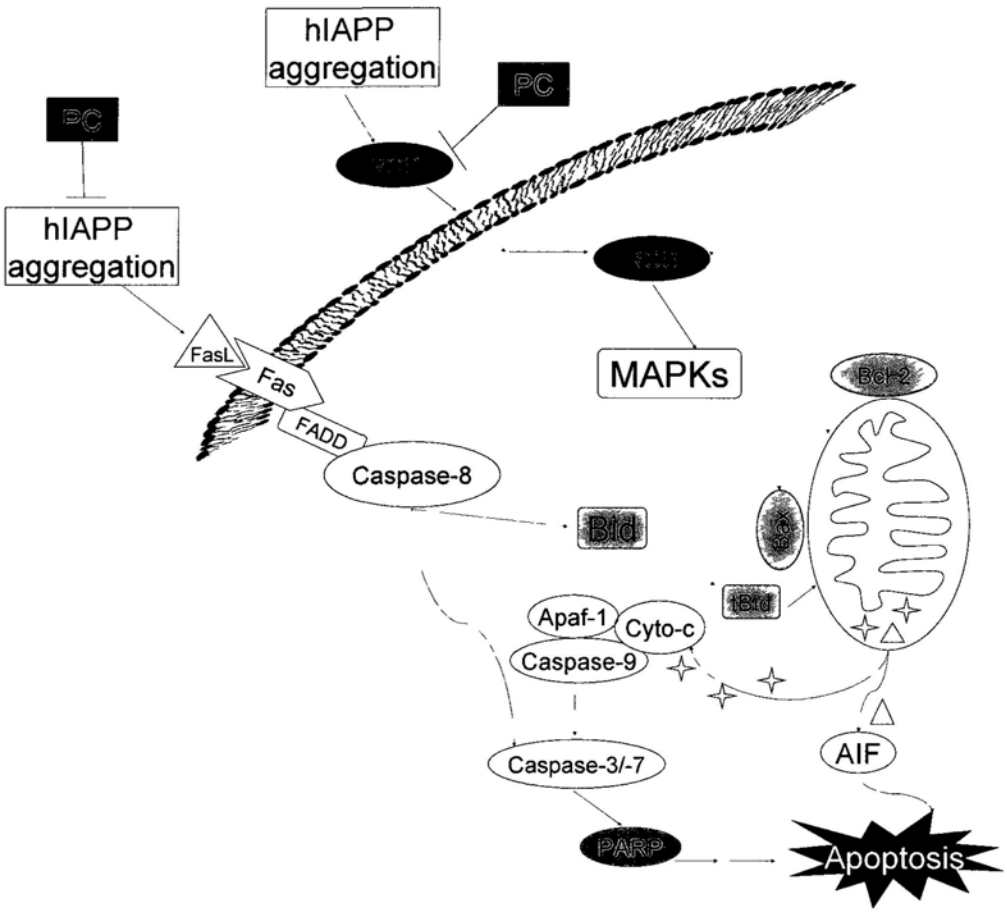

Fig. 4.1 Proposed signaling pathways of hIAPP-induced apoptosis and protection of phycocyanin (PC) in INS-1E cells. hIAPP induces apoptosis in INS-1E cells via both the extrinsic and the intrinsic apoptosis pathways. hIAPP elevates expression of

cell-surface death receptor, Fas, and then induces activation of caspase-8. The activated caspase-8 processes and activates Bid, which relays the signals from the extrinsic to the intrinsic apoptosis pathways with activation of caspase-9. hIAPP induces changes in expression of Bcl-2 family proteins, which results in depletion of $\Delta\Psi m$ and mitochondrial release of apoptogenic factors. Cytochrome c (Cyto-c) in the cytosol further activates caspase-9 and caspase-3, and subsequently causes PARP cleavage and cell apoptosis. hIAPP also induces generation of ROS and causes activation of MAPKs. These apoptotic pathways induced by hIAPP can be modulated by co-treatment with PC.

References

Aikin, R., Maysinger, D., and Rosenberg, L. (2004). Cross-talk between phosphatidylinositol 3-kinase/AKT and c-jun NH2-terminal kinase mediates survival of isolated human islets. Endocrinology *145*, 4522-4531.

Ammendrup, A., Maillard, A., Nielsen, K., Aabenhus Andersen, N., Serup, P., Dragsbaek Madsen, O., Mandrup-Poulsen, T., and Bonny, C. (2000). The c-Jun amino-terminal kinase pathway is preferentially activated by interleukin-1 and controls apoptosis in differentiating pancreatic beta-cells. Diabetes *49*, 1468-1476.

Asfari, M., Janjic, D., Meda, P., Li, G., Halban, P. A., and Wollheim, C. B. (1992). Establishment of 2-mercaptoethanol-dependent differentiated insulin-secreting cell lines. Endocrinology *130*, 167-178.

Blair, A. S., Hajduch, E., Litherland, G. J., and Hundal, H. S. (1999). Regulation of glucose transport and glycogen synthesis in L6 muscle cells during oxidative stress. Evidence for cross-talk between the insulin and SAPK2/p38 mitogen-activated protein kinase signaling pathways. J Biol Chem *274*, 36293-36299.

Bolt, M. W., Card, J. W., Racz, W. J., Brien, J. F., and Massey, T. E. (2001). Disruption of mitochondrial function and cellular ATP levels by amiodarone and N-desethylamiodarone in initiation of amiodarone-induced pulmonary cytotoxicity. J Pharmacol Exp Ther *298*, 1280-1289.

Bonny, C., Oberson, A., Negri, S., Sauser, C., and Schorderet, D. F. (2001). Cell-permeable peptide inhibitors of JNK: novel blockers of beta-cell death. Diabetes *50*, 77-82.

Briaud, I., Lingohr, M. K., Dickson, L. M., Wrede, C. E., and Rhodes, C. J. (2003). Differential activation mechanisms of Erk-1/2 and p70(S6K) by glucose in pancreatic beta-cells. Diabetes *52*, 974-983.

Butler, A. E., Janson, J., Bonner-Weir, S., Ritzel, R., Rizza, R. A., and Butler, P. C. (2003). Beta-cell deficit and increased beta-cell apoptosis in humans with type 2 diabetes. Diabetes *52*, 102-110.

Chang, W. K., Yang, K. D., Chuang, H., Jan, J. T., and Shaio, M. F. (2002). Glutamine protects activated human T cells from apoptosis by up-regulating glutathione and Bcl-2 levels. Clin Immunol *104*, 151-160.

Cory, S., and Adams, J. M. (2002). The Bcl2 family: regulators of the cellular life-or-death switch. Nat Rev Cancer *2*, 647-656.

Crompton, M. (2003). On the involvement of mitochondrial intermembrane junctional complexes in apoptosis. Curr Med Chem *10*, 1473-1484.

Czarna, M., and Jarmuszkiewicz, W. (2006). [Role of mitochondria in reactive oxygen species generation and removal; relevance to signaling and programmed cell death]. Postepy Biochem *52*, 145-156.

Darzynkiewicz, Z., Juan, G., Li, X., Gorczyca, W., Murakami, T., and Traganos, F. (1997). Cytometry in cell necrobiology: analysis of apoptosis and accidental cell death (necrosis). Cytometry *27*, 1-20.

Dineley, K. T., Westerman, M., Bui, D., Bell, K., Ashe, K. H., and Sweatt, J. D. (2001). Beta-amyloid activates the mitogen-activated protein kinase cascade via hippocampal alpha7 nicotinic acetylcholine receptors: In vitro and in vivo mechanisms related to Alzheimer's disease. J Neurosci *21*, 4125-4133.

Eguchi, Y., Shimizu, S., and Tsujimoto, Y. (1997). Intracellular ATP levels determine cell death fate by apoptosis or necrosis. Cancer Res *57*, 1835-1840.

Evans, J. L., Goldfine, I. D., Maddux, B. A., and Grodsky, G. M. (2002). Oxidative stress and stress-activated signaling pathways: a unifying hypothesis of type 2 diabetes. Endocr Rev *23*, 599-622.

Fischer, U., and Schulze-Osthoff, K. (2005). New approaches and therapeutics targeting apoptosis in disease. Pharmacol Rev *57*, 187-215.

Gouaze, V., Mirault, M. E., Carpentier, S., Salvayre, R., Levade, T., and Andrieu-Abadie, N. (2001). Glutathione peroxidase-1 overexpression prevents ceramide production and partially inhibits apoptosis in doxorubicin-treated human breast carcinoma cells. Mol Pharmacol *60*, 488-496.

Green, D. R., and Kroemer, G. (2004). The pathophysiology of mitochondrial cell death. Science *305*, 626-629.

Haataja, L., Gurlo, T., Huang, C. J., and Butler, P. C. (2008). Islet amyloid in type 2 diabetes, and the toxic oligomer hypothesis. Endocr Rev *29*, 303-316.

Halliwell, B., Gutteridge, J. M., and Cross, C. E. (1992). Free radicals, antioxidants, and human disease: where are we now? J Lab Clin Med *119*, 598-620.

Hammar, E., Parnaud, G., Bosco, D., Perriraz, N., Maedler, K., Donath, M., Rouiller, D. G., and Halban, P. A. (2004). Extracellular matrix protects pancreatic beta-cells against apoptosis: role of short- and long-term signaling pathways. Diabetes *53*, 2034-2041.

Hayden, M. R., Tyagi, S. C., Kerklo, M. M., and Nicolls, M. R. (2005). Type 2 diabetes mellitus as a conformational disease. Jop *6*, 287-302.

Jaeschke, H., Ho, Y. S., Fisher, M. A., Lawson, J. A., and Farhood, A. (1999). Glutathione peroxidase-deficient mice are more susceptible to neutrophil-mediated hepatic parenchymal cell injury during endotoxemia: importance of an intracellular oxidant stress. Hepatology *29*, 443-450.

Janciauskiene, S., and Ahren, B. (2000). Fibrillar islet amyloid polypeptide differentially affects oxidative mechanisms and lipoprotein uptake in correlation with cytotoxicity in two insulin-producing cell lines. Biochem Biophys Res Commun *267*, 619-625.

Jia, Z., and Misra, H. P. (2007). Reactive oxygen species in in vitro pesticide-induced neuronal cell (SH-SY5Y) cytotoxicity: role of NFkappaB and caspase-3. Free Radic Biol Med *42*, 288-298.

Jourdain, A., and Martinou, J. C. (2009). Mitochondrial outer-membrane permeabilization and remodelling in apoptosis. Int J Biochem Cell Biol *41*, 1884-1889.

Kahn, S. E., Andrikopoulos, S., and Verchere, C. B. (1999). Islet amyloid: a long-recognized but underappreciated pathological feature of type 2 diabetes. Diabetes *48*, 241-253.

Kannt, A., Lancaster, C. R., and Michel, H. (1998). The role of electrostatic interactions for cytochrome c oxidase function. J Bioenerg Biomembr *30*, 81-87.

Kayed, R., and Glabe, C. G. (2006). Conformation-dependent anti-amyloid oligomer

antibodies. Methods Enzymol *413*, 326-344.

Kayed, R., Head, E., Thompson, J. L., McIntire, T. M., Milton, S. C., Cotman, C. W., and Glabe, C. G. (2003). Common structure of soluble amyloid oligomers implies common mechanism of pathogenesis. Science *300*, 486-489.

Kim, R. (2005). Recent advances in understanding the cell death pathways activated by anticancer therapy. Cancer *103*, 1551-1560.

Kluck, R. M., Esposti, M. D., Perkins, G., Renken, C., Kuwana, T., Bossy-Wetzel, E., Goldberg, M., Allen, T., Barber, M. J., Green, D. R., and Newmeyer, D. D. (1999). The pro-apoptotic proteins, Bid and Bax, cause a limited permeabilization of the mitochondrial outer membrane that is enhanced by cytosol. J Cell Biol *147*, 809-822.

Konarkowska, B., Aitken, J. F., Kistler, J., Zhang, S., and Cooper, G. J. (2005). Thiol reducing compounds prevent human amylin-evoked cytotoxicity. Febs J *272*, 4949-4959.

Konarkowska, B., Aitken, J. F., Kistler, J., Zhang, S., and Cooper, G. J. (2006). The aggregation potential of human amylin determines its cytotoxicity towards islet beta-cells. Febs J *273*, 3614-3624.

Krantic, S., Mechawar, N., Reix, S., and Quirion, R. (2007). Apoptosis-inducing factor: a matter of neuron life and death. Prog Neurobiol *81*, 179-196.

Kroemer, G., Dallaporta, B., and Resche-Rigon, M. (1998). The mitochondrial death/life regulator in apoptosis and necrosis. Annu Rev Physiol *60*, 619-642.

Kroemer, G., and Reed, J. C. (2000). Mitochondrial control of cell death. Nat Med *6*, 513-519.

Kumar, S. (2007). Caspase function in programmed cell death. Cell Death Differ *14*, 32-43.

Kumarswamy, R., and Chandna, S. (2009). Putative partners in Bax mediated cytochrome-c release: ANT, CypD, VDAC or none of them? Mitochondrion *9*, 1-8.

Larsen, C. M., Wadt, K. A., Juhl, L. F., Andersen, H. U., Karlsen, A. E., Su, M. S., Seedorf, K., Shapiro, L., Dinarello, C. A., and Mandrup-Poulsen, T. (1998).

Interleukin-1beta-induced rat pancreatic islet nitric oxide synthesis requires both the p38 and extracellular signal-regulated kinase 1/2 mitogen-activated protein kinases. J Biol Chem *273*, 15294-15300.

Laybutt, D. R., Kaneto, H., Hasenkamp, W., Grey, S., Jonas, J. C., Sgroi, D. C., Groff, A., Ferran, C., Bonner-Weir, S., Sharma, A., and Weir, G. C. (2002). Increased expression of antioxidant and antiapoptotic genes in islets that may contribute to beta-cell survival during chronic hyperglycemia. Diabetes *51*, 413-423.

Leung, H. W., Lin, C. J., Hour, M. J., Yang, W. H., Wang, M. Y., and Lee, H. Z. (2007). Kaempferol induces apoptosis in human lung non-small carcinoma cells accompanied by an induction of antioxidant enzymes. Food Chem Toxicol *45*, 2005-2013.

Li, H., Zhu, H., Xu, C. J., and Yuan, J. (1998). Cleavage of BID by caspase 8 mediates the mitochondrial damage in the Fas pathway of apoptosis. Cell *94*, 491-501.

Liu, X., Kim, C. N., Yang, J., Jemmerson, R., and Wang, X. (1996). Induction of apoptotic program in cell-free extracts: requirement for dATP and cytochrome c. Cell *86*, 147-157.

Longpre, F., Garneau, P., Christen, Y., and Ramassamy, C. (2006). Protection by EGb 761 against beta-amyloid-induced neurotoxicity: involvement of NF-kappaB, SIRT1, and MAPKs pathways and inhibition of amyloid fibril formation. Free Radic Biol Med *41*, 1781-1794.

Lorenzo, A., Razzaboni, B., Weir, G. C., and Yankner, B. A. (1994). Pancreatic islet cell toxicity of amylin associated with type-2 diabetes mellitus. Nature *368*, 756-760.

Mingatto, F. E., Rodrigues, T., Pigoso, A. A., Uyemura, S. A., Curti, C., and Santos, A. C. (2002). The critical role of mitochondrial energetic impairment in the toxicity of nimesulide to hepatocytes. J Pharmacol Exp Ther *303*, 601-607.

Modjtahedi, N., Giordanetto, F., Madeo, F., and Kroemer, G. (2006). Apoptosis-inducing factor: vital and lethal. Trends Cell Biol *16*, 264-272.

Murray, B., Alessandrini, A., Cole, A. J., Yee, A. G., and Furshpan, E. J. (1998).

Inhibition of the p44/42 MAP kinase pathway protects hippocampal neurons in a cell-culture model of seizure activity. Proc Natl Acad Sci U S A *95*, 11975-11980.

Nagata, S. (1997). Apoptosis by death factor. Cell *88*, 355-365.

Nagata, S. (2000). Apoptotic DNA fragmentation. Exp Cell Res *256*, 12-18.

Nakano, H., Nakajima, A., Sakon-Komazawa, S., Piao, J. H., Xue, X., and Okumura, K. (2006). Reactive oxygen species mediate crosstalk between NF-kappaB and JNK. Cell Death Differ *13*, 730-737.

Nemoto, S., Xiang, J., Huang, S., and Lin, A. (1998). Induction of apoptosis by SB202190 through inhibition of p38beta mitogen-activated protein kinase. J Biol Chem *273*, 16415-16420.

Newmeyer, D. D., and Ferguson-Miller, S. (2003). Mitochondria: releasing power for life and unleashing the machineries of death. Cell *112*, 481-490.

Nigam, S., and Schewe, T. (2000). Phospholipase A(2)s and lipid peroxidation. Biochim Biophys Acta *1488*, 167-181.

Orrenius, S., Gogvadze, V., and Zhivotovsky, B. (2007). Mitochondrial oxidative stress: implications for cell death. Annu Rev Pharmacol Toxicol *47*, 143-183.

Paola, D., Domenicotti, C., Nitti, M., Vitali, A., Borghi, R., Cottalasso, D., Zaccheo, D., Odetti, P., Strocchi, P., Marinari, U. M., *et al.* (2000). Oxidative stress induces increase in intracellular amyloid beta-protein production and selective activation of betaI and betaII PKCs in NT2 cells. Biochem Biophys Res Commun *268*, 642-646.

Pavlovic, D., Andersen, N. A., Mandrup-Poulsen, T., and Eizirik, D. L. (2000). Activation of extracellular signal-regulated kinase (ERK)1/2 contributes to cytokine-induced apoptosis in purified rat pancreatic beta-cells. Eur Cytokine Netw *11*, 267-274.

Putt, K. S., Chen, G. W., Pearson, J. M., Sandhorst, J. S., Hoagland, M. S., Kwon, J. T., Hwang, S. K., Jin, H., Churchwell, M. I., Cho, M. H., *et al.* (2006). Small-molecule activation of procaspase-3 to caspase-3 as a personalized anticancer strategy. Nat Chem Biol *2*, 543-550.

Raff, M. (1998). Cell suicide for beginners. Nature *396*, 119-122.

Raman, M., Chen, W., and Cobb, M. H. (2007). Differential regulation and properties of MAPKs. Oncogene *26*, 3100-3112.

Razidlo, G. L., Kortum, R. L., Haferbier, J. L., and Lewis, R. E. (2004). Phosphorylation regulates KSR1 stability, ERK activation, and cell proliferation. J Biol Chem *279*, 47808-47814.

Ritzel, R. A., Meier, J. J., Lin, C. Y., Veldhuis, J. D., and Butler, P. C. (2007). Human islet amyloid polypeptide oligomers disrupt cell coupling, induce apoptosis, and impair insulin secretion in isolated human islets. Diabetes *56*, 65-71.

Robertson, R. P., Harmon, J., Tran, P. O., Tanaka, Y., and Takahashi, H. (2003). Glucose toxicity in beta-cells: type 2 diabetes, good radicals gone bad, and the glutathione connection. Diabetes *52*, 581-587.

Romay, C., Gonzalez, R., Ledon, N., Remirez, D., and Rimbau, V. (2003). C-phycocyanin: a biliprotein with antioxidant, anti-inflammatory and neuroprotective effects. Curr Protein Pept Sci *4*, 207-216.

Rumora, L., Hadzija, M., Barisic, K., Maysinger, D., and Grubiic, T. Z. (2002). Amylin-induced cytotoxicity is associated with activation of caspase-3 and MAP kinases. Biological chemistry *383*, 1751-1758.

Sakuraba, H., Mizukami, H., Yagihashi, N., Wada, R., Hanyu, C., and Yagihashi, S. (2002). Reduced beta-cell mass and expression of oxidative stress-related DNA damage in the islet of Japanese Type II diabetic patients. Diabetologia *45*, 85-96.

Schreiber, V., Dantzer, F., Ame, J. C., and de Murcia, G. (2006). Poly(ADP-ribose): novel functions for an old molecule. Nat Rev Mol Cell Biol *7*, 517-528.

Shi, Y. (2006). Mechanical aspects of apoptosome assembly. Curr Opin Cell Biol *18*, 677-684.

Simon, M. N., Azevedo-Martins, A. K., Amanso, A. M., Carvalho, C. R., and Curi, R. (2008). Persistent activation of Akt or ERK prevents the toxicity induced by saturated and polyunsaturated fatty acids in RINm5F beta-cells. Toxicol In Vitro *22*, 1018-1024.

Suh, Y. A., Arnold, R. S., Lassegue, B., Shi, J., Xu, X., Sorescu, D., Chung, A. B., Griendling, K. K., and Lambeth, J. D. (1999). Cell transformation by the

superoxide-generating oxidase Mox1. Nature *401*, 79-82.

Susin, S. A., Lorenzo, H. K., Zamzami, N., Marzo, I., Snow, B. E., Brothers, G. M., Mangion, J., Jacotot, E., Costantini, P., Loeffler, M., *et al.* (1999). Molecular characterization of mitochondrial apoptosis-inducing factor. Nature *397*, 441-446.

Tabner, B. J., El-Agnaf, O. M., German, M. J., Fullwood, N. J., and Allsop, D. (2005). Protein aggregation, metals and oxidative stress in neurodegenerative diseases. Biochem Soc Trans *33*, 1082-1086.

Tamagno, E., Bardini, P., Guglielmotto, M., Danni, O., and Tabaton, M. (2006). The various aggregation states of beta-amyloid 1-42 mediate different effects on oxidative stress, neurodegeneration, and BACE-1 expression. Free Radic Biol Med *41*, 202-212.

Tanaka, Y., Tran, P. O., Harmon, J., and Robertson, R. P. (2002). A role for glutathione peroxidase in protecting pancreatic beta cells against oxidative stress in a model of glucose toxicity. Proc Natl Acad Sci U S A *99*, 12363-12368.

Uemura, S., Matsushita, H., Li, W., Glassford, A. J., Asagami, T., Lee, K. H., Harrison, D. G., and Tsao, P. S. (2001). Diabetes mellitus enhances vascular matrix metalloproteinase activity: role of oxidative stress. Circ Res *88*, 1291-1298.

Valko, M., Leibfritz, D., Moncol, J., Cronin, M. T., Mazur, M., and Telser, J. (2007). Free radicals and antioxidants in normal physiological functions and human disease. Int J Biochem Cell Biol *39*, 44-84.

Valko, M., Morris, H., and Cronin, M. T. (2005). Metals, toxicity and oxidative stress. Curr Med Chem *12*, 1161-1208.

Wada, T., and Penninger, J. M. (2004). Mitogen-activated protein kinases in apoptosis regulation. Oncogene *23*, 2838-2849.

Wang, H., Xu, H., Dyck, L. E., and Li, X. M. (2005). Olanzapine and quetiapine protect PC12 cells from beta-amyloid peptide(25-35)-induced oxidative stress and the ensuing apoptosis. J Neurosci Res *81*, 572-580.

Westermark, P., Engstrom, U., Johnson, K. H., Westermark, G. T., and Betsholtz, C. (1990). Islet amyloid polypeptide: pinpointing amino acid residues linked to amyloid fibril formation. Proc Natl Acad Sci U S A *87*, 5036-5040.

Wisdom, R., Johnson, R. S., and Moore, C. (1999). c-Jun regulates cell cycle progression and apoptosis by distinct mechanisms. Embo J *18*, 188-197.

Xia, Z., Dickens, M., Raingeaud, J., Davis, R. J., and Greenberg, M. E. (1995). Opposing effects of ERK and JNK-p38 MAP kinases on apoptosis. Science *270*, 1326-1331.

Xiao, X. Q., Wang, R., and Tang, X. C. (2000). Huperzine A and tacrine attenuate beta-amyloid peptide-induced oxidative injury. J Neurosci Res *61*, 564-569.

Xiong, F. L., Sun, X. H., Gan, L., Yang, X. L., and Xu, H. B. (2006). Puerarin protects rat pancreatic islets from damage by hydrogen peroxide. Eur J Pharmacol *529*, 1-7.

Zha, J., Weiler, S., Oh, K. J., Wei, M. C., and Korsmeyer, S. J. (2000). Posttranslational N-myristoylation of BID as a molecular switch for targeting mitochondria and apoptosis. Science *290*, 1761-1765.

Zhang, S., Liu, H., Liu, J., Tse, C. A., Dragunow, M., and Cooper, G. J. (2006). Activation of activating transcription factor 2 by p38 MAP kinase during apoptosis induced by human amylin in cultured pancreatic beta-cells. Febs J *273*, 3779-3791.

Zhang, S., Liu, H., Yu, H., and Cooper, G. J. (2008). Fas-associated death receptor signaling evoked by human amylin in islet beta-cells. Diabetes *57*, 348-356.

Zhang, S., Liu, J., Dragunow, M., and Cooper, G. J. (2003). Fibrillogenic amylin evokes islet beta-cell apoptosis through linked activation of a caspase cascade and JNK1. J Biol Chem *278*, 52810-52819.

Zhao, B. (2009). Natural antioxidants protect neurons in Alzheimer's disease and Parkinson's disease. Neurochem Res *34*, 630-638.

Zraika, S., Hull, R. L., Udayasankar, J., Aston-Mourney, K., Subramanian, S. L., Kisilevsky, R., Szarek, W. A., and Kahn, S. E. (2009). Oxidative stress is induced by islet amyloid formation and time-dependently mediates amyloid-induced beta cell apoptosis. Diabetologia *52*, 626-635.

Zraika, S., Hull, R. L., Verchere, C. B., Clark, A., Potter, K. J., Fraser, P. E., Raleigh, D. P., and Kahn, S. E. (2010). Toxic oligomers and islet beta cell death: guilty by

association or convicted by circumstantial evidence? Diabetologia *53*, 1046-1056.

Appendix I: Publications

1. **Xiao-Ling Li**, Gang Xu, Tianfeng Chen, Yum-Shing Wong, Hai-Lu Zhao, Rong-Rong Fan, Xue-Mei Gu, Peter C.Y. Tong, Juliana C.N. Chan (2009). Phycocyanin protects INS-1E pancreatic beta cells against human islet amyloid polypeptide-induced apoptosis through attenuating oxidative stress and modulating JNK and p38 mitogen-activated protein kinase pathways. **The International Journal of Biochemistry & Cell Biology**. 41, 1526-1535.

2. **Xiao-Ling Li**, Tianfeng Chen, Yum-Shing Wong, Gang Xu, Hai-Lu Zhao, Rong-Rong Fan and Juliana C.N. Chan (2009). Human islet amyloid polypeptide -induced apoptosis in INS-1E pancreatic beta cells with involvement of mitochondrial dysfunction and the protection by Phycocyanin. (Submitted to **The International Journal of Biochemistry & Cell Biology**)

3. Rong-Rong Fan, **Xiao-Ling Li**, Gang Xu, Juliana C.N. Chan, Xue-Mei Gu (2010). Exendin-4 protects pancreatic beta cells from human islet amyloid polypeptide-induced cell damage: potential involvement of AKT and mitochondria biogenesis. **Diabetes Obesity and Metabolism**. 12, 815-824.

4. **Xiao-Ling Li**, Gang Xu, TianFeng Chen, Yum-Shing Wong, Hai-Lu Zhao, Peter C.Y. Tong, Juliana C.N. Chan. Phycocyanin protects INS-1E pancreatic beta cells against human islet amyloid-induced apoptosis through attenuating mitochondrial dysfunction. The 11th Hong Kong Diabetes and Cardiovascular Risk Factors-East Meets West Symposium. Hong Kong. 2009.

5. **Xiao-Ling Li**, Gang Xu, TianFeng Chen, Hai-Lu Zhao, Yum-Shing Wong, Peter C.Y. Tong1 Juliana C.N. Chan. Protective effects of phycocyanin on INS-1E pancreatic beta-cell against apoptosis induced by human islet amyloid polypeptide. The American Diabetes Association 68th Scientific Session. San Francisco, California, USA. Diabetes 2008; 57 (Suppl 1): A728 (2689-PO).

6. **Xiao-Ling Li**, Gang Xu, TianFeng Chen, Hai-Lu Zhao, Rong-Rong Fang, Xue-Mei

Gu, Yum-Shing Wong, Peter C.Y. Tong, Juliana C.N. Chan. Protective effects of phycocyanin against apoptotic cell death induced by human islet amyloid polypeptide in INS-1E pancreatic beta cells. The 5th Huaxia Congress of Endocrinology. Taipei. 4-9 December ,2008.

7. **Xiao-Ling Li**, Hai-Lu Zhao, Li-Zhong Liu, Peter C.Y. Tong, Juliana C.N. Chan. Induction of apoptosis by human islet amyloid polypeptide (hIAPP) in INS-1E pancreatic beta-cells. The 9th Hong Kong Diabetes and Cardiovascular Risk Factors-East Meets West Symposium. Hong Kong. 2007; Program Book 0024, P29.

8. Xue-Mei Gu, Kwan Li, **Xiao-Ling Li**, Rong-Rong Fang, Laybutt RD, Hai-Lu Zhao, Juliana C.N. Chan, Gang Xu. ER stress contributes to apoptosis induced by elevated fatty acids in HepG2 liver cells. The 45th Annual Meeting of the European-Association-for-the-Study-of-Diabetes. SEP 30-OCT 02, 2009 Vienna, AUSTRIA. Diabetologia. 52 (Suppl 1): S489-S489.
9. Xue-Mei Gu, Rong-Rong Fang, Kwan Li, **Xiao-Ling Li**, Laybutt RD, Gang Xu, Juliana C.N. Chan. Human islet amyloid peptide induced apoptosis of human liver cell line HepG2 via endoplasmic reticulum stress. Diabetologia 2008; 51(Suppl 1): S78-S78.
10. Gang Xu, Rong-Rong Fang, Xue-Mei Gu, **Xiao-Ling Li**, Kwan Li, Ronald Ma, Hai-Lu Zhao, Peter C.Y. Tong, Juliana C.N. Chan, Laybutt RD. Down regulation of GIP receptor by hyperlipidaemia: possible contribution to impaired incretin effects in type 2 diabetes. Diabetologia 2008; 51(Suppl 1): S257-S257.